12-14-2015

Novel Block Copolymer Architectures for Lithography-Relevant Self-Assembly

Jeffery Hakim Hayat
University of South Carolina - Columbia

NOVEL BLOCK COPOLYMER ARCHITECTURES FOR LITHOGRAPHY-RELEVANT SELF-ASSEMBLY

by

Jeffery Hakim Hayat

Bachelor of Science
University of Pittsburgh at Greensburg, 2011

Submitted in Partial Fulfillment of the Requirements

For the Degree of Doctor of Philosophy in

Chemistry

College of Arts and Sciences

University of South Carolina

2015

Accepted by:

Chuanbing Tang, Major Professor

Brian Benicewicz, Committee Member

Hui Wang, Committee Member

Ehsan Jabbarzadeh, Committee Member

Lacy Ford, Senior Vice Provost and Dean of Graduate Studies

DEDICATION

To my wife, my family, and all my friends, without their support and encouragement, none of my accomplishments would be possible.

ACKNOWLEDGEMENTS

First, I would like to show my sincerest gratitude to my advisor, Dr. Chuanbing Tang, who gave me the opportunity to work in his research group, and offered endless support and guidance on my research projects. I feel very fortunate to have the opportunity to learn from such an enthusiastic and knowledgeable person and it has proved invaluable in my development as a scientist. His enthusiasm for polymer science has influenced me a great deal and I am thankful for the foundation he has created for me and only hope to learn more from him in the future.

I would also like to thank my research committee Dr. Brian Benicewicz, Dr. Hui Wang, and Dr. Ehsan Jabbarzadeh for their advice, encouragement, and valuable suggestions on my research during graduate school. Further, I would like to acknowledge the research collaborations formed with Dr. Gila Stein's research group from the University of Houston and Dr. Morgan Stefik's research group from USC as they were instrumental in the research presented herein.

I am very appreciative of the experiences shared and friendships formed with other graduate students and post-docs at USC. Members of Tang group, Dr. Christopher Hardy, Dr. Kejian Yao, Dr. Perry Wilbon, Dr. Jiuyang Zhang, Dr. Yali Qiao, Dr. Yi Yan, Dr. Alper Nese, Dr. Xiaodong Yin, Dr. Zhongkai Wang, Mitra Ganewatta, Liang Yuan, Nathan Trenor, Paras Pageni, Anis Rahman, Pabel Kabir, Meghan Lamm, and many great others. It was a great pleasure to work with all of you and learn from you. I would

also like to thank Mike, Tony, Mohammad, Amrita, Andrew, and Zach for your help both within and outside of lab.

Further, I would like especially like to thank Kayley Fishel-Hayat for her constant support, listening, and help throughout my academic career, as it allowed me to reach this stage. Holly and Benji-thank you for always being there for mom so she could be there for me. Thank you very much!

Finally, I would like to acknowledge all the funding supports from the University of South Carolina, the SRC, and the ACS Petroleum Research Fund.

ABSTRACT

This dissertation is focused on the synthesis, characterization, self-assembly, and materials processing of various functionalized block copolymer systems. A variety of monomers were prepared and polymerized through various polymerization techniques including atom transfer radical polymerization, reversible addition-fragmentation chain transfer polymerization, and ring-opening metathesis polymerization. Self-assembly of the functionalized block copolymers led to well-defined nanostructures in bulk and thin films. These materials have the capability to be utilized in various applications including ordered catalysts and templates for nanolithography.

In Chapter 1, the overall background of diblock and triblock copolymers and their preparation methods is in this dissertation. Major research objectives of my doctoral work are described.

Chapter 2 focuses on the reduction of annealing time and use of industrially compatible solvents in high-humidity solvent annealing with poly(ethylene oxide)-*block*-poly(styrene). Chapters 3-5 describe the design, synthesis, and characterization of various diblock and triblock polymeric architectures and their self-assembly in both bulk and thin-films. Incorporating desirable functional groups into block copolymer systems can lead to confinement of the functional group to a specific domain upon microphase

separation of block copolymers. The resulting materials display desirable characteristics of the functional group in a well-ordered nanostructure.

Finally, chapter 6 provides a summary of the work described herein, and provides an outlook into future research with these block copolymer systems.

TABLE OF CONTENTS

LIST OF TABLES

LIST OF FIGURES

LIST OF SYMBOLS

T_g	glass transition temperature
M_n	number average molecular weight
χ	Flory-Huggins interaction parameter
N	degree of polymerization
f	volume fraction

List of Abbreviations

AFM ..... Atomic Force Microscopy

AIBN ..... Azobisisobutyronitrile

ATRP ..... Atom Transfer Radical Polymerization

BCP ..... Block Copolymer

CPPA ..... 4-Cyano-4-(phenylcarbonothioylthio) pentanoic acid

CRP ..... Controlled Radical Polymerization

Cu(I)Br ..... Copper (I) Bromide

Đ ..... Dispersity

DCM ..... Dichloromethane

DMF ..... *N*,*N*-Dimethylformamide

DSC ..... Differential Scanning Calorimetry

FTIR ..... Fourier Transform Infrared Spectrometry

GISAXS ..... Grazing Incidence Small-Angle X-ray Scattering

GPC ..... Gel Permeation Chromatography

ISP ..... poly(2-vinylpyridine-styrene-isoprene)

P2VP ..... poly(2-vinylpyridine)

PDI ..... Polydispersity Index

PEO ..... poly(ethylene oxide)

PI ..... polyisoprene

PMDETA ..... *N,N,N',N'',N''*-Pentamethyldiethylenetriamine

PMMA ..... poly(methyl methacrylate)

PS ..... polystyrene

RAFT ..... Reversible Addition-Fragmentation Chain-Transfer

SAXS ..... Small-Angle X-ray Scattering

TEM ..... Transmission Electron Microscopy

TGA ..... Thermogravimetric Analysis

THF ..... Tetrahydrofuran

CHAPTER 1

INTRODUCTION

1.1 Background

International Technology Roadmap for Semiconductors projects dynamic random-access memory (DRAM) ½ pitch at 22 nm and at 16 nm to be achieved at 2016 and 2019; a hurdle which the semiconductor industry will face in continuing to decrease the size of integrated circuit components, as photolithographic techniques currently employed in complementary metal oxide semiconductor transistors are reaching their lower limit.[1] Block copolymer nanolithography is a promising technique to drive further device miniaturization due to the nanometer-scale size of structures by self-assembly.[1, 2] However, significant challenges remain to be solved before block copolymer nanolithography can be realized as a practical solution to the semiconductor industries problems. Smaller feature size, uniform porous films, long-range order, and industrial benign processes are a few of the main requirements demanded by the nanotechnology industry as outlined in the ITRS.[1, 3-7]

1.2 Diblock Copolymers

Block copolymers are a class of materials that are composed of two covalently linked polymer chains.[8] The thermodynamic immiscibility of these polymers drives the formation of microphase separated structures with tunable size, shape, and periodicity.[9] These polymeric nanostructures can be utilized in a variety of applications ranging from lithographic masks, microelectronic device templates, magnetic storage media, and inorganic nano-objects, etc. [10-18] The microphase separated structures are controlled by three experimental parameters: Flory-Huggins interaction parameter (χ), degree of polymerization (N, proportional to molecular weight), and volume fraction of one of the

blocks (*f*) (Figure 1.1A).[19-22] The most common morphologies studied in A-B diblock copolymers are hexagonally packed cylinders, body-centered cubic spheres, and lamella, as shown in the phase diagram in Figure 1.1B. The segregation strength of the polymeric material is determined by the χN, while the phases are controlled by altering *f*.

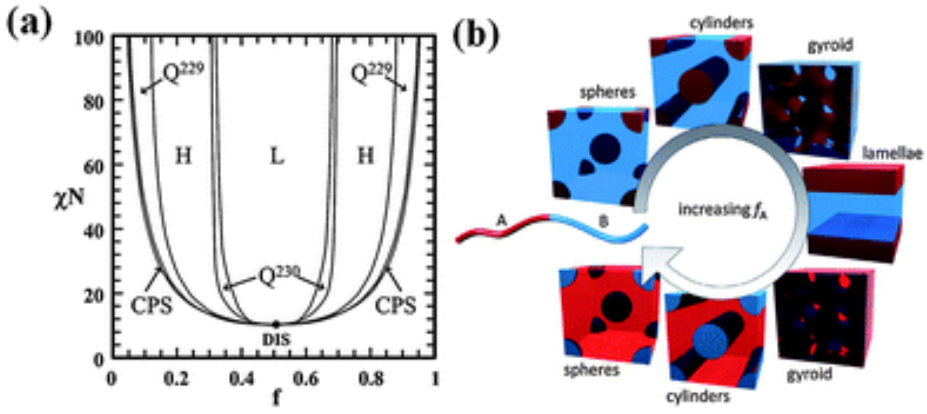

Figure 1.1 Diblock Copolymer Phase Diagram (**A**) and Architectures (**B**) [19-22]

Self-assembly and processing of these systems is what leads to arrays of highly ordered microphase separated structures. The periodicity of the nanostructures are usually in the range of 10-100 nm.[23] Long-range order and orientational control are done through various processing strategies including topographical and chemical graphoepitaxy, external fields, temperature gradients, and solvent annealing.[24-31] Furthermore, linear block copolymers can also be incorporated into different polymeric architectures such as grafted and star block copolymers to form nanostructures not possible from simple linear block copolymers.[32] Various polymeric architectures derived from different linear A-B diblock copolymers will be described in this thesis.

1.3 Triblock Copolymers

Although A-B diblock copolymers present many interesting characteristics, it is important to study block copolymer systems that can provide new ordered morphologies. Linear A-B-C triblock copolymers have gained tremendous attention due to their vast range of potential morphologies. The diverse morphological architectures are dictated by the three binary interaction parameters, two independent volume fractions and three different block sequences.[3, 33-37] In contrary to one binary interaction parameter, one volume fraction, and a single block sequence as seen in diblock copolymers, triblock copolymer morphologies range from tetragonal lattices of cylinders, periodic arrays core/shell spheres and cylinders, and novel bi and tri-continuous ordered mesophases, as seen in Figure 1.2.[38-40]

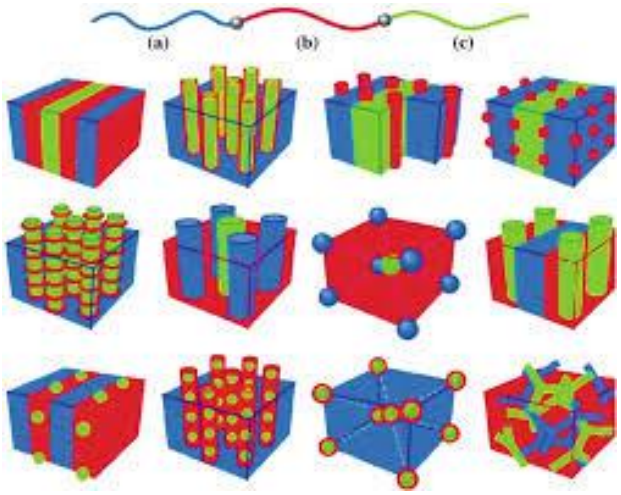

Figure 1.2 Architectures of Triblock Copolymers

Blends of diblock copolymers such as A-B/B-C and A-B/C-D have also been explored in the search for novel architectures; however, macrophase separation limits their ability to form more complex structures.[41, 42] In a related approach, blends of A-

B/B'-C block copolymers improve the compatibility and limit the macrophase separation as the B/B' interaction between the blend (usually hydrogen bonding) allows the B and B' block to form homogenous domains.[2, 43, 44] Among the various morphologies obtainable from the microphase separated structures, square arrays of cylinders are of particular importance for many applications. Compared to hexagonal arrays, square arrays are more compatible with current integrated circuit design based on the rectilinear system, however, more difficult to achieve due to their unique requirements on compositions.[2, 37, 43-47] Square arrays have been well predicted by numerical self-consistent field theory (SCFT) simulations which predict the formation of square cylinders in bulk in a symmetric triblock system, when A and C blocks are of similar volume fractions and the middle block as the major volume fraction ($\chi_{AB} \approx \chi_{BC} << \chi_{AC}$).[39, 40]

1.4 Polymerization Techniques and "Click" Chemistry

Atom Transfer Radical Polymerization (ATRP)[48-50] ATRP is one of the most used controlled radical polymerization (CRP) techniques. This polymerization provides great control over the reaction to develop well-defined polymeric architectures with predetermined molecular weight and narrow molecular weight distributions. The general mechanism for ATRP is shown below in Figure 1.3. The conditions of the polymerization use transition-metal complexes, by which the equilibrium between dormant and active species is strongly shifted toward dormant species in order to establish a low concentration of propagating radicals. The radicals (active species) $P_n\bullet$ are generated by a reversible redox process in the presence of the transition metal complex. The dormant species P_n-X are made through an reducing reaction between the transition metal complex

Cu(II)X/L and the propagating radicals.. Finally, many factors need to be considered to use this polymerization method, such as initiators, monomers, catalyst systems, temperature, and solvents.

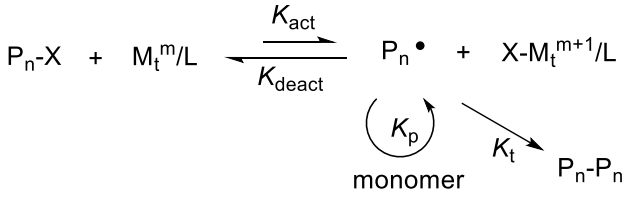

Figure 1.3 Overall mechanism of ATRP

Reversible Addition Fragmentation Chain Transfer Polymerization (RAFT)[51-53]

RAFT polymerization is another common controlled radical polymerization technique used to obtain predetermined molecular weight, and narrow molecular weight distribution in polymeric systems. RAFT was first reported by Rizzardo et al. in 1998.[52] This polymerization involves reversible addition-fragmentation chain transfer using a dithioester RAFT agent that contains appropriate R and Z groups. The use of the RAFT agent promotes chain transfer between the active and dormant species (Figure 1.4). Specifically, the R groups are those that can leave as a free-radical leaving group and also reinitiate the polymerization. Since RAFT is a radical process, the R group is vital to the stability of the radical intermediate and its ability to fragment. Some common R groups are cumyl and cyano alkyl groups. On the other hand, Z groups favor the stability of the RAFT agent and influences the rate of radical addition/fragmentation. Phenyl rings are the most common Z groups used in the RAFT. While there are numerous RAFT agents used, dithiobenzoates are readily used because their ability to provide control over many monomers and radical initiators. RAFT polymerization has been used to prepare

polymers of various architectures, including diblock copolymers, triblock copolymers, grafted polymers, and star polymers.

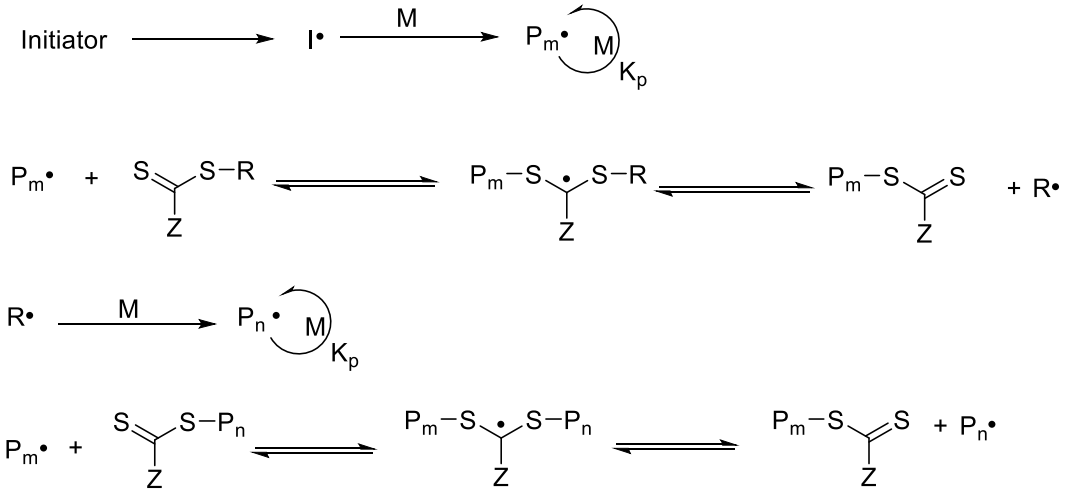

Figure 1.4 Overall mechanism of RAFT polymerization

Ring-Opening Metatheses Polymerization (ROMP)[54, 55] ROMP is an olefin metathesis chain-growth type polymerization. ROMP is an attractive technique to prepare new polymers with controlled molecular architectures since it is robust, highly efficient. The overall mechanism of ROMP is a metal-mediated carbon-carbon double bond exchange. Polymers prepared by ROMP contain unsaturated double bonds in each repeating unit. Most commonly, norbornene monomers are used as the relief of ring strain serves as the driving force. The catalysts used in ROMP include a variety of metals, but the most common and well-known ones are ruthenium based Grubbs' catalysts. Figure 1.5 shows the general mechanism and three different generations of Grubbs' catalysts.

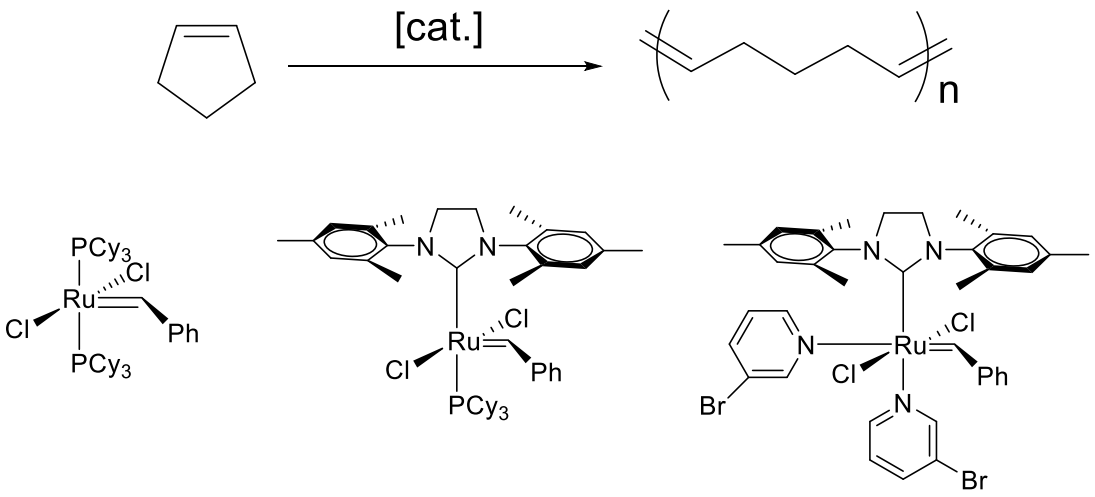

Grubbs' I catalyst Grubbs' II catalyst Grubbs' III catalyst

Figure 1.5 General Mechanism and Grubbs' catalysts for ROMP

"Click" Chemistry[56-58] "Click Chemistry" denotes certain reactions coined by Sharpless et al.[57] Click chemistry includes copper (I)-catalyzed azide-alkyne cycloaddition, thiol-ene, and Diels-Alder cycloaddition. Particularly the copper(I)-catalyzed azide-alkyne cycloaddition (CuAAC) was first categorized as a click reaction in 2002 by Sharpless and Meldal, and has become one of the most prominent methods used for post-polymerization modification.[57] CuAAC is a variation of the Huisgen 1,3-dipolar cycloaddition, it transforms organic azides and terminal alkynes into 1,4-disubstituted 1,2,3-triazoles (Figure 1.6). This reaction has been used in conjunction with ATRP and RAFT to produce a wide variety of functional polymers.[59-62]

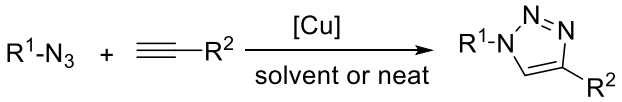

Figure 1.6 Copper catalyzed azide-alkyne cycloaddition (CuAAC)

All polymeric architectures have been designed from each of the abovementioned methods (ATRP, RAFT, and ROMP) through chain-extension with a second monomer,

or through post-polymerization modification to attach a second polymer ("click" chemistry) and produce functional polymeric materials (Scheme 1.1).[63]

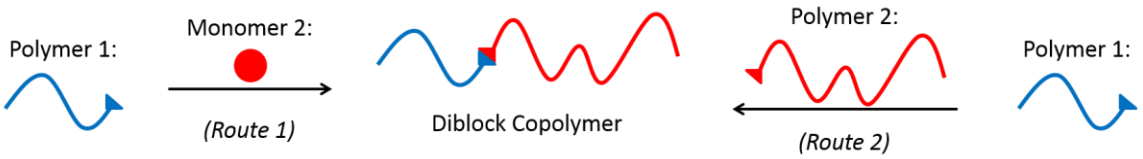

Scheme 1.1 Preparation of block copolymers by chain extension (*Route 1*) and polymer coupling (*Route 2*)

1.5 Dissertation Outline

This dissertation has two main research objectives. The first objective is to develop an industrial friendly and faster solvent annealing process. Understanding of the kinetics involved in solvent annealing using commonly employed solvents was carried out. Next, implementation of two industrially benign solvents and the kinetics, as well as efficiency, was studied.

The second objective of this thesis was to design, synthesize, and characterize functional polymeric materials for the use in advanced applications. Mainly, diblock, triblock, grafted, and star block copolymers containing various functional groups were designed and their self-assembly was studied

In Chapter 2, the reduction of solvent annealing time using poly(ethylene oxide)-*block*-polystyrene (PEO-*b*-PS) with toluene as the solvent was explored. Annealing time was reduced by nearly an order or magnitude by simply decreasing the solvent chamber volume. Also, implementation of industrially benign solvents, methyl ethyl ketone (MEK), and propylene glycol monomethyl ether acetate (PGMEA), was used to obtain ordered surface patterns with PEO-*b*-PS block copolymer.

In Chapter 3, novel grafted and star block copolymers were synthesized using a combination of ATRP, ROMP, and "click" chemistry. These architectures were developed to overcome severe de-wetting and to target low feature sizes and periodicity that proved near impossible for linear diblock copolymer PEO-*b*-PS from previous studies.

In Chapter 4, details of the preparation, polymerization, and self-assembly of novel P2VP-*b*-PS-*b*-PI triblock copolymer using RAFT and "click" chemistry were discussed. This system was aimed to target numerous morphology.

In Chapter 5, grafted diblock copolymers were prepared via RAFT, ATRP, ROMP, and "click" chemistry. As compared to Chapter 3's PEO-*b*-PS grafted and star diblock copolymers, these architectures were derived from PS-*b*-PMMA. This series of polymers provide great insights for future work.

Finally, a summary is given in Chapter 6. In addition, some suggestions about continued and future research of block copolymer self-assembly are provided.

1.6 References

1. Park, S.; Lee, D. H.; Xu, J.; Kim, B.; Hong, S. W.; Jeong, U.; Xu, T.; Russell, T. P., Macroscopic 10-Terabit–per–Square-Inch Arrays from Block Copolymers with Lateral Order. *Science* **2009,** *323* (5917), 1030-1033.
2. Tang, C.; Lennon, E. M.; Fredrickson, G. H.; Kramer, E. J.; Hawker, C. J., Evolution of Block Copolymer Lithography to Highly Ordered Square Arrays. *Science* **2008,** *322* (5900), 429-432.
3. Bang, J.; Kim, S. H.; Drockenmuller, E.; Misner, M. J.; Russell, T. P.; Hawker, C. J., Defect-Free Nanoporous Thin Films from ABC Triblock Copolymers. *Journal of the American Chemical Society* **2006,** *128* (23), 7622-7629.
4. Bita, I.; Yang, J. K. W.; Jung, Y. S.; Ross, C. A.; Thomas, E. L.; Berggren, K. K., Graphoepitaxy of Self-Assembled Block Copolymers on Two-Dimensional Periodic Patterned Templates. *Science* **2008,** *321* (5891), 939-943.

5. Ross, C., Patterned Magnetic Recording Media. *Annual Review of Materials Research* **2001,** *31*, 203-235.
6. Ruiz, R.; Kang, H.; Detcheverry, F. A.; Dobisz, E.; Kercher, D. S.; Albrecht, T. R.; de Pablo, J. J.; Nealey, P. F., Density Multiplication and Improved Lithography by Directed Block Copolymer Assembly. *Science* **2008,** *321* (5891), 936-939.
7. Ryu, D. Y.; Ham, S.; Kim, E.; Jeong, U.; Hawker, C. J.; Russell, T. P., Cylindrical Microdomain Orientation of PS-b-PMMA on the Balanced Interfacial Interactions: Composition Effect of Block Copolymers. *Macromolecules* **2009,** *42* (13), 4902-4906.
8. Bates, F. S.; Fredrickson, G. H., Block Copolymer Thermodynamics: Theory and Experiment. *Annual Review of Physical Chemistry* **1990,** *41*, 525-557.
9. Bates, F. S.; Fredrickson, G. H., Block Copolymers: Designer Soft Materials. *Physics Today* **1999,** *52*, 32-38.
10. Albert, J. N. L.; Epps III, T. H., Self-Assembly in Block Copolymer Thin Films. *Materials Today* **2010,** *13*, 24-33.
11. Bang, J.; Jeong, U.; Ryu, D. Y.; Russell, T. P.; Hawker, C. J., Block Copolymer Nanolithography: Translation of Molecular Level Control to Nanoscale Patterns. *Advanced Materials* **2009,** *21* (47), 4769-4792.
12. Hadjichristidis, N.; Pispas, S.; Floudas, G., *Block Copolymers: Synthetic Strategies, Physical Properties, and Applications*. John Wiley & Sons, Inc.: Hoboken, NJ, 2003.
13. Hamley, I. W., *The Physics of Block Copolymers*. Oxford University Press: Oxford, U.K., 1998.
14. Hamley, I. W., Ordering in thin films of block copolymers: Fundamentals to potential applications. *Progress in Polymer Science* **2009,** *34* (11), 1161-1210.
15. Kim, H.-C.; Park, S.-M.; Hinsberg, W. D., Block Copolymer Based Nanostructures: Materials, Processes, and Applications to Electronics. *Chemical Reviews* **2010,** *110* (1), 146-177.
16. Lazzari, M.; Liu, G.; Lecommandoux, S., *Block Copolymers in Nanoscience*. Wiley-VCH: Weinheim, 2007.
17. Park, C.; Yoon, J.; Thomas, E. L., Enabling Nanotechnology with Self Assembled Block Copolymer Patterns. *Polymer* **2003,** *44* (22), 6725-6760.
18. Park, M.; Harrison, C.; Chaikin, P. M.; Register, R. A.; Adamson, D. H., Block Copolymer Lithography: Periodic Arrays of ~1011 Holes in 1 Square Centimeter. *Science* **1997,** *276* (5317), 1401-1404.
19. Hajduk, D. A.; Harper, P. E.; Gruner, S. M.; Honeker, C. C.; Kim, G.; Thomas, E. L.; Fetters, L. J., The Gyroid: a New Equlibrium. *Macromolecules* **1994,** *27*, 4063-4075.
20. Helfand, E.; Wasserman, Z. R., Block Copolymer Theory .5. Spherical Domains. *Macromolecules* **1978,** *11* (5), 960-966.
21. Helfand, E.; Wasserman, Z. R., Block Co-Polymer Theory .6. Cylindrical Domains. *Macromolecules* **1980,** *13* (4), 994-998.
22. Matsushita, Y.; Mori, K.; Saguchi, R.; Nakao, Y.; Noda, I.; Nagasawa, M., Molecular-Weight Dependence of Lamellar Domain Spacing of Diblock Copolymers in Bulk. *Macromolecules* **1990,** *23* (19), 4313-4316.
23. Bates, F. S.; Fredrickson, G. H., Block Copolymers---Designer Soft Materials. *Physics Today* **1999,** *52* (2), 32-38.

24. Mansky, P.; DeRouchey, J.; Russell, T. P.; Mays, J.; Pitsikalis, M.; Morkved, T.; Jaeger, H., Large-Area Domain Alignment in Block Copolymer Thin Films Using Electric Fields. *Macromolecules* **1998,** *31* (13), 4399-4401.
25. Mansky, P.; Liu, Y.; Huang, E.; Russell, T. P.; Hawker, C., Controlling Polymer-Surface Interactions with Random Copolymer Brushes. *Science* **1997,** *275* (5305), 1458-1460.
26. Morkved, T. L.; Lu, M.; Urbas, A. M.; Ehrichs, E. E.; Jaeger, H. M.; Mansky, P.; Russell, T. P., Local Control of Microdomain Orientation in Diblock Copolymer Thin Films with Electric Fields. *Science* **1996,** *273* (5277), 931-933.
27. Ouk Kim, S.; Solak, H. H.; Stoykovich, M. P.; Ferrier, N. J.; de Pablo, J. J.; Nealey, P. F., Epitaxial self-assembly of block copolymers on lithographically defined nanopatterned substrates. *Nature* **2003,** *424* (6947), 411-414.
28. Rockford, L.; Mochrie, S. G. J.; Russell, T. P., Propagation of Nanopatterned Substrate Templated Ordering of Block Copolymers in Thick Films. *Macromolecules* **2001,** *34* (5), 1487-1492.
29. Segalman, R. A.; Yokoyama, H.; Kramer, E. J., Graphoepitaxy of Spherical Domain Block Copolymer Films. *Advanced Materials* **2001,** *13* (15), 1152-1155.
30. Stein, G. E.; Kramer, E. J.; Li, X.; Wang, J., Single-Crystal Diffraction from Two-Dimensional Block Copolymer Arrays. *Physical Review Letters* **2007,** *98* (8), 086101.
31. Tang, C.; Wu, W.; Smilgies, D.-M.; Matyjaszewski, K.; Kowalewski, T., Robust Control of Microdomain Orientation in Thin Films of Block Copolymers by Zone Casting. *Journal of the American Chemical Society* **2011,** *133* (30), 11802-11809.
32. Feng, C.; Li, Y.; Yang, D.; Hu, J.; Zhang, X.; Huang, X., Well-defined graft copolymers: from controlled synthesis to multipurpose applications. *Chemical Society Reviews* **2011,** *40* (3), 1282-1295.
33. Bailey, T. S.; Pham, H. D.; Bates, F. S., Morphological Behavior Bridging the Symmetric AB and ABC States in the Poly(styrene-b-isoprene-b-ethylene oxide) Triblock Copolymer System. *Macromolecules* **2001,** *34*, 6994-7008.
34. Chen, H.-Y.; Fredrickson, G. H., Morphologies of ABC triblock copolymer thin films. *Journal of Chemical Physics* **2002,** *116*, 1137-1146.
35. Nakazawa, H.; Ohta, T., Microphase Separation of ABC-Type Triblock Copolymers. *Macromolecules* **1993,** *26*, 5503-5511.
36. Rzayev, J.; Hillmyer, M. A., Nanochannel Array Plastics with Tailored Surface Chemistry. *Journal of the American Chemical Society* **2005,** *127*, 13373-13379.
37. Tang, C.; Bang, J.; Stein, G. E.; Fredrickson, G. H.; Hawker, C. J.; Kramer, E. J.; Sprung, M.; Wang, J., Square Packing and Structural Arrangement of ABC Triblock Copolymer Spheres in Thin Films. *Macromolecules* **2008,** *41*, 4328-4339.
38. Fredrickson, G. H.; Bates, F. S., Dynamics of Block Copolymers: Theory and Experiment. *Annual Review of Materials Research* **1996,** *26* (1), 501-550.
39. Mogi, Y.; Kotsuji, H.; Kaneko, Y.; Mori, K.; Matsushita, Y.; Noda, I., Preparation and Morphology of Triblock Copolymers of the ABC Type. *Macromolecules* **1992,** *25*, 5408-5411.
40. Mogi, Y.; Nomura, M.; Kotsuji, H.; Ohnishi, K.; Matsushita, Y.; Noda, I., Superlattice Structures in Morphologies of the ABC Triblock Copolymers. *Macromolecules* **1994,** *27*, 6755-6760.

41. Abetz, V.; Goldacker, T., Formation of superlattices via blending of block copolymers. *Macromolecular Rapid Communications* **2000,** *21*, 16-34.
42. Kimishima, K.; Jinnai, H.; Hashimoto, T., Control of Self-Assembled Structures in Binary Mixtures of A-B Diblock Copolymer and A-C Diblock Copolymer by Changing the Interaction between B and C Block Chains. *Macromolecules* **1999,** *32*, 2585-2596.
43. Tang, C.; Hur, S.-m.; Stahl, B. C.; Sivanandan, K.; Dimitriou, M.; Pressly, E.; Fredrickson, G. H.; Kramer, E. J.; Hawker, C. J., Thin Film Morphology of Block Copolymer Blends with Tunable Supramolecular Interactions for Lithographic Applications. *Macromolecules* **2010,** *43* (6), 2880-2889.
44. Tang, C.; Sivanandan, K.; Stahl, B. C.; Fredrickson, G. H.; Kramer, E. J.; Hawker, C. J., Multiple Nanoscale Templates by Orthogonal Degradation of a Supramolecular Block Copolymer Lithographic System. *ACS Nano* **2009,** *4* (1), 285-291.
45. Chuang, V. P.; Gwyther, J.; Mickiewicz, R. A.; Manners, I.; Ross, C. A., Templated Self-Assembly of Square Symmetry Arrays from an ABC Triblock Terpolymer. *Nano Letters* **2009,** *9* (12), 4364-4369.
46. Park, S.-M.; Craig, G. S. W.; La, Y.-H.; Solak, H. H.; Nealey, P. F., Square Arrays of Vertical Cylinders of PS-b-PMMA on Chemically Nanopatterned Surfaces. *Macromolecules* **2007,** *40* (14), 5084-5094.
47. Son, J. G.; Gwyther, J.; Chang, J.-B.; Berggren, K. K.; Manners, I.; Ross, C. A., Highly Ordered Square Arrays from a Templated ABC Triblock Terpolymer. *Nano Letters* **2011,** *11* (7), 2849-2855.
48. Matyjaszewski, K., Atom Transfer Radical Polymerization (ATRP): Current Status and Future Perspectives. *Macromolecules* **2012,** *45* (10), 4015-4039.
49. Siegwart, D. J.; Oh, J. K.; Matyjaszewski, K., ATRP in the design of functional materials for biomedical applications. *Progress in Polymer Science* **2012,** *37* (1), 18-37.
50. Wang, J.-S.; Matyjaszewski, K., Controlled/"living" radical polymerization. atom transfer radical polymerization in the presence of transition-metal complexes. *Journal of the American Chemical Society* **1995,** *117* (20), 5614-5615.
51. Barner-Kowollik, C., *Handbook of RAFT Polymerization*. Wiley: 2008.
52. Chiefari, J.; Chong, Y. K.; Ercole, F.; Krstina, J.; Jeffery, J.; Le, T. P. T.; Mayadunne, R. T. A.; Meijs, G. F.; Moad, C. L.; Moad, G.; Rizzardo, E.; Thang, S. H., Living Free-Radical Polymerization by Reversible Addition−Fragmentation Chain Transfer: The RAFT Process. *Macromolecules* **1998,** *31* (16), 5559-5562.
53. Chiefari, J.; Mayadunne, R. T. A.; Moad, C. L.; Moad, G.; Rizzardo, E.; Postma, A.; Thang, S. H., Thiocarbonylthio Compounds (SC(Z)S−R) in Free Radical Polymerization with Reversible Addition-Fragmentation Chain Transfer (RAFT Polymerization). Effect of the Activating Group Z. *Macromolecules* **2003,** *36* (7), 2273-2283.
54. Bielawski, C. W.; Grubbs, R. H., Living ring-opening metathesis polymerization. *Progress in Polymer Science* **2007,** *32* (1), 1-29.
55. Hejl, A.; Scherman, O. A.; Grubbs, R. H., Ring-Opening Metathesis Polymerization of Functionalized Low-Strain Monomers with Ruthenium-Based Catalysts. *Macromolecules* **2005,** *38* (17), 7214-7218.

56. Hein, J. E.; Fokin, V. V., Copper-catalyzed azide-alkyne cycloaddition (CuAAC) and beyond: new reactivity of copper(i) acetylides. *Chemical Society Reviews* **2010,** *39* (4), 1302-1315.
57. Rostovtsev, V. V.; Green, L. G.; Fokin, V. V.; Sharpless, K. B., A Stepwise Huisgen Cycloaddition Process: Copper(I)-Catalyzed Regioselective "Ligation" of Azides and Terminal Alkynes. *Angewandte Chemie International Edition* **2002,** *41* (14), 2596-2599.
58. Sumerlin, B. S.; Vogt, A. P., Macromolecular Engineering through Click Chemistry and Other Efficient Transformations. *Macromolecules* **2010,** *43* (1), 1-13.
59. Altintas, O.; Hizal, G.; Tunca, U., ABC-type hetero-arm star terpolymers through "Click" chemistry. *Journal of Polymer Science Part A: Polymer Chemistry* **2006,** *44* (19), 5699-5707.
60. Golas, P. L.; Tsarevsky, N. V.; Matyjaszewski, K., Structure–Reactivity Correlation in "Click" Chemistry: Substituent Effect on Azide Reactivity. *Macromolecular Rapid Communications* **2008,** *29* (12-13), 1167-1171.
61. Mantovani, G.; Ladmiral, V.; Tao, L.; Haddleton, D. M., One-pot tandem living radical polymerisation-Huisgens cycloaddition process ("click") catalysed by N-alkyl-2-pyridylmethanimine/Cu(i)Br complexes. *Chemical Communications* **2005,** (16), 2089-2091.
62. O'Reilly, R. K.; Joralemon, M. J.; Hawker, C. J.; Wooley, K. L., Fluorogenic 1,3-Dipolar Cycloaddition within the Hydrophobic Core of a Shell Cross-Linked Nanoparticle. *Chemistry – A European Journal* **2006,** *12* (26), 6776-6786.
63. Hardy, C. G. Functional Block Copolymers for Applications in Advanced Materials, Energy Storage, and Lithography. University of South Carolina, Columbia, SC, 2013.

CHAPTER 2

IMPROVING HUMIDITY-CONTROLLED SOLVENT ANNEALING PROCESSES FOR BLOCK COPOLYMER POLY(ETHYLENE OXIDE)-*B*-POLYSTYRENE[†]

[†] Hayat, J.; Mitra, I.; Qiao, Y.; Stein, G. E.; Tang, C. *European Polymer Journal* **2015**, *71*, 476-489. Reprinted here with permission of publisher.

2.1 Abstract

This chapter addresses two challenges in humidity-controlled solvent annealing of poly(ethylene oxide)-*b*-polystyrene thin films: (1) reduction in annealing time by nearly an order of magnitude for toluene under high humidity, which is achieved by decreasing the annealing chamber volume; (2) utilization of two industry-benign solvents, methyl ethyl ketone (MEK) and propylene glycol monomethyl ether acetate (PGMEA), to achieve ordered surface patterns under high humidity. When toluene is employed for annealing, the rate of block copolymer ordering is controlled by the time required to saturate the vapor phase, which depends on the chamber size in this study. The kinetics with MEK and PGMEA are more complex: While saturation time plays a role, these solvents reduce the incompatibility between PS and PEO, so longer annealing times are required to achieve good lateral order. We also present evidence that lateral ordering is faster than lattice swelling in the small chamber, so large grains are achieved without inflating the domain size and periodicity.

2.2 Introduction

Block copolymers are comprised of chemically distinct segments that are covalently bonded together. The thermodynamic immiscibility of these polymers drives the formation of microphase separated domains with tunable size, shape, and periodicity. The morphologies of block copolymers are controlled by their molecular characteristics.[1-5] There are three principal experimental parameters that dictate how a diblock copolymer microphase separates: Flory-Huggins interaction parameter (χ), degree of polymerization (N, proportional to molecular weight), and volume fraction of one of the blocks (f).[6] The

product χN controls the strength of segregation. The size and periodicity of nanostructures is tuned through changes in N, while phases are largely controlled by f.

Block copolymer thin films are used for nanolithographic masks,[7-12] templates for inorganic nano-objects,[8, 13-15] magnetic storage media,[16] and devices.[17, 18] These applications require good lateral ordering of the domains, and for anisotropic morphologies (lamellae and cylinders), the orientation of domains with respect to the interfaces must also be controlled. Lamellae and cylinders can align either parallel or perpendicular to a substrate depending on interfacial energetics and external structure-directing potentials. Popular examples of external potentials include electric fields,[19-22] chemically patterned substrates (chemoepitaxy),[23, 24] and topographically patterned substrates (graphoepitaxy).[25, 26]

This chapter focuses on two challenges in the high-humidity solvent annealing process of poly(ethylene oxide-*b*-styrene) (PEO-*b*-PS) diblock copolymer thin films: reduction of annealing time and implementation of two industry-benign solvents. Solvent annealing can induce domain ordering by plasticizing the copolymer to allow diffusion, modifying the effective χ parameter, and tuning energetics at the air interface to favor lateral ordering.[27-35] In addition to controlling solvent vapor pressure, humidity controls can be used to tailor surface interactions in copolymers with a hydrophilic block (such as PEO) and facilitate lateral ordering.[36-43] These procedures are well-documented with PEO-*b*-PS copolymers that form PEO cylinders or spheres in a PS matrix, and can induce long-range lateral ordering with grain sizes on the order of micrometers.[44-47]

High-humidity solvent annealing requires control over critical parameters such as solvent type, relative humidity (RH%), and annealing time. An appropriate solvent will solubilize both copolymer blocks. While many organic solvents meet this criterion for PEO-*b*-PS, the most commonly-employed reagents are carcinogenic or suspected carcinogenic, so they are not desirable for industrial processes. RH controls the lateral ordering of PEO domains at the film surface. For example, earlier work on cylindrical PEO-*b*-PS demonstrated that high RH (>90%) promotes perpendicular orientation at the surface whereas low RH (<80%) leads to parallel layers through the film thickness.[46] Furthermore, solvent vapor pressure and the solubility between the block copolymer and solvent partly determine the time needed for annealing.

Scheme 2.1 Humidity-controlled solvent annealing process for block copolymer PEO-*b*-PS in thin films

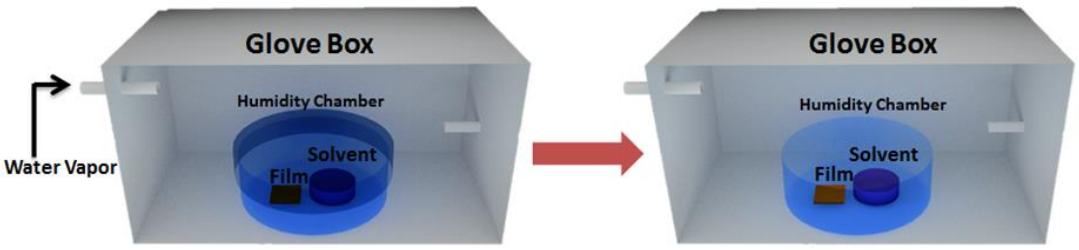

Scheme 2.1 illustrates the solvent annealing process that is employed in this work. A thin film of PEO-*b*-PS is placed inside a small chamber that includes a solvent reservoir, and the chamber was placed in a humid glove box. The small chamber consists of an upside-down petri dish over a petri dish containing the solvent reservoir and film. The upside-down petri dish acts a cover in the system. The small chamber was sealed by placing a heavy metal on top of the cover. The chamber becomes saturated with solvent vapor, which causes the film to form a swollen and homogenous polymer layer on the

substrate. The top of the small chamber (upside-down petri dish) was then opened and removed from inside the humid glove box. The exposure of the thin film to the large reservoir of the humid environment (>90%) would initiate a "de-swelling" process where the solvent evaporates from the film surface and leads to the formation of a concentration gradient in the film. Simultaneously, water vapor (humid environment) is preferentially solubilized by hydrophilic PEO segments and induces ordering of PEO domains on the surface. As solvent continues to evaporate, the ordering at the surface can propagate into the film.[17, 37, 38, 45, 48] It is important to note that de-swelling of the thin film is not affected by the volume of the small chamber since the de-swelling occurs only after the top of the chamber is removed.

There are two underlying practical challenges for this high-humidity solvent annealing process. First, annealing time needs to be significantly reduced. The typical timescale to achieve long-range lateral order in PEO-*b*-PS copolymers is hours to days, so it is not appropriate for high throughput production. Second, we demonstrate that long-range lateral order in PEO-*b*-PS thin films is achieved in minutes with humid toluene vapor by simply decreasing the annealing chamber volume. We also report the use of industry-benign solvents, such as methyl ethyl ketone (MEK) and propylene glycol monomethyl ether acetate (PGMEA), to achieve ordered surface patterns. These simple changes to high-humidity solvent annealing protocols are easily implemented in any laboratory environment.

2.3 Experimental Section

2.3.1 Materials

Tetrahydrofuran (THF) and dimethylformamide (DMF) were dried over molecular sieves and distilled before use. Styrene was passed through a basic alumina column before use. *N,N,N',N'',N''*-pentamethyldiethylenetriamine (PMDETA, Aldrich) and triethylamine (Et_3N, 99%, Aldrich) were distilled before use. Cu(I)Br (99.999% Aldrich) and 2-bromoisobutyryl bromide (Aldrich) used as received. Toluene (99%), methyl ethyl ketone (MEK, 99.0%), and propylene glycol monomethyl ether acetate (PGMEA, 99.5%) were purchased from Sigma Aldrich and used as received. All other reagents and solvents were purchased from Sigma Aldrich or Alfa Aesar and used as received.

2.3.2 Synthesis of PEO-*b*-PS

As shown in Scheme 2.2, the preparation of block copolymer poly(ethylene oxide)-*block*-polystyrene (PEO-*b*-PS) followed procedures reported earlier.[38, 40, 49] This block copolymer has a number-average molecular weight of 18,000 Da with the PEO fraction at 28 wt% and a dispersity of 1.10.

2.3.3 Characterization

Gel permeation chromatography (GPC) was performed at 50 °C on a Varian system equipped with a Varian 356-LC refractive index detector and a Prostar 210 pump. The columns were STYRAGEL HR1, HR2 (300 × 7.5 mm) from Agilent. HPLC grade DMF was used as eluent flow rate of 1.0 mL/min. Polystyrene standards were used for calibration.

2.3.4 Preparation of Thin Films

A block copolymer (1.5 wt%) toluene solution was spin coated (3000 RPM, 60 s) onto oxidized silicon substrates (100 nm thick thermal oxide). The thin films were annealed in a glove box with controlled humidity as shown in Scheme 2.1. Three different solvents were used for solvent annealing: toluene, MEK, and PGMEA. Annealing time was varied for each solvent. All films were saturated with solvent vapor in a chamber before exposure in the humid glove box. Grain sizes were determined by measuring areas of complete grains from at least five different micrographs and calculating an average of selected areas. Film thicknesses were measured with a J.A. Woollam spectroscopic ellipsometer with an incident angle of 70°. Ellipsometry data (Δ, Ψ) were modeling using the Cauchy dispersion relation to describe the refractive index of the polymer film, i.e., $n(\lambda) = A + B/\lambda^2$, where *A*, *B*, and polymer film thickness were adjustable parameters for regression analysis (all positive values). All film thicknesses were in the range of 55 to 65 nm.

2.3.5 Atomic Force Microscopy

Atomic force microscopy (AFM) was performed using a Multimode Nanoscope V system (Bruker, Santa Barbara, CA). Tapping mode AFM was used to map the topography by tapping the surface using an oscillating tip. The measurements were performed using commercial Si cantilevers with a nominal spring constant and resonance frequency at 20–80 N m^{-1} and 230–410 kHz, respectively (TESP, Bruker AFM Probes, Santa Barbara, CA). The spacing between close-packed rows of dots or adjacent parallel cylinders was calculated from the power spectral density using the Bruker software. The sizes of ordered "grains" were calculated from AFM micrographs using ImageJ software:

Grain boundaries were traced using the polygon option. We calculate the area of each polygon, and then define a circle of equal area to calculate the grain "diameter". (Grains that extend outside the range of the image were excluded from the analysis.) The image sizes used for this analysis ranged from 2 μm at short times up to 4 μm at longer times. The standard deviation is based on the average from 2-3 images per sample.

2.3.6 Grazing-Incidence Small Angle X-ray Scattering (GISAXS)

GISAXS experiments were performed at beam line 8-ID-E at the Advanced Photon Source of Argonne National Laboratory. Samples were placed in a low vacuum chamber and illuminated with 7.35 keV (λ=0.168 nm) radiation at incident angles in the range of 0.1-0.24º (critical angle of the polymer is approximately 0.16º). The off-specular scattering was recorded with a Pilatus 1MF pixel array detector (pixel size = 172 μm) positioned 2175 mm away from the sample. Slit sizes were 50 μm (vertical) and 100 μm (horizontal). Acquisition times were on the order of 10 sec for each incident angle. Each data set is stored as a 981×1043 32-bit tiff image with 20-bit dynamic range. Note that α_i, α_f, and α_c denote the incident angle, exit angle, and critical angle of the polymer, respectively.

2.4 Results and Discussion

A linear diblock copolymer was synthesized using mono-functional poly(ethylene oxide) (PEO), as shown in Scheme 2.2.[49]

Scheme 2.2 Synthesis of block copolymer PEO-*b*-PS according to previous reported literature[38, 40, 49]

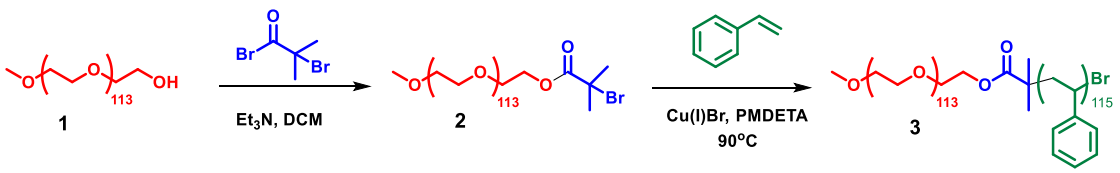

Mono-hydroxyl terminated PEO (**1**) with a number-averaged molecular weight 5000 Da was converted into an atom transfer radical polymerization (ATRP) macroinitiator (**2**) by reacting the terminal hydroxide group with 2-bromoisobutyrl bromide in the presence of triethylamine. Block copolymer PEO-*b*-PS (**3**) was synthesized by chain extension of the macroinitiator (**2**) with styrene using Cu(I)Br and PMDETA as the catalyst system at 90 °C. The molecular weight of polystyrene was monitored by proton NMR (Figure 2.1). The monomer conversion was obtained by calculating the decrease in styrene monomer signals at 5.74 and 5.22 ppm as compared to the PEO backbone protons at 3.47-3.77 ppm. The final block copolymer has a molecular weight 18,000 Da with a PEO fraction of 28.0 wt% and dispersity (*Đ*) of 1.10. It has been well demonstrated that PEO-*b*-PS with a PEO (5000 Da) block in the range of 20-30 wt% can produce cylindrical morphologies both in bulk and thin films under humidity-controlled solvent annealing.[36-39, 41-45]

Films of PEO-*b*-PS with thicknesses of ~60 nm were spin-cast on silicon/silicon oxide substrates from 1.5 wt% toluene solutions. The films were then subjected to the high-humidity annealing protocol introduced in Scheme 2.1. The chamber sizes were 1236 cm^3 ("large") and 64 cm^3 ("small") (Scheme 2.3). The solvent reservoir inside the chamber has a volume of 15.7 cm^3. Three solvents were compared: toluene, MEK and PGMEA. The efficacy of toluene in high-humidity solvent annealing processes has been established by other studies,[36-39, 41-45] and thus these outcomes serve as a reference for the current work with more benign MEK and PGMEA. All films were solvent annealed for times ranging from 0.5 hours to 20 hours, and then “de-swelled’’ for a period of time in the humid glove box.

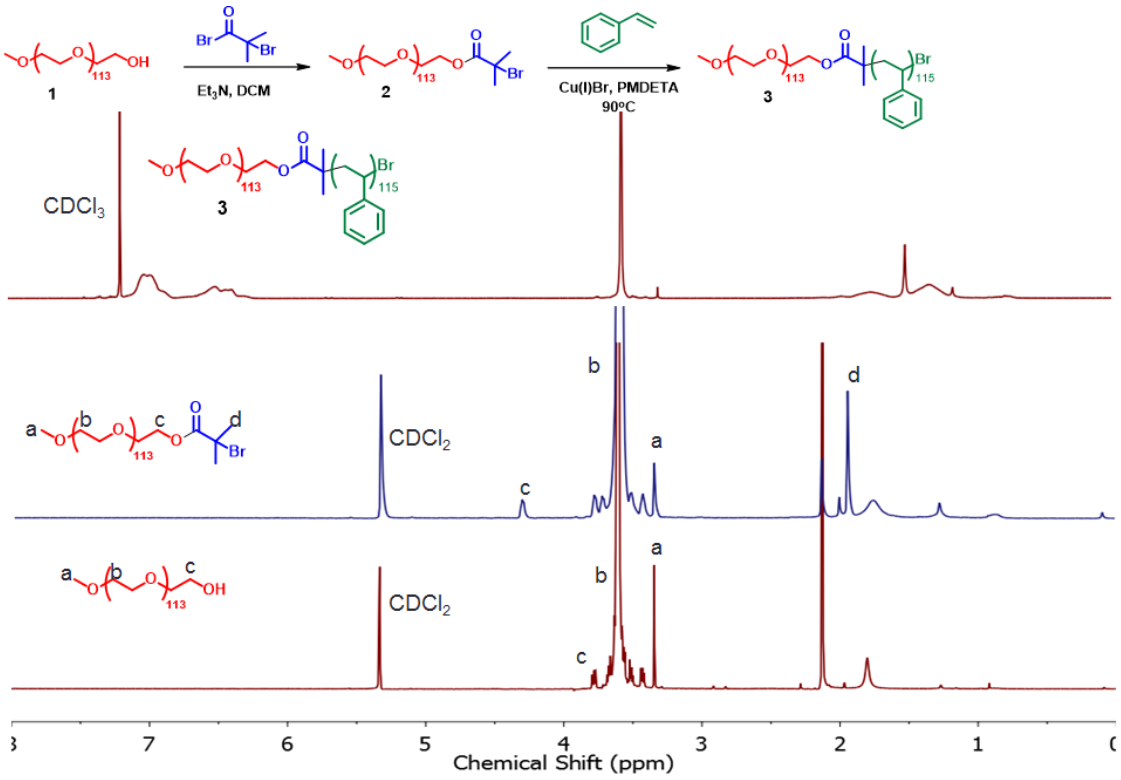

Figure 2.1 ^{1}H NMR spectra of PEO-*b*-PS, PEO-Br and PEO

Scheme 2.3 Solvent Annealing Chambers

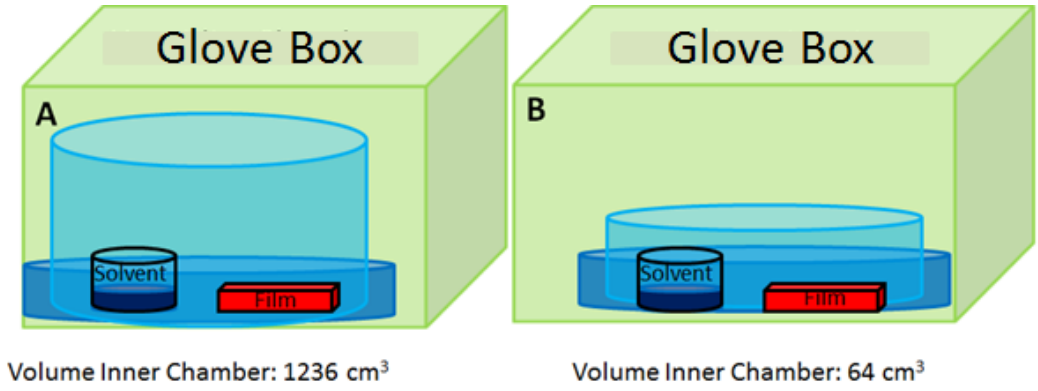

Hansen solubility parameters for PS, PEO, and each solvent are summarized in Table 2.1, and were used to predict the Flory-Huggins χ-parameter for each polymer/solvent pair:[50]

$$\chi = \frac{v_s A_{12}}{RT} \tag{2.1}$$

where v_s is the solvent molar volume, and the exchange-energy density of two components is:

$$A_{12} = (\delta_d^1 - \delta_d^2)^2 + 0.25(\delta_p^1 - \delta_p^2)^2 + 0.25(\delta_h^1 - \delta_h^2)^2 \tag{2.2}$$

Predicted χ-parameters are summarized in Table 2.2. Toluene is selective to the PS domains, while all other solvents are selective to PEO. Note that the values for PS/solvent pairs are consistent with other predictions and experimental measurements.[50]

Table 2.1 Hansen solubility parameters

Material	δ_d ($MPa^{1/2}$)	δ_p ($MPa^{1/2}$)	δ_h ($MPa^{1/2}$)
PS[51]	18.6	0.2	0
PEO[52]	16.3	6.1	9.4
Toluene[50]	18.0	1.4	2.0
MEK[50]	16.0	9.0	5.1
PGMEA[53]	16.1	6.1	6.6
Water[52]	15.5	16.0	42.4

The vapor pressures of toluene, MEK, and PGMEA are summarized in Table 2.3 for 25 ^oC. The vapor pressure (P^{vap}) will control the concentration of solvent vapor in the chamber, while both P^{vap} and χ will determine the solvent fraction in the film (φ^s).

Table 2.2 Estimated χ-parameters at 298K for each polymer/solvent system

	PS	PEO
Toluene	0.26	0.94
MEK	0.43	0.26
PGMEA	0.41	0.11
Water	2.84	2.15

The equilibrium solvent fraction is estimated with Flory-Huggins theory: The chemical potential of solvent in the vapor phase and the film must be equal at equilibrium, leading to Equation 2.3:

$$\ln(P^{vap}/P^0) = \chi(1-\varphi^s) + \ln(\varphi^s) + (1-1/N)(1-\varphi^s) \qquad (2.3)$$

where P^0 is a reference state of 1.01 bar (normal boiling). Results are reported in Table 2.3. Vapor pressure has the strongest impact on solvent concentration in the film, and polymer-solvent compatibility plays a secondary role. The predicted concentration for the toluene/PS system is consistent with other literature studies that directly measure solvent uptake.[54]

Table 2.3 Solvent vapor pressure at 25 °C and equilibrium concentration of solvent in the PS and PEO domains (volume fractions φ^s)

Solvent	**P^{vap} at 25 °C (bar)**	**φ^s (PS)**	**φ^s (PEO)**
Toluene	0.038	0.01	0.006
MEK	0.127	0.03	0.04
PGMEA	0.007	0.002	0.002

The first solvent employed was toluene. All films annealed under toluene were allowed to de-swell for 15 minutes. It typically takes more than 10 hours to achieve highly ordered PEO-*b*-PS thin films in a large chamber (volume of 1236 cm^3). When the annealing time was less than 1 hour, the films (1a, 1b and 1c in Table 2.4 and Figure 2.2) were either disordered or had extremely small grains of hexagonally-packed arrays. Only annealing times in excess of 6 hours could result in ordered thin films (1e and 1f in Table 2.4 and Figure 2.2). However, when the chamber volume was decreased to 64 cm^3, laterally ordered films were obtained in a matter of minutes, and further annealing up to 3 hours produced single grains spanning more than 2.5 μm^2. Figure 2.3 shows AFM height images that illustrate the evolution of order achieved with a small chamber volume (samples 2a-d in Table 2.4). After 0.25 hour of annealing, the PEO domains are hexagonally ordered at the air surface. Some areas of the film exhibit long-range order, while other regions exhibit liquid-like order. Such extremity indicates that the system is highly unbalanced. Nevertheless, the distance between close-packed rows is d = 23 nm. After 0.5 hr, the domains at the air interface are laterally-ordered into large hexagonal grains that span nearly 1.5 μm × 1.5 μm with d = 25 nm (Figure 2.3B). This is a significant observation as this level of ordering is sufficient for many applications.[55-57] A 1 hr annealing increased the average grain size to 1.9 μm × 1.9 μm with d = 26 nm. When the annealing time was extended to 3 hours, a highly ordered thin film with an average grain size of 2.8 μm × 2.8 μm and d = 26 nm was obtained. The grain size was similar to or even better than those films annealed for more than 16 hours in the large chamber (sample 1f in Table 2.4 and Figure 2.2).

Table 2.4 Annealing conditions and results for block copolymer PEO-*b*-PS thin films in large and small chambers with toluene as annealing solvent. "Disordered" grain size consists of both parallel and perpendicular domains on the surface with no degree of ordering to determine average grain size. "=" means cylinders parallel to the surface, "⊥"means hexagonally-packed domains on the surface. Average grain size depicts the size of continuous ordered grains in the AFM micrographs only if perpendicular or parallel domains were present. De-swelling time = 15 minutes

Sample	Chamber Size (Volume)	Annealing Time	Relative Humidity (+/- 3%)	d (nm)	Average Grain Size
1a	1236 cm^3	0.25 hour	88%	25	Disordered
1b	1236 cm^3	0.5 hour	89%	25	"⊥", 0.22 μm × 0.22 μm
1c	1236 cm^3	1 hour	88%	26	"⊥", 0.49 μm × 0.49 μm
1d	1236 cm^3	3 hours	90%	27	"⊥", 1.2 μm × 1.2 μm
1e	1236 cm^3	6 hours	90%	31	"⊥", 2 μm × 2 μm
1f	1236 cm^3	16 hours	90%	33	"⊥", 2.4μm × 2.4 μm
2a	64 cm^3	0.25 hour	88%	23	Ordered/Disordered
2b	64 cm^3	0.5 hour	89%	25	"⊥", 1.5 μm × 1.5μm
2c	64 cm^3	1 hour	88%	26	"⊥", 1.9 μm × 1.9 μm
2d	64 cm^3	3 hours	90%	26	"⊥", 2.8μm × 2.8 μm

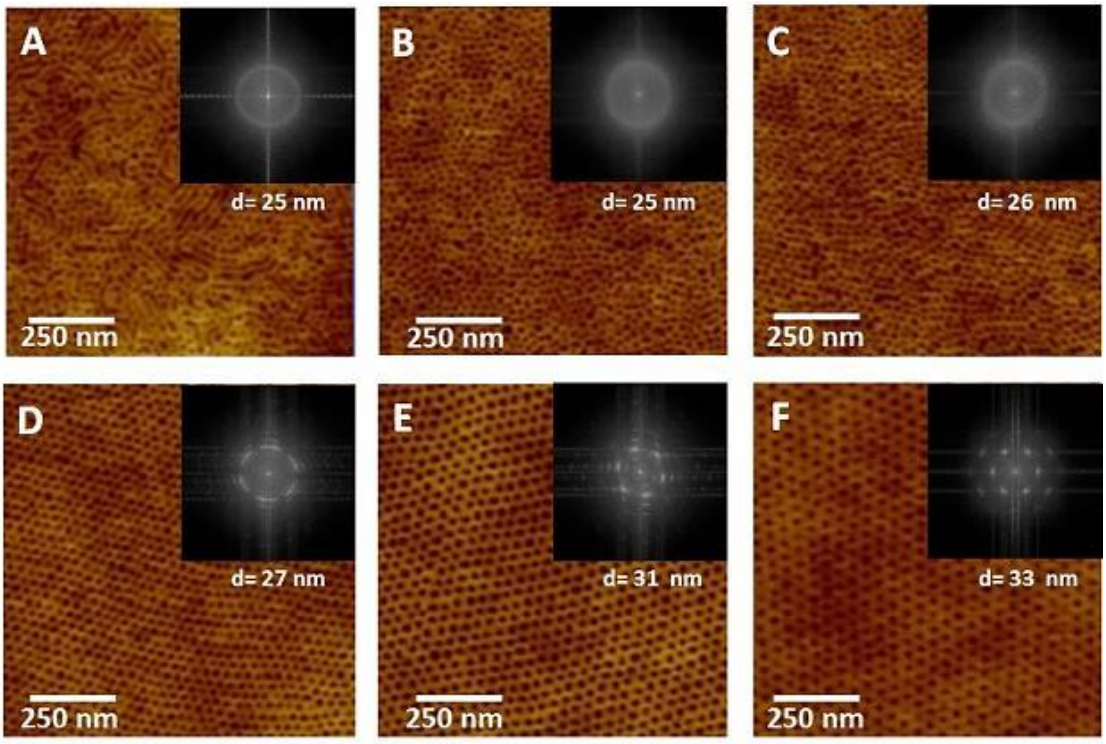

Figure 2.2 AFM height images of thin films of block copolymer PEO-*b*-PS processed by high humidity solvent annealing in toluene under varied annealing time in a large chamber: (A= **1a**, 0.25 hr; B = **1b**, 0.5 hr; C = **1c**, 1 hr; D = **1d**, 3 hr; E = **1e**, 6 hr; F = **1f**, 16 hr)

Figure 2.4 directly compares the effect of chamber size on the ordering of block copolymers in thin films as a function of annealing time using toluene as the solvent. We omit the data for Figure 2.3A, as the sample exhibited coexistence between highly ordered and highly disordered grains. Another point of interest relates to swelling of the lattice during the annealing process (captured by changes in *d*). The swelling is a strong function of annealing time and a weak function of chamber size, without any clear coupling to the extent of lateral order. This is a significant observation for lithography, as these data demonstrate that the smaller chamber not only reduces the annealing time, but results in patterns with smaller pitch (Figure 2.5).

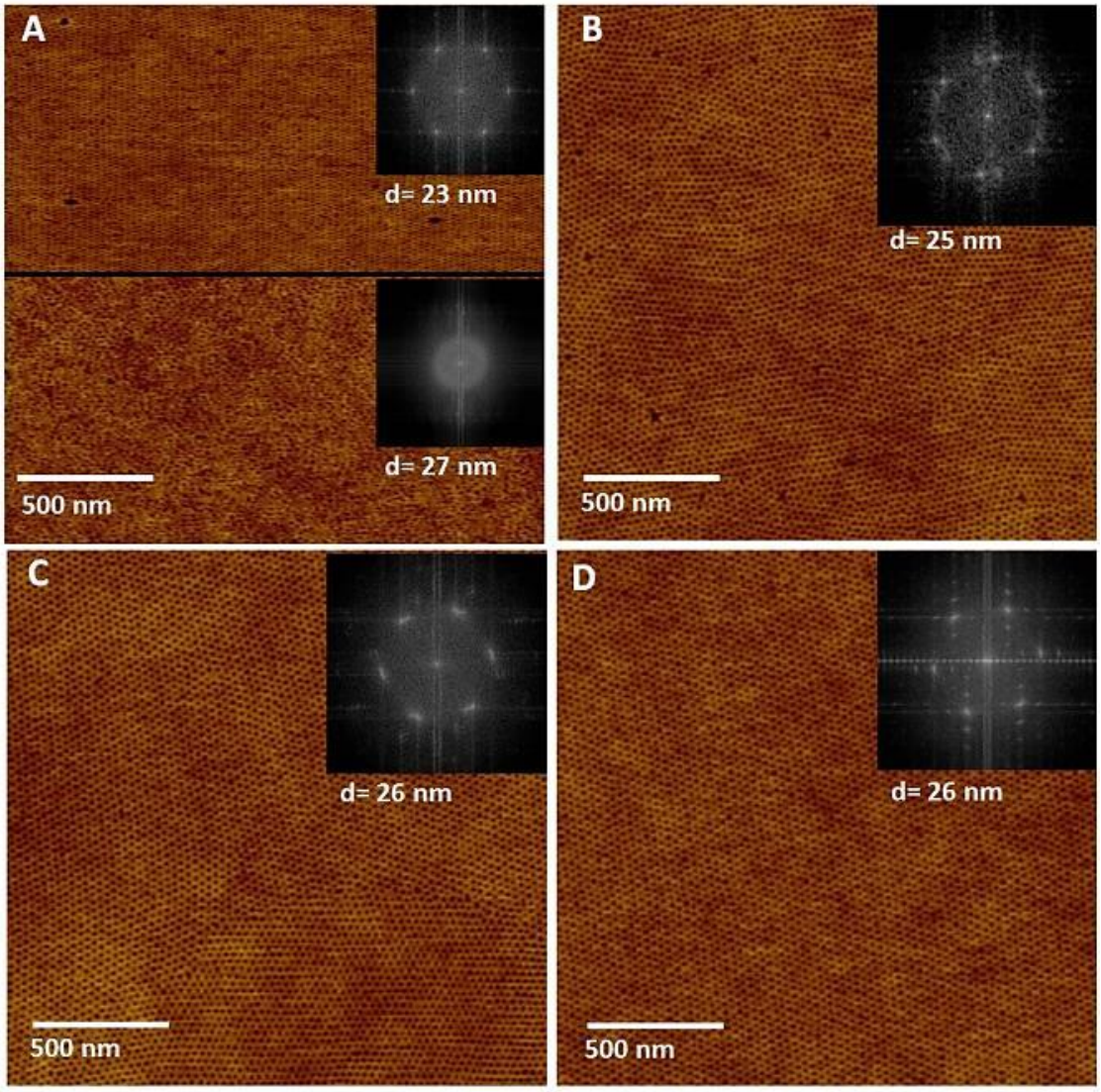

Figure 2.3 AFM height images of thin films of block copolymer PEO-*b*-PS processed by high humidity solvent annealing in toluene under varied annealing time in a small chamber: (A = **2a**, 0.25 hr; B = **2b**, 0.5 hr; C = **2c**, 1 hr; D = **2d**, 3 hr)

The smaller chamber clearly reduces the annealing time that is needed to achieve good lateral order, so we now discuss the cause of the enhanced ordering kinetics. We model the transient concentration profiles in the chamber with Fick's second law,

$$\frac{\partial c_s}{\partial t} = D_{sa} \frac{\partial^2 c_s}{\partial z^2} \qquad (2.4)$$

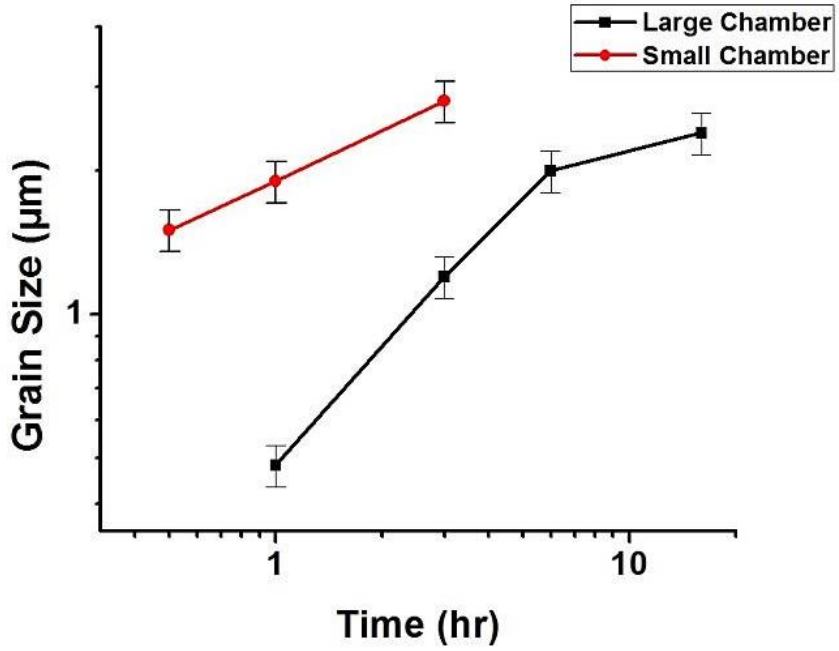

Figure 2.4 Lateral grain size in PEO-b-PS thin films as a function of time. High-humidity toluene solvent annealing in large and small chambers (Small Chamber 2b-2d and Large Chamber 1c-1f)

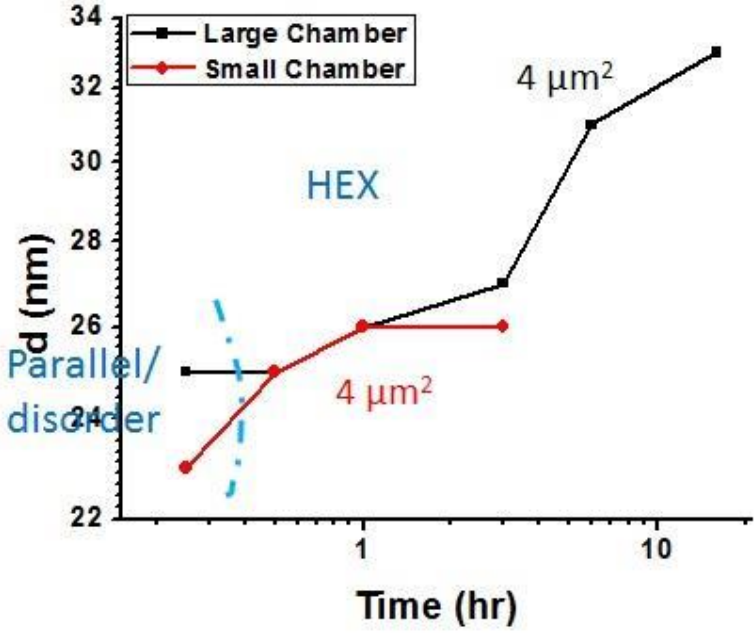

Figure 2.5 d-spacing in PEO-b-PS thin films as a function of time. High-humidity toluene solvent annealing in large and small chambers (Small Chamber 2a-2d and Large Chamber 1a-1f)

where $c_s[t,z]$ is the concentration of solvent in the vapor phase, D_{sa} is the diffusivity of solvent in the vapor phase, and z is the linear distance from the source. A one-dimensional model is selected for simplicity (and visualization.). It is important to note that the calculations based on a 1D model do not account for chamber shapes. Herein, we assume that evaporation proceeds under isothermal and isobaric conditions.

The chamber initially has no solvent vapor, so the first boundary condition we apply is:

$$c_s[0,z] = 0 \qquad (2.5)$$

At the surface of the liquid ($z = 0$) we assume the partial pressure of solvent in the vapor phase can be modeled as an ideal gas, i.e., $p_s[t,0] = P^{vap}$. This leads to the second boundary condition:

$$c_s[t,0] = \frac{P^{vap}}{RT} \qquad (2.6)$$

where R = 83.14 bar cm^3 mol^{-1} K^{-1} and T = 298 K is the temperature in the glove box. The third boundary condition pertains to the wall of the chamber (at $z = L$). We start with the assumption that the boundary is impermeable:

$$\left.\frac{\partial c_s}{\partial z}\right|_{z=L} = 0 \qquad (2.7)$$

The vapor pressure of toluene is 0.038 bar at 298 K, so $c_s[t,0] = 1.5\text{x}10^{-6}$ mol/cm^3. The diffusivity of toluene in air at 298 K can be approximated from empirical correlations adapted from classical kinetic theory, such as equation 1 in Wilke and Lee et al,[58] and is approximately 0.2 cm^2/sec. We set the chamber "length" L based on the sizes

of each chamber: The small chamber has a diameter of 9 cm and height 1 cm, while the large chamber has a diameter of 15 cm and a height of 7 cm. The liquid source inside each chamber has diameter and height of 5 cm and 0.8 cm, respectively. Since we use a 1D model, we define a length scale L for each chamber with the following formula: $L = (V_{chamber} - V_{source})/A_{source}$, where the numerator reflects the unoccupied volume of the chamber and the denominator is the surface area of the liquid source. We find L = 0.75 cm for the small chamber, and L = 19 cm for the large chamber.

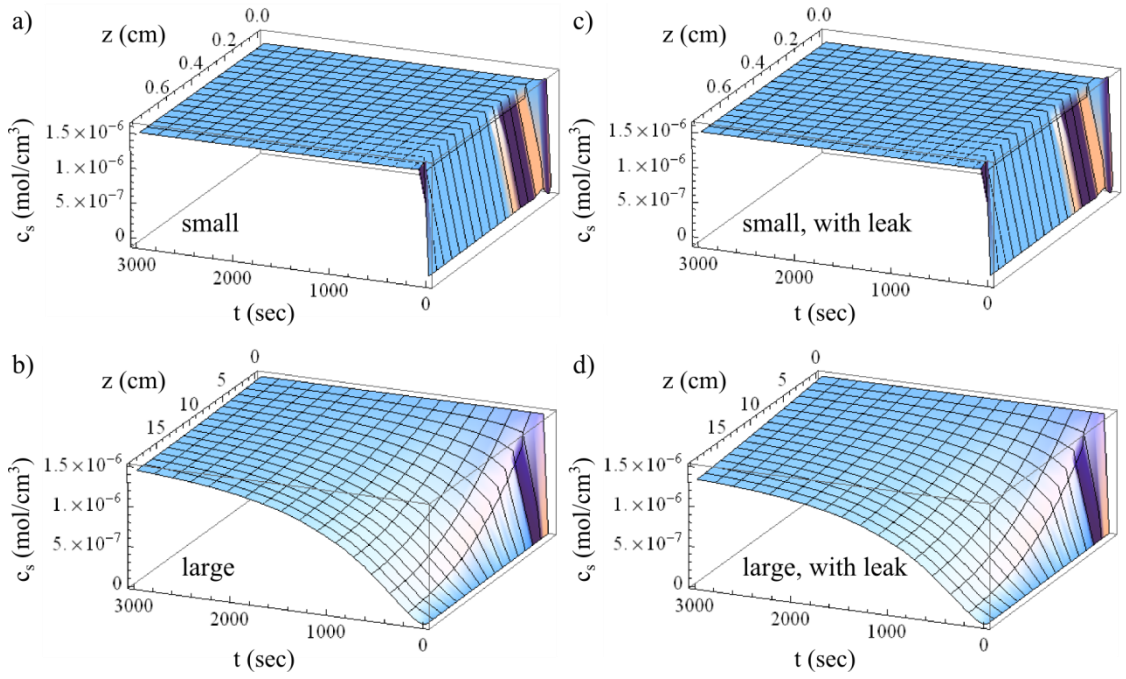

Figure 2.6 Toluene concentration in the vapor phase c_s as a function of t and z for a) small chamber; b) large chamber; c) leaky small chamber; d) leaky large chamber

Figures 2.6A and 2.6B summarize the transient concentration profiles from z = 0 to L over 3000 sec. The small chamber is filled with vapor at a partial pressure of $p_s = P^{vap}$ within 10 seconds. However, the large chamber requires nearly an hour to reach the same steady-state concentration. This model suggests that slow ordering kinetics in the

large chamber is at least partly associated with the long time scales to achieve a saturated vapor phase.

Another point to consider is the solvent leakage rate. Each chamber is merely an upside-down glass dish placed on the bottom of the glove box, meaning there is no seal at the base. The gradient in solvent composition could drive diffusion out of the chamber into the large glove box, where the ambient solvent composition is approximately 0. Therefore, the third boundary condition might be better described as:

$$\left.\frac{\partial c_s}{\partial z}\right|_{z=L} = -Cs[t, L] * constant \qquad (2.8)$$

The constant captures the effective solvent diffusivity (D_{eff}) through the narrow gap and the mass transfer coefficient (k_c) for diffusion of solvent inside the glove box (as the surrounding gas is not stagnant). It is difficult to estimate these parameters for the present system, so we assume the constant is approximately k_c/D_{eff} = 0.005. Outcomes are reported in Figures 2.6C and 2.6D. The transient concentration profiles in the small chamber are largely unaffected by a small leak, while the large chamber does not reach a concentration of 1.5×10^{-6} mol/cm^3 within 3000 seconds. If we increase the constant by an order of magnitude, producing a bigger leak, then we find an even larger discrepancy between the two chambers in the long time limit. This is illustrated by Figure 2.7 as shown below.

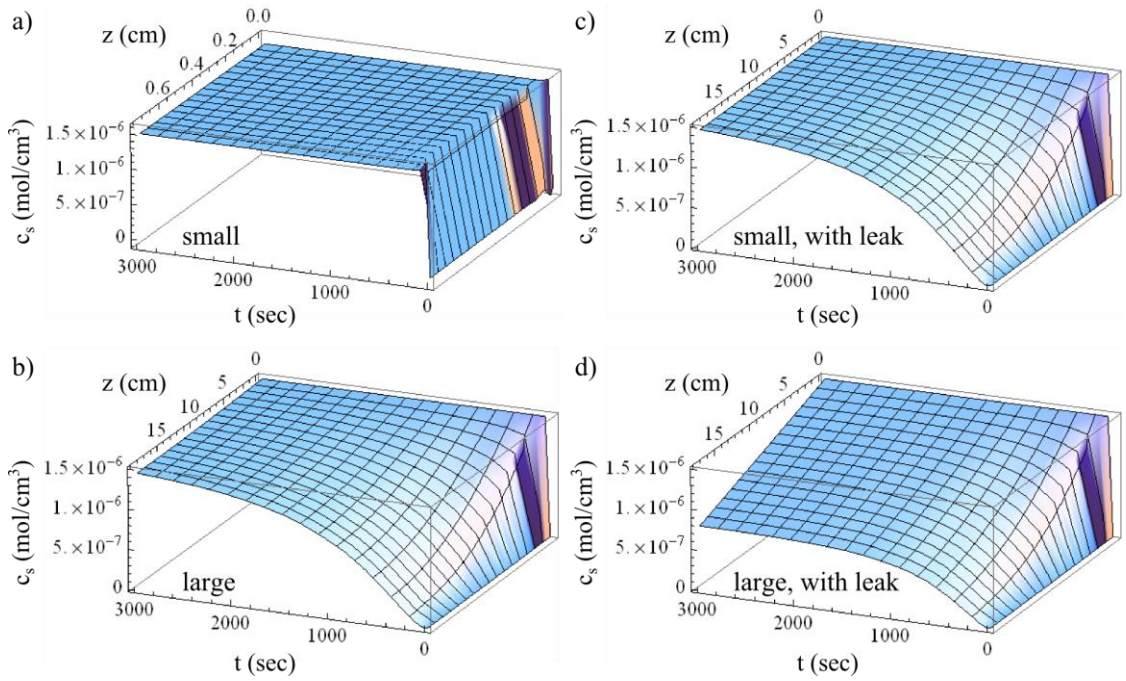

Figure 2.7 Toluene concentration in the vapor phase c_s as a function of t and z for a) small chamber; b) large chamber; c) leaky small chamber; d) leaky large chamber. The leak in these calculations is an order of magnitude larger than in Figure 2.6; i.e., $k_c/D_{\text{eff}} = 0.05$.[58]

The second challenge to address was replace toluene with industry-benign solvents (MEK and PGMEA) to see whether the same degree of surface order could be attained. Following the previously discussed methods, we can predict the saturation time for each solvent system in the small and large chambers. For MEK, the vapor pressure is 0.126 bar at 298 K, so $c_s[t,0] = 5.1\text{x}10^{-6}$ mol/cm^3. The diffusivity of MEK in air is approximately 0.24 cm^2/sec.[58] For PGMEA, the vapor pressure is 0.007 bar at 298 K, so $c_s[t,0] = 2.7\text{x}10^{-7}$ mol/cm^3. The diffusivity of PGMEA in air is approximately 0.17 cm^2/sec.[58] Figure 2.8 reports the time required to achieve a saturated vapor state. The saturation time is very fast (nearly instantaneous) for both solvents in the small chamber, while saturation is slow in the large chamber. However, as discussed in Table 2.5, the solvent concentration in the film is much higher for MEK than PGMEA, so we do not anticipate similar ordering kinetics in the two systems.

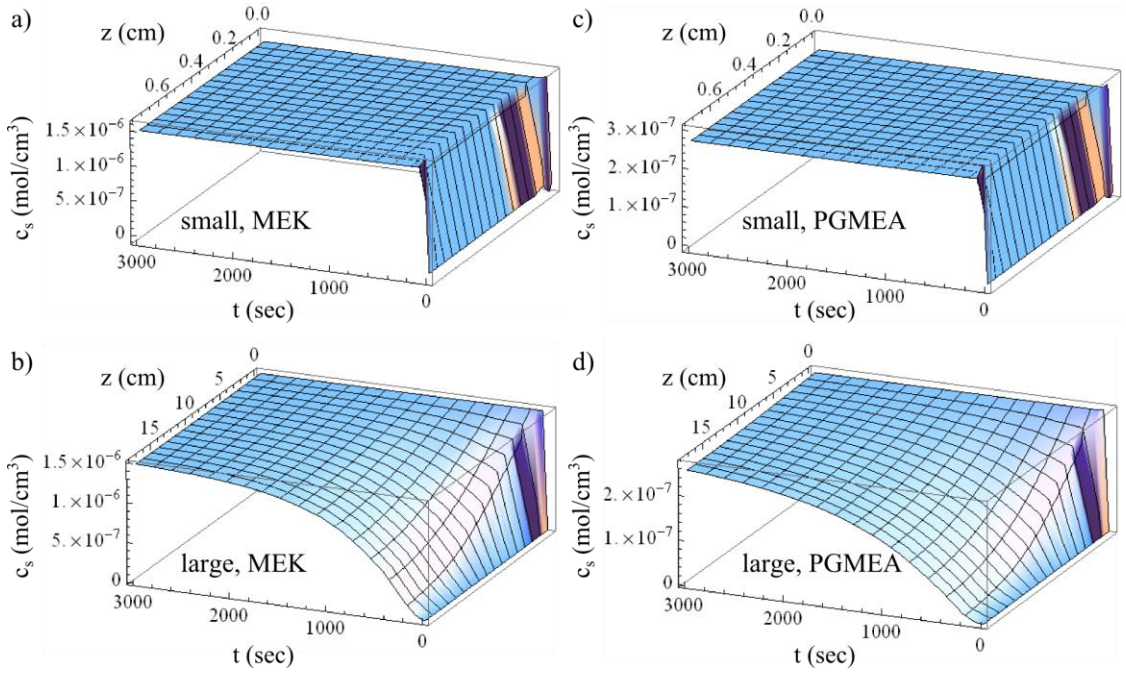

Figure 2.8 Solvent concentration c_s as a function of t and z for a) small chamber with MEK; b) large chamber with MEK; c) small chamber with PGMEA; d) large chamber with PGMEA

Table 2.5 summarizes the experimental conditions and results for the annealing process under MEK. All films annealed under MEK were allowed de-swell time for 5 minutes. As shown in Figure 2.9A, annealing times less than 3 hours in the small chamber produced parallel cylinders with d = 23 nm. Annealing times in excess of 12 hours in the small chamber produced ordered hexagonal domains at the surface of the film with grain sizes of approximately 0.70 μm × 0.70 μm and d = 23 nm, although the surface was rough (Figure 2.9B). An increase in annealing time to 18 hours in the small chamber showed significantly improved ordering, with highly ordered hexagonal domains on the surface having an average of grain size about 1.6 μm × 1.6 μm and d = 25 nm (Figure 2.9C). The results for the smaller chamber were much better than those for the large chamber with 18 hours of annealing, where the latter case produced poorly

ordered hexagonal domains with d = 30 nm. The domains at the film surface had non-uniform sizes and many pinhole defects (Figure 2.9D).

The parallel cylinders shown in Figure 2.9A could be caused by the different surface energy of PEO and PS segments under humid MEK vapor, as this solvent environment is selective to PEO. The pitch d for parallel and perpendicular cylinders are the distance between nearest-neighbors and the distance between close-packed rows, respectively. Therefore, if the cylinders re-orient normal to the film with increased annealing time, then the d-spacing is reduced by a factor of $\sqrt{3}/2$. Such behavior is not observed here, which suggests that the ordered surface structure is in fact "perforations" rather than vertical cylinders.

Like the case of toluene, the time required to achieve large grains is reduced with decreasing chamber size. However, the time scales to reach grain sizes on the order of 1 μm^2 are longer than achieved with toluene. As summarized in Tables 2.2 and 2.3, the uptake of MEK in the film is larger than that of toluene, even though MEK is less soluble than toluene in PS. This is associated with the higher P^{vap} at 25^0C of MEK compared with toluene. Therefore, we conclude that kinetics of ordering is suppressed because MEK enhances the compatibility between PEO and PS.[59-62] Another interesting point is that changes in d as a function of annealing time and chamber size are consistent with toluene: d ranges from 23 to 25 nm in the small chamber, while d reaches 30 nm at long times in the large chamber (Figure 2.10).

Table 2.5 Annealing conditions and results for PEO-*b*-PS thin films in large and small chambers with MEK as annealing solvent. "Disordered" grain size consists of both parallel and perpendicular domains on the surface with no degree of ordering to determine average grain size, "=" means cylinders parallel to the surface, "⊥"means hexagonally-packed domains on the surface. Average grain size depicts the size of continuous ordered grains in the AFM micrographs only if perpendicular or parallel domains were present. De-swelling time = 5 min

Sample	Chamber Size (Volume)	Annealing Time	Relative Humidity	d (nm)	Average Grain Size
1a	1236 cm^3	0.5 hour	88%	23	Disordered
1b	1236 cm^3	1 hour	89%	23	Disordered
1c	1236 cm^3	3 hours	88%	24	Disordered
1d	1236 cm^3	6 hours	90%	25	"⊥", 0.20 μm × 0.20 μm
1e	1236 cm^3	18 hours	90%	30	"⊥", 0.70 μm × 0.70 μm
2a	64 cm^3	0.5 hour	88%	23	Disordered
2b	64 cm^3	1 hour	89%	23	Disordered
2c	64 cm^3	3 hours	88%	23	"=", 0.30 μm × 0.30μm
2d	64 cm^3	6 hours	90%	23	"⊥", 0.35 μm × 0.35 μm
2e	64 cm^3	12 hours	88%	23	"⊥", 0.70 μm × 0.70 μm
2f	64 cm^3	16 hours	88%	24	"⊥", 0.80 μm × 0.80 μm
2g	64 cm^3	18 hours	88%	25	"⊥", 1.60 μm × 1.60 μm

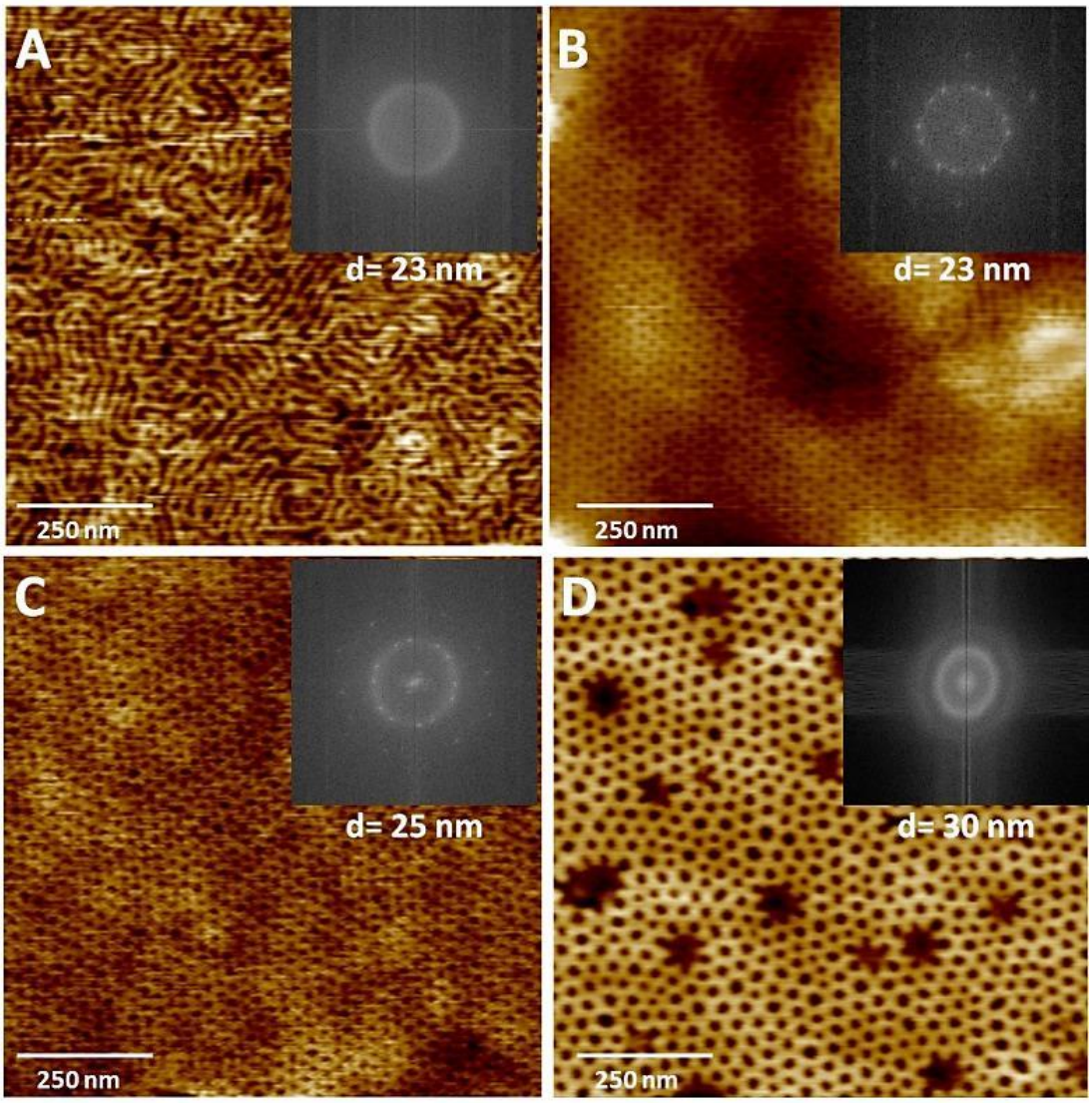

Figure 2.9 AFM height images of thin films of block copolymer PEO-*b*-PS processed by solvent annealing under MEK: Effect of annealing time (A = **2c**, small chamber, 3 hr; B = **2e**, small chamber, 12 hr; C = **2g**, small chamber, 18 hr; D = **1e**, large chamber, 18 hr).

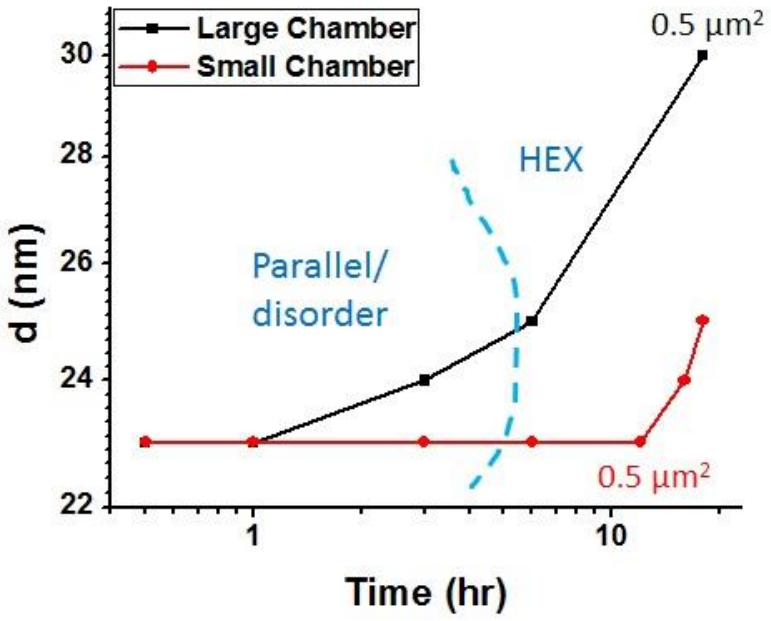

Figure 2.10 d-spacing in PEO-b-PS thin films as a function of time. High-humidity MEK solvent annealing in large and small chambers (Small Chamber 2a-2g and Large Chamber 1a-1e)

Next we carried out solvent annealing with PGMEA vapor. Table 2.6 summarizes the experimental conditions and results. When the film was annealed for 18 hours under PGMEA in the large chamber, but de-swelled for only 5 minutes, the films were characterized by parallel cylinders with d = 26 nm (Figure 2.11A). When the de-swelling time was increased from 5 min to 2.5 hours, disordered hexagonal domains with an average grain size of 0.7 µm × 0.7 µm and d = 27 nm were observed at the film surface (Figure 2.11B). A long solvent annealing time in the small chamber (~20 hours) with a long de-swelling time (2.5 hours) generated a highly ordered film with hexagonally packed domains, which have an average grain size of 1.6 µm × 1.6 µm and d = 29 nm as shown in Figure 2.11C. When the de-swell time was kept at 2.5 hour, but the annealing time was decreased to 6 hours, the films exhibit hexagonally-packed domains with an average grain size of 0.4 µm × 0.4 µm and d = 28 nm (Figure 2.11D).

Table 2.6 Annealing conditions and results for PEO-*b*-PS block copolymer thin films in large and small chambers with PGMEA as annealing solvent. "Disordered" grain size consists of both parallel and perpendicular domains on the surface with no degree of ordering to determine average grain size. "=" means cylinders parallel to the surface, "⊥"means hexagonally-packed domains on the surface. Average grain size depicts the size of continuous ordered grains in the AFM micrographs only if perpendicular or parallel domains were present.

Sample	Chamber Size (Volume)	Annealing Time	De-swelling Time	Relative Humidity	d (nm)	Average Grain Size
1a	1236 cm^3	0.5 hour	2.5 hours	92%	23	Disordered
1b	1236 cm^3	1 hour	2.5 hours	92%	23	Disordered
1c	1236 cm^3	3 hours	2.5 hours	92%	24	Disordered
1d	1236 cm^3	18 hours	5 min	92%	26	"=", 1.1 μm × 1.1 μm
1e	1236 cm^3	18 hours	2.5 hours	92%	27	"⊥", 0.7 μm × 0.7 μm
2a	64 cm^3	0.5 hour	2.5 hours	92%	22	Disordered
2b	64 cm^3	1 hour	2.5 hours	92%	22	Disordered
2c	64 cm^3	3 hours	2.5 hours	92%	22	"⊥", 0.3 μm × 0.3 μm
2d	64 cm^3	6 hours	2.5 hours	92%	27	"⊥", 0.4 μm × 0.4 μm
2e	64 cm^3	12 hours	2.5 hours	92%	27	"⊥", 0.5 μm × 0.5 μm
2f	64 cm^3	20 hours	2.5 hours	92%	29	"⊥", 1.6 μm × 1.6 μm

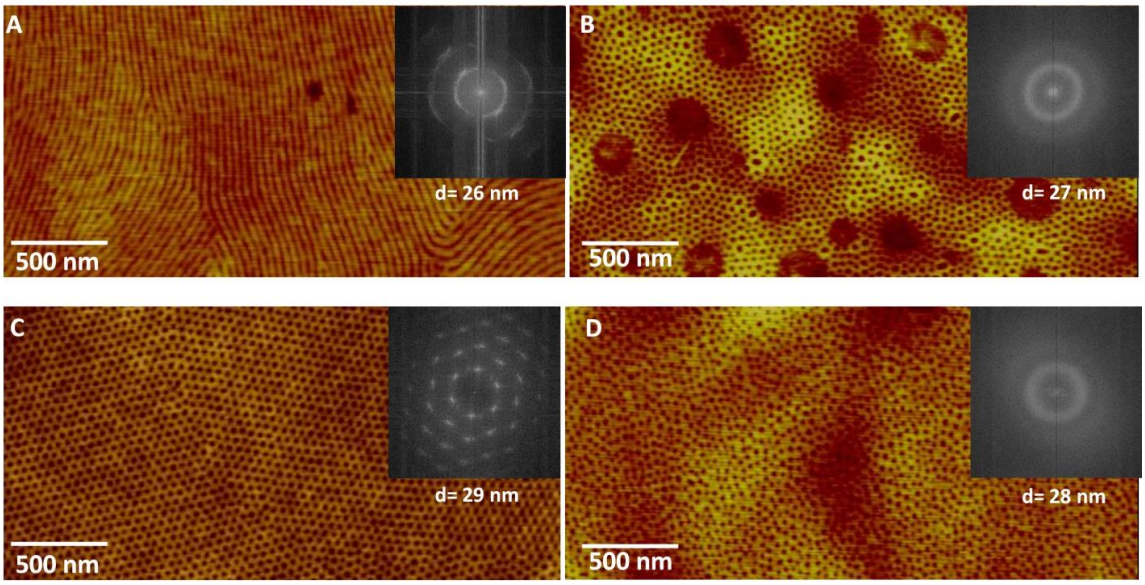

Figure 2.11 AFM height images of thin films of block copolymer PEO-*b*-PS processed by solvent annealing under PGMEA: Effect of annealing time (A = **1d**, large chamber, 18 hr, 5 min de-swell; B = **1e**, large chamber, 18 hr, 2.5 hr de-swell; C = **2f**, small chamber, 20hr, 2.5 hr de-swell; D = **2d**, small chamber, 6hr, 2.5 hr de-swell).

As shown in Figure 2.8, saturation time is very fast for both solvents in the small chamber. However, as summarized in Tables 2.2 and 2.3, the uptake of PGMEA in the film is much lower than that of MEK and toluene. This is associated with the lower P^{vap} at 25^{0}C of PGMEA compared with the other two solvents. Also, the diffusivity of PGMEA (0.17 cm^2/sec) compared with MEK (0.24 cm^2/sec), and toluene (0.2 cm^2/sec) is much lower. This contributes to the longer de-swell time needed for PGMEA rather than MEK and toluene, since there is little solvent in the film, so when evaporation occurs there is not much cooling at the surface which drives water condensation on the film.

GISAXS measurements were performed to evaluate ordering induced by the high-humidity solvent annealing processes. Films were measured by varying the incident angle near the polymer's critical angle ($\alpha_c \approx 0.16^o$)**,** which produces controlled X-ray penetration depths in the range of 10 nm up to the full film thickness.[63]

For the first set of experiments, films were annealed in toluene using the small chamber for 3 hours, and then de-swelled under high humidity for 15 min. This corresponds to Sample 2d in Table 2.4 and Figure 2.3D. The scattering profiles recorded above and below the polymer's critical angle are nearly identical (Figure 2.12). If perpendicular cylinders persist throughout the film thickness, then the in-plane first-order diffraction rod should exhibit "oscillations" with a period that is inversely proportional to the cylinder height (i.e., the form factor).[64, 65] Instead, we observe a broad "streak" along the α_f axis at all incident angles, meaning a thin surface structure is dominating the scattering.

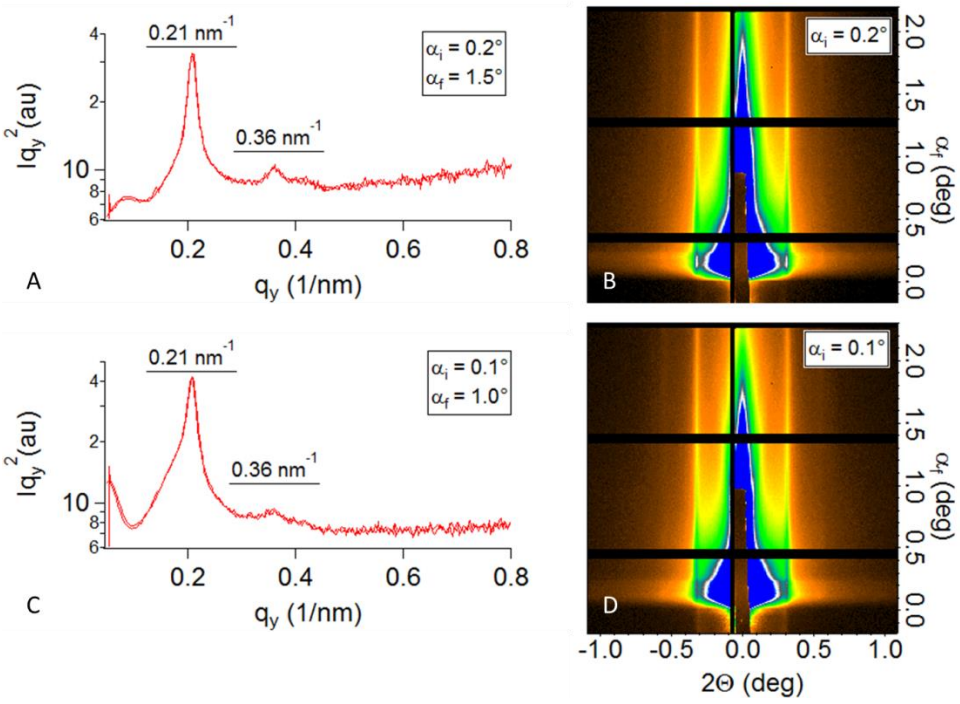

Figure 2.12 GISAXS measurement of films with toluene solvent annealing: (A,B) above the polymer's critical angle, sampling the full film thickness; (C,D) below the polymer's critical angle, sampling the top ~10 nm.

The symmetry of the surface structure is hexagonal, which is determined from the relative positions of the first- and second-order in-plane scattering peaks (1:√3). The distance between close-packed rows in the hexagonal lattice is approximately d = 30 nm, which is a few nanometers larger than AFM measurements. It is important to note that the √3 peak is not detected at low values of α_f, which is a signature of surface scattering from "dimples". This point is further discussed at the end of the GISAXS discussion

For the second set of experiments, films were annealed in MEK using the small chamber for 18 hours, and then de-swelled under high humidity for 5 min. This corresponds to Sample 2g in Table 2.5 and Figure 2.9C. Much like the samples annealed in toluene, the scattering profiles recorded above and below the polymer's critical angle are nearly identical, and there is no sign of perpendicular cylinders that persist throughout the film's thickness (Figure 2.13). However, the in-plane symmetry is consistent with parallel cylinders, which is determined from the relative positions of first- and second-order in-plane scattering peaks (1:2). The cylinder-to-cylinder distance is approximately d = 25 nm, which is two nanometers larger than the AFM measurement of parallel cylinders. There is no evidence of layering, which means there is not a complete unit cell (at most two layers of cylinders). Note that the second order peak is only detected at exit angles near the polymer's critical angle ($\alpha_f \approx 1.2\alpha_c$).

For the final set of experiments, films were annealed in PGMEA using the small chamber for 20 hours, and de-swelled for 2.5 hours. This condition corresponds to Sample 2f in Table 2.6 and Figure 2.11C. The scattering profiles (Figure 2.14) are very similar to the case of toluene solvent annealing, but with the appearance of higher order in-plane peaks (ratios of 1:√3:√4:√7). The distance between close-packed rows is

approximately 29 nm, which is nearly identical to the outcomes of toluene solvent annealing and matches the AFM data. The improvement in lateral order makes it easier to see the out-of-plane structure. For example, in Figure 2.14D, it is clear that the √3 peak is trongest near $\alpha_f \approx 1^o$. The solid pink line is a guide to eye that marks the maxima of in-plane peaks, and this demonstrates that the surface structure has "sloped" sidewalls ($\gamma \approx 30^o$), meaning the PEO domains have collapsed to form a "dimpled" surface.[46]

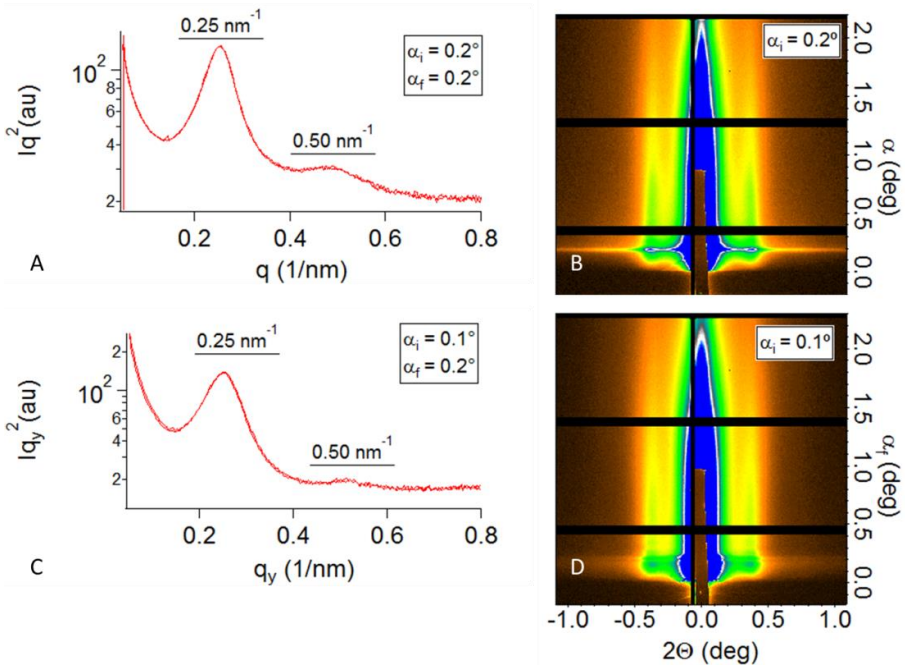

Figure 2.13 GISAXS measurement of films by solvent annealing under MEK: (A,B) above the polymer's critical angle, sampling the full film thickness; (C,D) below the polymer's critical angle, sampling the top ~10 nm.

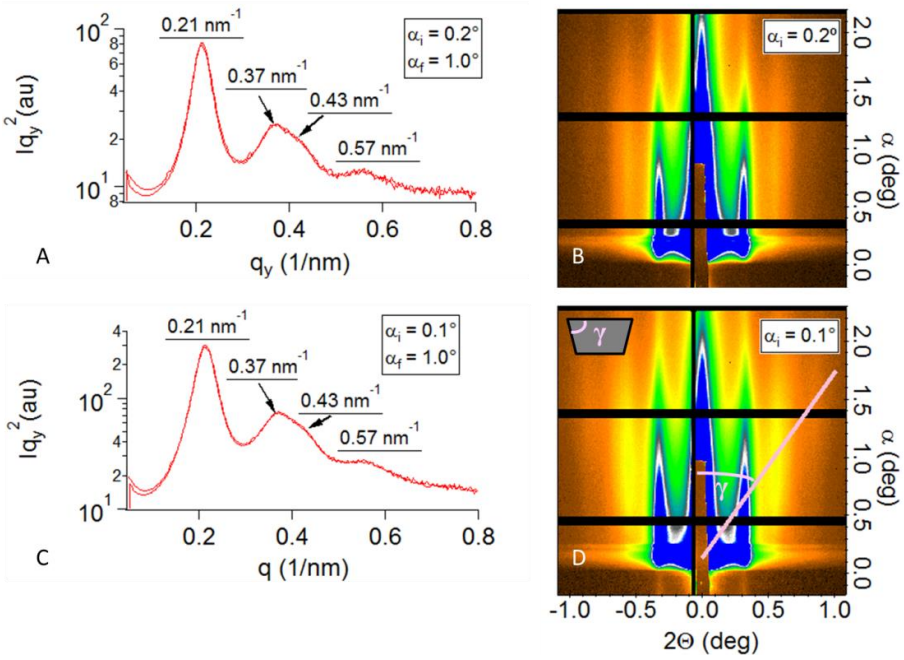

Figure 2.14 GISAXS measurement of films by solvent annealing under PGMEA: (A,B) above the polymer's critical angle, sampling the full film thickness; (C,D) below the polymer' critical angle, sampling the top ~10 nm.

Both AFM and GISAXS data suggest the lattice parameter for the PEO-b-PS block copolymer ranges from 23 nm to 30 nm depending on the solvent, annealing time, and lattice symmetry (hexagonal or parallel cylinders). It is important to note that transitions from parallel cylinders to hexagonal order are observed in both MEK and PGMEA processes, and these structures have nearly the same row-to-row spacing. If the hexagonal surface patterns are associated with perpendicular cylinders, then the row-to- row spacing should be $\sqrt{3}/2$ of the parallel cylinder-to-cylinder distance. Therefore, we conclude that hexagonal dimples at the film surface are a result of parallel cylinders that perforate at the top. GISAXS results are dominated by scattering from the dimpled surface, but the data are consistent with the AFM measurements: the peaks from cylinders will overlap with

the hexagonal structure at 1 and √4. Scheme 2.4 illustrates the proposed surface structure of PEO-*b*-PS thin films solvent annealed under high humidity.

Scheme 2.4 Proposed surface structure of block copolymer PEO-*b*-PS thin films solvent annealed under high humidity. Pink = PEO; Green = PS.

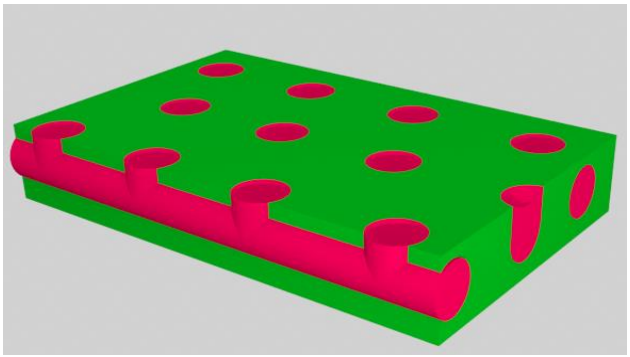

2.5 Conclusion

We investigated high humidity solvent annealing in thin films of amphilic PEO-*b*-PS block copolymers. Using toluene solvent we reduced the annealing time from hours to minutes by decreasing the chamber volume to reduce the saturation time. We then evaluated the benign solvents MEK and PGMEA and showed that both can drive ordering, but they are less effective than toluene because they enhance the compatibility between PS and PEO segments. The combination of AFM and GISAXS data suggest that hexagonal domains at the polymer/air interface do not propagate throughout the thickness of the film. The lattice periodicity increases in each solvent environment as a function of time, a challenge that is apparently mitigated by use of the small annealing chamber.

2.6 References

1. Bates, F. S., Polymer-Polymer Phase Behavior. *Science* **1991,** *251* (4996), 898-905.

2. Fredrickson, G. H.; Bates, F. S., Dynamics of Block Copolymers: Theory and Experiment. *Annual Review of Materials* **1996,** *26* (1), 501-550.
3. Bates, F. S.; Hillmyer, M. A.; Lodge, T. P.; Bates, C. M.; Delaney, K. T.; Fredrickson, G. H., Multiblock Polymers: Panacea or Pandora's Box? *Science* **2012,** *336* (6080), 434-440.
4. Hawker, C. J.; Wooley, K. L., The Convergence of Synthetic Organic and Polymer Chemistries. *Science* **2005,** *309* (5738), 1200-1205.
5. Stuparu, M. C.; Khan, A.; Hawker, C. J., Phase separation of supramolecular and dynamic block copolymers. *Polymer Chemistry* **2012,** *3* (11), 3033-3044.
6. Bates, F. S.; Fredrickson, G. H., Block Copolymers---Designer Soft Materials. *Physics Today* **1999,** *52* (2), 32-38.
7. Bates, C. M.; Maher, M. J.; Janes, D. W.; Ellison, C. J.; Willson, C. G., Block Copolymer Lithography. *Macromolecules* **2013,** *47* (1), 2-12.
8. Park, M.; Harrison, C.; Chaikin, P. M.; Register, R. A.; Adamson, D. H., Block Copolymer Lithography: Periodic Arrays of ~1011 Holes in 1 Square Centimeter. *Science* **1997,** *276* (5317), 1401-1404.
9. Hawker, C. J.; Russell, T. P., Block Copolymer Lithography: Merging "Bottom-Up" with "Top-Down" Processes. *MRS Bulletin* **2005,** *30* (12), 952-966.
10. Luo, M.; Epps, T. H., Directed Block Copolymer Thin Film Self-Assembly: Emerging Trends in Nanopattern Fabrication. *Macromolecules* **2013,** *46* (19), 7567-7579.
11. Hardy, C. G.; Tang, C., Advances in square arrays through self-assembly and directed self-assembly of block copolymers. *Journal of Polymer Science Part B: Polym Physics* **2013,** *51* (1), 2-15.
12. Kempe, K.; Killops, K. L.; Poelma, J. E.; Jung, H.; Bang, J.; Hoogenboom, R.; Tran, H.; Hawker, C. J.; Schubert, U. S.; Campos, L. M., Strongly Phase-Segregating Block Copolymers with Sub-20 nm Features. *ACS Macro Letters* **2013,** *2* (8), 677-682.
13. Kim, H. C.; Jia, X.; Stafford, C. M.; Kim, D. H.; McCarthy, T. J.; Tuominen, M.; Hawker, C. J.; Russell, T. P., A Route to Nanoscopic SiO2 Posts via Block Copolymer Templates. *Advanced Materials* **2001,** *13* (11), 795-797.
14. Kim, D. H.; Kim, S. H.; Lavery, K.; Russell, T. P., Inorganic Nanodots from Thin Films of Block Copolymers. *Nano Letters* **2004,** *4* (10), 1841-1844.
15. Thurn-Albrecht, T.; Schotter, J.; Kästle, G. A.; Emley, N.; Shibauchi, T.; Krusin-Elbaum, L.; Guarini, K.; Black, C. T.; Tuominen, M. T.; Russell, T. P., Ultrahigh-Density Nanowire Arrays Grown in Self-Assembled Diblock Copolymer Templates. *Science* **2000,** *290* (5499), 2126-2129.
16. Cheng, J. Y.; Ross, C. A.; Chan, V. Z. H.; Thomas, E. L.; Lammertink, R. G. H.; Vancso, G. J., Formation of a Cobalt Magnetic Dot Array via Block Copolymer Lithography. *Advanced Materials* **2001,** *13* (15), 1174-1178.
17. Park, S.; Lee, D. H.; Xu, J.; Kim, B.; Hong, S. W.; Jeong, U.; Xu, T.; Russell, T. P., Macroscopic 10-Terabit–per–Square-Inch Arrays from Block Copolymers with Lateral Order. *Science* **2009,** *323* (5917), 1030-1033.
18. Bao, X.-Y.; Yi, H.; Bencher, C.; Chang, L.-W.; Dai, H.; Chen, Y.; Chen, P. T. J.; Wong, H. S. P., SRAM, NAND, DRAM contact hole patterning using block copolymer directed self-assembly guided by small topographical templates. *Electron Devices Meeting (IEDM), 2011 IEEE International* **2011**, 7.7.1-7.7.4.

19. Mansky, P.; DeRouchey, J.; Russell, T. P.; Mays, J.; Pitsikalis, M.; Morkved, T.; Jaeger, H., Large-Area Domain Alignment in Block Copolymer Thin Films Using Electric Fields. *Macromolecules* **1998,** *31* (13), 4399-4401.
20. Mansky, P.; Liu, Y.; Huang, E.; Russell, T. P.; Hawker, C., Controlling Polymer-Surface Interactions with Random Copolymer Brushes. *Science* **1997,** *275* (5305), 1458-1460.
21. Morkved, T. L.; Lu, M.; Urbas, A. M.; Ehrichs, E. E.; Jaeger, H. M.; Mansky, P.; Russell, T. P., Local Control of Microdomain Orientation in Diblock Copolymer Thin Films with Electric Fields. *Science* **1996,** *273* (5277), 931-933.
22. Tang, C.; Wu, W.; Smilgies, D.-M.; Matyjaszewski, K.; Kowalewski, T., Robust Control of Microdomain Orientation in Thin Films of Block Copolymers by Zone Casting. *Journal of the American Chemical Society* **2011,** *133* (30), 11802-11809.
23. Ouk Kim, S.; Solak, H. H.; Stoykovich, M. P.; Ferrier, N. J.; de Pablo, J. J.; Nealey, P. F., Epitaxial self-assembly of block copolymers on lithographically defined nanopatterned substrates. *Nature* **2003,** *424* (6947), 411-414.
24. Rockford, L.; Mochrie, S. G. J.; Russell, T. P., Propagation of Nanopatterned Substrate Templated Ordering of Block Copolymers in Thick Films. *Macromolecules* **2001,** *34* (5), 1487-1492.
25. Segalman, R. A.; Yokoyama, H.; Kramer, E. J., Graphoepitaxy of Spherical Domain Block Copolymer Films. *Advanced Materials* **2001,** *13* (15), 1152-1155.
26. Stein, G. E.; Kramer, E. J.; Li, X.; Wang, J., Single-Crystal Diffraction from Two-Dimensional Block Copolymer Arrays. *Physical Review Letters* **2007,** *98* (8), 086101.
27. Sinturel, C.; Vayer, M.; Morris, M.; Hillmyer, M. A., Solvent Vapor Annealing of Block Polymer Thin Films. *Macromolecules* **2013,** *46* (14), 5399-5415.
28. Jung, Y. S.; Ross, C. A., Solvent-Vapor-Induced Tunability of Self-Assembled Block Copolymer Patterns. *Advanced Materials* **2009,** *21* (24), 2540-2545.
29. Lin, Z. Q.; Kim, D. H.; Wu, X. D.; Boosahda, L.; Stone, D.; LaRose, L.; Russell, T. P., A Rapid Route to Arrays of Nanostructures in Thin Films. *Advanced Materials* **2002,** *14* (19), 1373-1376.
30. Jung, Y. S.; Chang, J. B.; Verploegen, E.; Berggren, K. K.; Ross, C. A., A Path to Ultranarrow Patterns Using Self-Assembled Lithography. *Nano Letters* **2010,** *10* (3), 1000-1005.
31. Gotrik, K. W.; Hannon, A. F.; Son, J. G.; Keller, B.; Alexander-Katz, A.; Ross, C. A., Morphology Control in Block Copolymer Films Using Mixed Solvent Vapors. *ACS Nano* **2012,** *6* (9), 8052-8059.
32. Wadley, M. L.; Hsieh, I. F.; Cavicchi, K. A.; Cheng, S. Z. D., Solvent Dependence of the Morphology of Spin-Coated Thin Films of Polydimethylsiloxane-Rich Polystyrene-block-Polydimethylsiloxane Copolymers. *Macromolecules* **2012,** *45* (13), 5538-5545.
33. Osuji, C. O., Alignment of Self-Assembled Structures in Block Copolymer Films by Solvent Vapor Permeation. *Macromolecules* **2010,** *43* (7), 3132-3135.
34. Albert, J. N. L.; Bogart, T. D.; Lewis, R. L.; Beers, K. L.; Fasolka, M. J.; Hutchison, J. B.; Vogt, B. D.; Epps, T. H., Gradient Solvent Vapor Annealing of Block Copolymer Thin Films Using a Microfluidic Mixing Device. *Nano Letters* **2011,** *11* (3), 1351-1357.

35. Qiang, Z.; Xue, J.; Stein, G. E.; Cavicchi, K. A.; Vogt, B. D., Control of Ordering and Structure in Soft Templated Mesoporous Carbon Films by Use of Selective Solvent Additives. *Langmuir* **2013,** *29* (27), 8703-8712.
36. Bang, J.; Kim, S. H.; Drockenmuller, E.; Misner, M. J.; Russell, T. P.; Hawker, C. J., Defect-Free Nanoporous Thin Films from ABC Triblock Copolymers. *Journal of the American Chemical Society* **2006,** *128* (23), 7622-7629.
37. Tang, C.; Bang, J.; E. Stein, G.; Fredrickson, G. H.; Hawker, C. J.; Kramer, E. J.; Sprung, M.; Wang, J., Square Packing and Structural Arrangement of ABC Triblock Copolymer Spheres in Thin Films. *Macromolecules* **2008,** *41* (12), 4328-4339.
38. Tang, C.; Hur, S.-m.; Stahl, B. C.; Sivanandan, K.; Dimitriou, M.; Pressly, E.; Fredrickson, G. H.; Kramer, E. J.; Hawker, C. J., Thin Film Morphology of Block Copolymer Blends with Tunable Supramolecular Interactions for Lithographic Applications. *Macromolecules* **2010,** *43* (6), 2880-2889.
39. Tang, C.; Sivanandan, K.; Stahl, B. C.; Fredrickson, G. H.; Kramer, E. J.; Hawker, C. J., Multiple Nanoscale Templates by Orthogonal Degradation of a Supramolecular Block Copolymer Lithographic System. *ACS Nano* **2009,** *4* (1), 285-291.
40. Hardy, C. G.; Ren, L.; Ma, S.; Tang, C., Self-assembly of well-defined ferrocene triblock copolymers and their template synthesis of ordered iron oxide nanoparticles. *Chemical Communications* **2013,** *49* (39), 4373-4375.
41. Rao, J.; De, S.; Khan, A., Synthesis and self-assembly of dynamic covalent block copolymers: towards a general route to pore-functionalized membranes. *Chemical Communications* **2012,** *48* (28), 3427-3429.
42. Rao, J.; Khan, A., Using reversibility of the dynamic covalent bond to create porosity in highly ordered polymer thin films under mild conditions and nano-pore functionalization in the gas phase. *Polymer Chemistry* **2013,** *4* (9), 2691-2695.
43. Rao, J.; Paunescu, E.; Mirmohades, M.; Gadwal, I.; Khaydarov, A.; Hawker, C. J.; Bang, J.; Khan, A., Supramolecular mimics of phase separating covalent diblock copolymers. *Polymer Chemistry* **2012,** *3* (8), 2050-2056.
44. Kim, S. H.; Misner, M. J.; Russell, T. P., Solvent-Induced Ordering in Thin Film Diblock Copolymer/Homopolymer Mixtures. *Advanced Materials* **2004,** *16* (23-24), 2119-2123.
45. Kim, S. H.; Misner, M. J.; Xu, T.; Kimura, M.; Russell, T. P., Highly Oriented and Ordered Arrays from Block Copolymers via Solvent Evaporation. *Advanced Materials* **2004,** *16* (3), 226-231.
46. Bang, J.; Kim, B. J.; Stein, G. E.; Russell, T. P.; Li, X.; Wang, J.; Kramer, E. J.; Hawker, C. J., Effect of Humidity on the Ordering of PEO-Based Copolymer Thin Films. *Macromolecules* **2007,** *40* (19), 7019-7025.
47. Killops, K. L.; Gupta, N.; Dimitriou, M. D.; Lynd, N. A.; Jung, H.; Tran, H.; Bang, J.; Campos, L. M., Nanopatterning Biomolecules by Block Copolymer Self-Assembly. *ACS Macro Letters* **2012,** *1* (6), 758-763.
48. Mokarian-Tabari, P.; Collins, T. W.; Holmes, J. D.; Morris, M. A., Cyclical "Flipping" of Morphology in Block Copolymer Thin Films. *ACS Nano* **2011,** *5* (6), 4617-4623.
49. Kang, M.; Moon, B., Synthesis of Photocleavable Poly(styrene-block-ethylene oxide) and Its Self-Assembly into Nanoporous Thin Films. *Macromolecules* **2008,** *42* (1), 455-458.

50. Hansen, C. M., *Hansen Solubility Parameters: A User's Handbook, Second Edition* CRC Press: Boca Raton, FL, 2007.
51. Barton, A. F. M., *CRC Handbook of Solubility Parameters and Other Cohesion Parameters, Second Edition*. CRC Press: 1991.
52. Brandrup, J.; Immergut, E. H.; Grulke, E. A.; Abe, A.; Bloch, D. R., *Polymer Handbook, 4th Ed.* John Wiley & Sons: New York, 1999.
53. Company, D. C. DOWANOL™ PMA Propylene Glycol Methyl Ether Acetate. http://www.dow.com/assets/attachments/business/pcm/dowanol/dowanol_pma/tds/dowanol_pma.pdf (accessed November 24, 2014).
54. Elbs, H.; Krausch, G., Ellipsometric determination of Flory-Huggins interaction parameters in solution. *Polymer* **2004,** *45* (23), 7935-7942.
55. Ham, S.; Shin, C.; Kim, E.; Ryu, D. Y.; Jeong, U.; Russell, T. P.; Hawker, C. J., Microdomain Orientation of PS-b-PMMA by Controlled Interfacial Interactions. *Macromolecules* **2008,** *41* (17), 6431-6437.
56. Hong, A. J.; Liu, C.-C.; Wang, Y.; Kim, J.; Xiu, F.; Ji, S.; Zou, J.; Nealey, P. F.; Wang, K. L., Metal Nanodot Memory by Self-Assembled Block Copolymer Lift-Off. *Nano Letters* **2009,** *10* (1), 224-229.
57. Ji, S.; Liu, C.-C.; Liao, W.; Fenske, A. L.; Craig, G. S. W.; Nealey, P. F., Domain Orientation and Grain Coarsening in Cylinder-Forming Poly(styrene-b-methyl methacrylate) Films. *Macromolecules* **2011,** *44* (11), 4291-4300.
58. Wilke, C. R.; Lee, C. Y., Estimation of Diffusion Coefficients for Gases and Vapors. *Industrial & Engineering Chemistry* **1955,** *47* (6), 1253-1257.
59. Chang, J.-B.; Son, J. G.; Hannon, A. F.; Alexander-Katz, A.; Ross, C. A.; Berggren, K. K., Aligned Sub-10-nm Block Copolymer Patterns Templated by Post Arrays. *ACS Nano* **2012,** *6* (3), 2071-2077.
60. Hamley, I. W., Ordering in thin films of block copolymers: Fundamentals to potential applications. *Progress in Polymer Science* **2009,** *34* (11), 1161-1210.
61. Kim, S. H.; Misner, M. J.; Yang, L.; Gang, O.; Ocko, B. M.; Russell, T. P., Salt Complexation in Block Copolymer Thin Films. *Macromolecules* **2006,** *39* (24), 8473-8479.
62. Rasappa, S.; Schulte, L.; Borah, D.; Morris, M. A.; Ndoni, S., Rapid, Brushless Self-assembly of a PS-b-PDMS Block Copolymer for Nanolithography. *Colloids and Interface Science Communications* **2014,** *2* (0), 1-5.
63. Stein, G. E.; Kramer, E. J.; Li, X.; Wang, J., Layering Transitions in Thin Films of Spherical-Domain Block Copolymers. *Macromolecules* **2007,** *40* (7), 2453-2460.
64. Renaud, G.; Lazzari, R.; Leroy, F., Probing surface and interface morphology with Grazing Incidence Small Angle X-Ray Scattering. *Surface Science Reports* **2009,** *64* (8), 255-380.
65. Zhang, J.; Posselt, D.; Sepe, A.; Shen, X.; Perlich, J.; Smilgies, D.-M.; Papadakis, C. M., Structural Evolution of Perpendicular Lamellae in Diblock Copolymer Thin Films during Solvent Vapor Treatment Investigated by Grazing-Incidence Small-Angle X-Ray Scattering. *Macromolecular Rapid Communications* **2013,** *34* (16), 1289-1295.

CHAPTER 3

HIGH QUALITY FILMS WITH SUB-10 NM FEATURE SIZES UTILIZING NOVEL GRAFTED AND STAR BLOCK COPOLYMERS

3.1 Abstract

This chapter addresses the synthesis, characterization, and thin films self-assembly of novel polystyrene-*block*-poly(ethylene oxide) (PS-*b*-PEO) grafted and star block copolymers. These novel architectures were designed to overcome a severe dewetting problem in low molecular weight linear PS-*b*-PEO thin film systems while maintaining small features and pitch respectively. Low molecular weight PS-*b*-PEO block copolymers potentially lead to minimal phase separation and increase dewetting due to the χN falling below 10.5 and depleted chain entanglement. One approach to overcome this problem with linear PS-*b*-PEO is to complex the block copolymer with a salt-additive to increase the segregation strength (χ), which in-turn increases χN. Although this complexation helps, it does not overcome the total dewetting occurring in the film. The grafted and star block copolymer architectural design overcomes dewetting due to their high overall total molecular weight. Thus, the increase in the number of side-chains or arms causes enhanced chain entanglement between adjacent polymer chains to ensure a high quality film after annealing. Furthermore, the relative molecular weight of the side chains or arms dictates the feature size and pitch of the ordered surface domains.

3.2 Introduction

The development of highly ordered surface patterns with decreased feature size and pitch is still an issue the semiconductor industry faces. The current photolithographic techniques employed are reaching their lower limits due to high cost with currently used methods and technical difficulties.[1, 2] Block copolymer (BCP) nanolithography is a promising technique to drive further miniaturization due to the nanometer-scale size of

structures obtained after self-assembly.[2-8] Since the size of the nanodomains is ultimately defined by the molecular weight (N) of the block copolymer, decreasing the total molecular weight would reduce the feature sizes and also reduce χN. However, there is a limit as to how low in molecular weight of a linear block copolymer can be before it passes the order-disorder transition (ODT). A common way to overcome this problem is to complex the low molecular weight block copolymer with a salt additive to increase chi (χ), which in-turn increases the χN.[9, 10] Block copolymers with high χ can utilize lower molecular weight polymers before the order-disorder transition (ODT) is reached.[5, 11-15] However, during the annealing phase, macroscopic phase separation occurs for low molecular weight linear block copolymers systems due to limited polymer chain entanglement. These issues generate the need for further exploration of other block copolymer architectures with enhanced chain entanglement to overcome dewetting while maintaining small feature sizes in thin films.

Long-range order and orientational control has been achieved with various block copolymer systems through various external potentials including topographically patterned substrates (graphoepitaxy),[16, 17] chemically patterned substrates (chemoepitaxy),[18, 19] electric fields,[20-23], and solvent annealing.[2, 3, 24] Specifically, a dual-humidity solvent annealing process using polystyrene-*block*- poly(ethylene oxide) (PS-*b*-PEO) is a fast and cheap technique to promote long-range ordered nanostructures in thin films. However, for all linear block copolymers there exists a vast film dewetting during annealing for low molecular weight block copolymer systems.[25] We recently found a lower molecular weight threshold for linear PS-*b*-PEO.[25] Below a total molecular weight of 3000 Da (PEO 750 Da and PS 2,250 Da), the polymer film completely dewet during

annealing showing no feature formation from AFM measurements even after incorporation of a salt additive.[25]

Grafted and star block copolymers have gained much attention due to their ability to form nanostructures which are impossible from their linear block copolymer counterparts.[26-42] Such structures have been utilized to prepare microphase separated spherical, cylindrical and lamellae structures with domain size below 100 nm in various applications.[43-45] These block copolymer systems can potentially provide access to microphase structures of A-B diblock copolymers. The grafted and star block copolymer systems contain linking components as A-B linear diblock copolymers as side-chains (grafted BCP), and arms (star BCP) to avoid dewetting during a solvent annealing process by offering increased chain entanglement between adjacent polymer chains. Specifically, due to the confinement of the component block copolymers to a common backbone (grafted BCP) or a central core (star BCP). The A and B blocks on the polymer side-chain form microphase separated domains, thus, providing access to the microphase structures of A-B diblock, while surpassing the lower limit of feature sizes obtainable by linear A-B diblock. Scheme 3.1 illustrates the chemical compositions of the three types of block copolymers to target sub 10 nm and 20 nm feature size and pitch respectively. All three types of architectures were designed using PEO-*b*-PS sub units to take advantage of dual humidity solvent annealing to induce lateral ordering.

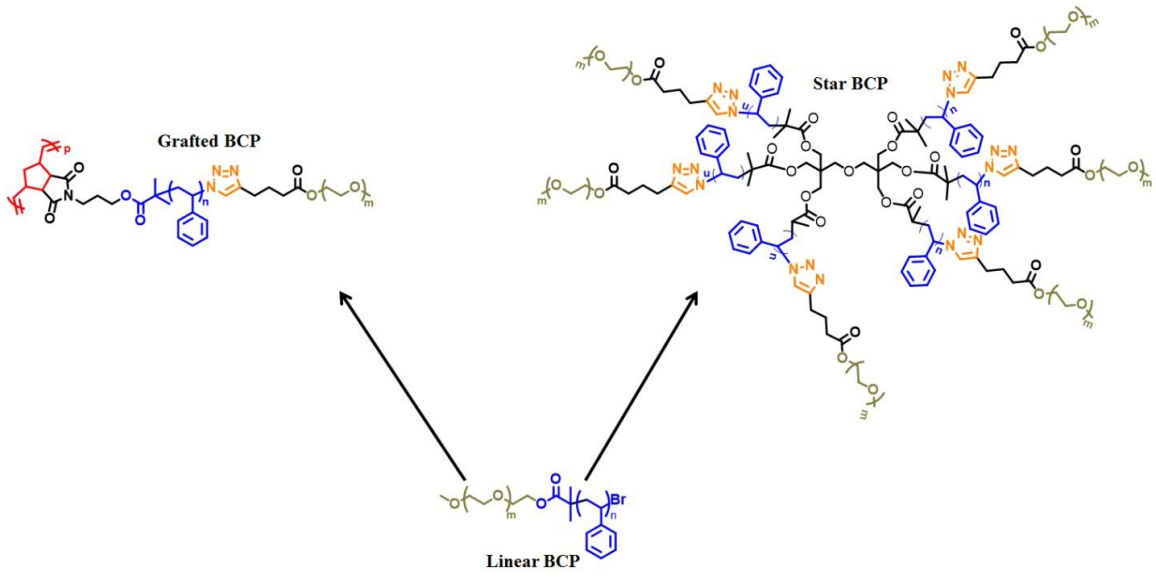

Scheme 3.1 Grafted and Star Block Copolymers derived from Linear PS-*b*-PEO

Herein, we describe the synthesis, characterization and thin-film studies of novel grafted and star block copolymers prepared via a combination of atom transfer radical polymerization (ATRP), ring-opening metathesis polymerization (ROMP), and copper-catalyzed "click" reactions. Specifically, we have utilized grafted and star block copolymers in which the side-chains and arms consist of low molecular weight PEO-*b*-PS diblock copolymers to prepare films with feature sizes below what is possible for the linear diblock copolymer analogues. While macrophase separation led to dewet films for linear diblock copolymers with the same molecular weight as the grafted and star copolymer side-chains and arms, the grafted and star block copolymers systems retained high quality films due to their overall higher molecular weight. This could increase in chain entanglement between adjacent polymer chains. Furthermore, the feature sizes of the microphase separated structures of grafted and star block copolymer systems were similar to those of the linear diblock copolymer analogues, suggesting that for grafted and

star block copolymer systems with low backbone lengths and low number of arms, the block copolymer on the side-chain or arms determines the feature sizes upon self-assembly, while the total molecular weight dictates the segregation strength (χN) and ensures the microscopic phase separation still above the order-disorder transition (ODT).

3.3 Experimental Section

3.3.1 Materials

Sodium azide, and ethyl vinyl ether (EVE, 99%) were from Acros Organics. Tetrahydrofuran (THF) and *N,N*-dimethylformamide (DMF) were dried over molecular sieves and distilled before use. Styrene was passed through a basic alumina column before use. *N,N,N',N'',N''*-pentamethyldiethylenetriamine (PMDETA, Aldrich) and triethylamine (Et_3N, 99%, Aldrich) were distilled before use. Cu(I)Br (99.999% Aldrich), Dipentaerythritol hexakis(2-bromoisobutyrate) (Aldrich) and 2-bromoisobutyryl bromide (Aldrich) were used as received. Grubbs 3rd generation catalyst, N-[3-Hydroxylpropyl]-*cis*-5-Norbornene-*exo*-2,3-Dicarboximide (NPH), and 5-hexynoic acid chloride were prepared according to previous reports.[46-48] All other reagents and solvents were purchased from Sigma Aldrich or Alfa Aesar and used as received.

3.3.2 Characterization

Gel permeation chromatography (GPC) was performed at 50 °C on a Varian system equipped with a Varian 356-LC refractive index detector and a Prostar 210 pump. The columns were STYRAGEL HR1, HR2 (300 × 7.5 mm) from Agilent. HPLC grade DMF was used as eluent flow rate of 1.0 mL/min. Polystyrene standards were used for calibration. DMF and samples were filtered through micro-filters with a pore size of 0.2 μm (Teflon, 17 mm Syringes Filters, National Scientific, USA). FT-IR spectra were

recorded on a PerkinElmer Spectrum 100 FT-IR spectrometer equipped with a Universal ATR sampling accessory. ^{1}H NMR (300 MHz) spectra was recorded on a Bruker 300 spectrometer with tetramethylsilane (TMS) as an internal reference.

3.3.3 Atomic Force Microscopy

Atomic force microscopy (AFM) was performed using a Multimode Nanoscope V system (Bruker, Santa Barbara, CA). Tapping mode AFM was used to map the topography by tapping the surface using an oscillating tip. The measurements were performed using commercial Si cantilevers with a nominal spring constant and resonance frequency at 20–80 N m^{-1} and 230–410 kHz, respectively (TESP, Bruker AFM Probes, Santa Barbara, CA).

3.3.4 Preparation of Thin Films

A grafted and star block copolymer (1.5 wt %) toluene solution was spin coated (3000 RPM, 60 s) onto oxidized silicon substrates (100 nm thick thermal oxide). The thin films were annealed in a glove box under controlled humidity with toluene as the solvent. All films were saturated with solvent vapor in a chamber before exposure in the humid glove box. Grain sizes were determined by measuring areas of complete grains from at least five different micrographs to calculate an average grain size. The lateral grain size reported in this manuscript is defined as the diameter of a circle or equal area. Film thicknesses were measured with a J.A. Woollam spectroscopic ellipsometer with an incident angle of 70°. All film thicknesses were in the range of 55 to 65 nm.

3.3.5 Synthesis of Grafted Monomers and Polymers

Norbornene-terminated ATRP initiator (N-[3-propyl-2-bromo-2-methylproponate]-cis-5-Norbornene-exo-2,3-Dicarboximide, (NP-Br, 2).

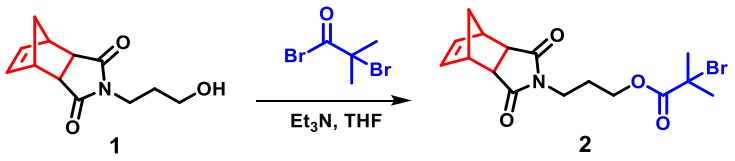

NPH (**1**, 0.31 g, 1.4 $\times 10^{-3}$ mol) was added to a 100 mL round bottom flask equipped with a stir bar and purged with nitrogen. Dry tetrahydrofuran (25 mL) was added and the reaction was cooled to 0 °C before triethylamine (0.39 mL, 2.8 $\times 10^{-3}$ mol) was added. A solution of 2-bromoisobutyryl bromide (0.26 mL, 2.1 $\times 10^{-3}$ mol) in dry tetrahydrofuran (15 mL) was added dropwise to the cooled solution. The solution was stirred at 0 °C for 30 minutes, then at room temperature overnight. The mixture was filtered and concentrated to dryness. The solids were then dissolved in DCM. The DCM was extracted with deionized H_2O twice. The aqueous layers were combined and extracted with DCM three times. The organic layers were combined, dried over anhydrous sodium sulfate, filtered, concentrated, and the products were separated using column chromatography (silica gel, eluent: DCM). The product was collected, concentrated, and vacuum dried. Yield: 0.40 g, 76.9%. ^{1}H NMR (300 MHz, CD_2Cl_2): δ (ppm) 6.30 (s, 2H, C*H*=C*H*), 4.15 (t, 2H, $CH_2CH_2OC(O)$), 3.59 (t, 2H, NCH_2CH_2), 3.33 (s, 2H, C*H*C(O)N), 2.69 (s, 2H, CH_2CH), 1.88-2.08 (m, 8s, $CH_2CH_2CH_2$ + $(CH_3)_2C(O)$), 1.51 and 1.23 (dd, 2H, CH_2CH). FT-IR (cm^{-1}): 2980, 1760, 1690, 1465, 1440, 1390, 1340, 1110, 1170, 890, 720.

Bromide-terminated NP-polystyrene (NP-PS-Br, 3).

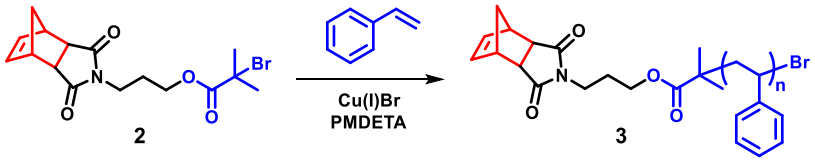

2 3

Copper (I) bromide (1 eq.) was charged into a 10 mL schlenk line flask and purged with nitrogen. NP-Br (**2**, 1 eq.), styrene (*n* eq.), and *N,N,N',N'',N''*-pentamethyldiethylenetriamine (PMDETA, 1.5 eq.) were added to a 5 mL pearl shaped flask, degassed by bubbling nitrogen through the solution for 20 minutes, and transferred to the schlenk line flask. The solution was then allowed to stir at room temperature for 20 minutes before a sample was taken for NMR analysis. The schlenk line flask was then put to an oil bath preheated to 90 °C. The polymerization was monitored by ^{1}H NMR and the reaction was stopped at the desired monomer conversion by cooling in an ice bath and then diluting the solution with THF. The solution was then precipitated into methanol twice. The solid white product was collected by filtration and vacuum dried. ^{1}H NMR (300 MHz, CD_2Cl_2) δ (ppm): 6.35-7.33 (br, Ar*H*), 6.30 (s, 2H, C*H*=C*H*), 3.59 (t, 2H, NCH_2CH_2), 3.33 (s, 2H, C*H*C(O)N), 2.69 (s, 2H, CH_2C*H*), 1.0-2.4 (br, -CH_2C*H*-). FT-IR (cm^{-1}): 3090, 3050, 3020, 2960, 2840, 1700, 1590, 1490, 1460.

Azide-terminated NP-polystyrene (NP-PS-N_3, 4).

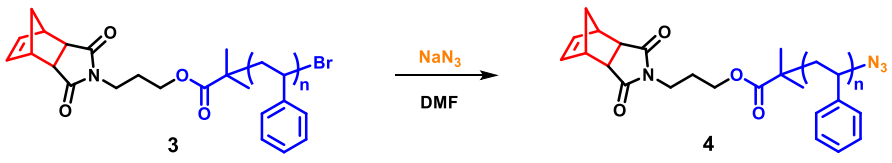

3 4

The terminal bromide groups were converted to azide groups through reaction with NaN_3 in DMF as previously reported.[46] ^{1}H NMR (300 MHz, CD_2Cl_2): δ (ppm) 6.35-7.33 (br, Ar*H*), 6.30 (s, 2H, C*H*=C*H*), 3.59 (t, 2H, NC*H*$_2$CH$_2$), 3.33 (s, 2H, C*H*C(O)N), 2.69 (s, 2H, CH$_2$C*H*), 1.0-2.4 (br, -C*H*$_2$C*H*-). FT-IR (cm^{-1}): 3090, 3050, 3020, 2960, 2840, 2100, 1700, 1590, 1490, 1460.

Alkyne-terminated poly(ethylene oxide) (PEO-alkyne,5).

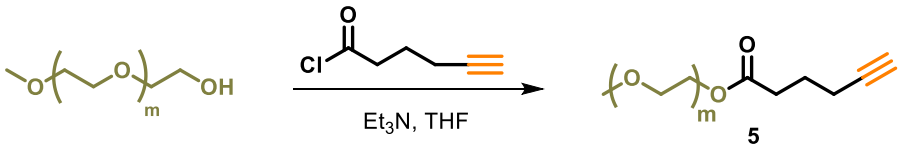

Polyethylene glycol monomethyl ether (1 eq.) was dissolved in 30 mL dry THF and the flask was purged with nitrogen. Triethylamine (1.5 eq.) was added and the solution was cooled to 0 °C. A solution of 5-hexynoic acid chloride (1.5 eq.) in 10 mL dry THF was added over 30 minutes. After stirring at room temperature overnight, the reaction mixture was filtered and concentrated to dryness. The solids were dissolved in dichloromethane and extracted with water twice. The aqueous layers were combined and extracted with dichloromethane three times. The organic layers were combined and stirred over anhydrous sodium sulfate. The solution was filtered, concentrated, and precipitated into diethyl ether three times. The product was collected by centrifuge and vacuum dried. ^{1}H NMR (300 MHz, CD_2Cl_2): δ (ppm) 4.22 (t, 2H, CH$_2$C*H*$_2$COC(O)), 3.4-3.8 (m, -OC*H*$_2$C*H*$_2$-), 3.35 (s, 3H, -OC*H*$_3$), 2.48 (t, 2H, C(O)C*H*$_2$CH$_2$), 2.25 (td, 2H, CH$_2$C*H*$_2$C≡CH), 2.02 (t, 1H, C≡C*H*), 1.84 (quin, 2H, CH$_2$C*H*$_2$CH$_2$). FT-IR (cm^{-1}): 3290, 3070, 2880, 1710, 1450, 1290.

Norbornene-terminated diblock copolymer PS-b-PEO (NP-g-(PS-b-PEO), 6).

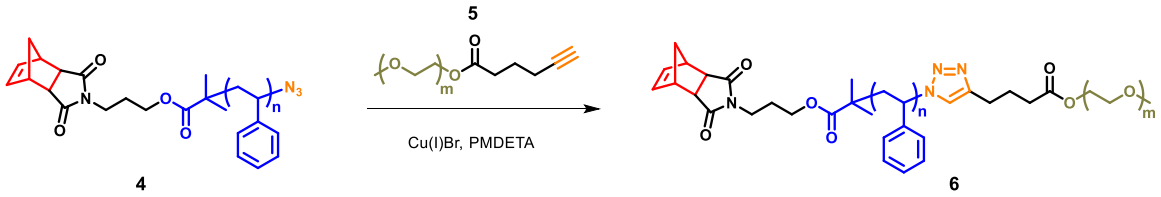

Cu(I)Br (0.1 eq.) was charged into a round bottom flask and purged with nitrogen. PEO-alkyne (**5**, 2 eq.), NP-PS-N_3 (**4**, 1 eq.), and PMDETA (0.15 eq.) were added to a pear shaped flask, dissolved in THF, and bubbled with nitrogen for 30 minutes. The mixture in the pear shaped flask was transferred to the round bottom flask and stirred at 40 °C overnight. The reaction mixture was then concentrated to dryness, dissolved in dichloromethane, and extracted with water three times. The organic layer was dried over anhydrous sodium sulfate, filtered, and concentrated. The solution was then precipitated into methanol two times. The product was collected by centrifuge and vacuum dried overnight. ^{1}H NMR (300 MHz, CD_2Cl_2): δ (ppm**)** 6.35-7.33 (br, Ar*H*), 6.30 (s, 2H, C*H*=C*H*), 4.22 (t, 2H, CH_2CH_2COC(O)), 3.4-3.8 (m, -OCH_2CH_2-), 3.35 (s, 3H, -OCH_3), 2.69 (s, 2H, CH_2C*H*), 2.48 (t, 2H, C(O)C$H_2$$CH_2$), 1.0-2.4 (br, -C$H_2$C*H*-)**.** FT-IR ($cm^{-1}$): 3090, 3050, 3020, 2960, 2840, 1700, 1590, 1490, 1460.

Grafted block copolymer poly(norbornene-graft-(PS-b-PEO)) (PNP-g-(PS-b-PEO), 7).

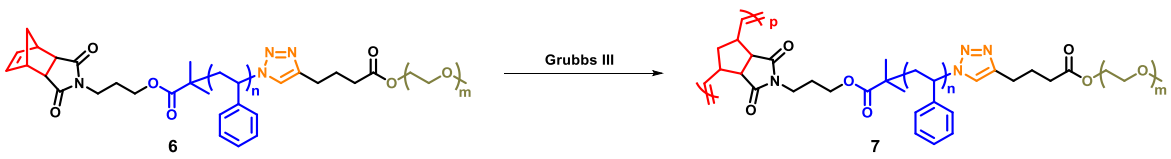

Grubbs 3rd generation catalyst (1 eq.) and anhydrous DMF (1 mL) were added to a schlenk line flask and bubbled with nitrogen for 10 minutes. NP-*g*-(PS-*b*-PEO) (6, *p* eq.) was added to a pear shaped flask, dissolved in DMF (4 mL), and bubbled with nitrogen for 10 minutes. The mixture in the pear shaped flask was transferred to the schlenk line flask and stirred at 60 °C. The polymerization was monitored by GPC and terminated by addition of ethyl vinyl ether (5 equiv.) when all macromonomer **6** was consumed. The reaction mixture was precipitated into diethyl ether two times. The solid product was collected by centrifuge and vacuum dried overnight. ^{1}H NMR (300 MHz, CD_2Cl_2): δ (ppm) 6.35-7.33 (br, Ar*H*), 5.42 and 5.60 (br, C*H*=C*H*), 4.22 (br, $CH_2CH_2COC(O)$), 3.4-3.8 (m, -OCH_2CH_2-), 3.35 (br, -OCH_3), 2.69 (br, CH_2CH), 2.48 (br, C(O)CH_2CH_2), 1.0-2.4 (br, -CH_2C*H*-)**.**

3.3.6 Synthesis of Star Monomers and Polymers

Bromine-terminated 6f-BiB-polystyrene (PS-Br, 9).

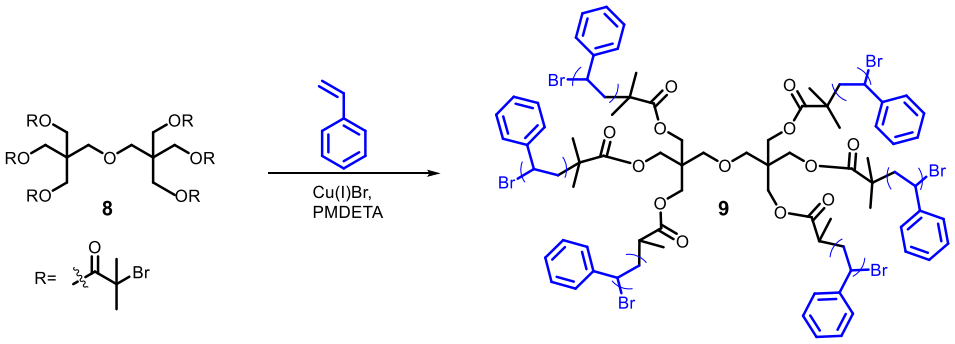

Copper(I) bromide (1 eq.) was charged into a 10 mL schlenk line flask and purged with nitrogen. Dipentaerythritol hexakis(2-bromoisobutyrate) (**8**) (1 eq.), styrene (*n* eq.), and *N,N,N',N'',N''*-pentamethyldiethylenetriamine (PMDETA, 1.5 eq.) were added to a 5 mL pearl shaped flask, degassed by bubbling nitrogen through the solution for 20 minutes,

and transferred to the schlenk line flask. The solution was then allowed to stir at room temperature for 20 minutes before a sample was taken for NMR analysis. The schlenk line flask was then added to an oil bath preheated to 90 °C. The polymerization was monitored by ^{1}H NMR and the reaction was stopped at the desired monomer conversion by cooling in an ice bath and then diluting the solution with THF. The solution was then precipitated into methanol twice. The solid white product was collected by filtration and vacuum dried. ^{1}H NMR (300 MHz, $CDCl_3$): δ (ppm) 6.35-7.33 (br, Ar*H*), 6.30 (s, 2H, C*H*=C*H*, 1.0-2.4 (br, -CH_2C*H*-).

Azide terminated 6f-BiB-polystyrene (PS-N_3, 10).

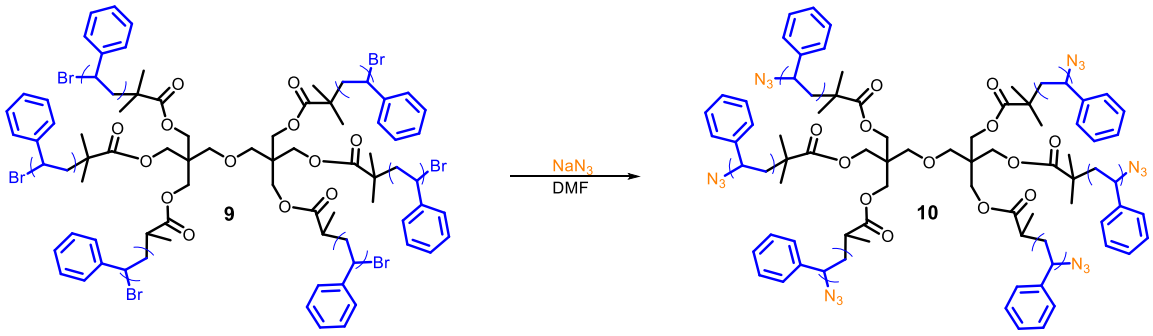

The terminal bromine groups were converted to azide groups through reaction with NaN_3 in DMF as previously reported.[46] ^{1}H NMR (300 MHz, $CDCl_3$): δ (ppm) 6.35-7.33 (br, Ar*H*), 1.0-2.4 (br, -CH_2C*H*-). FT-IR (cm^{-1}): 2100.

6f-BiB-Star diblock copolymer PS-b-PEO (PS-b-PEO), 11).

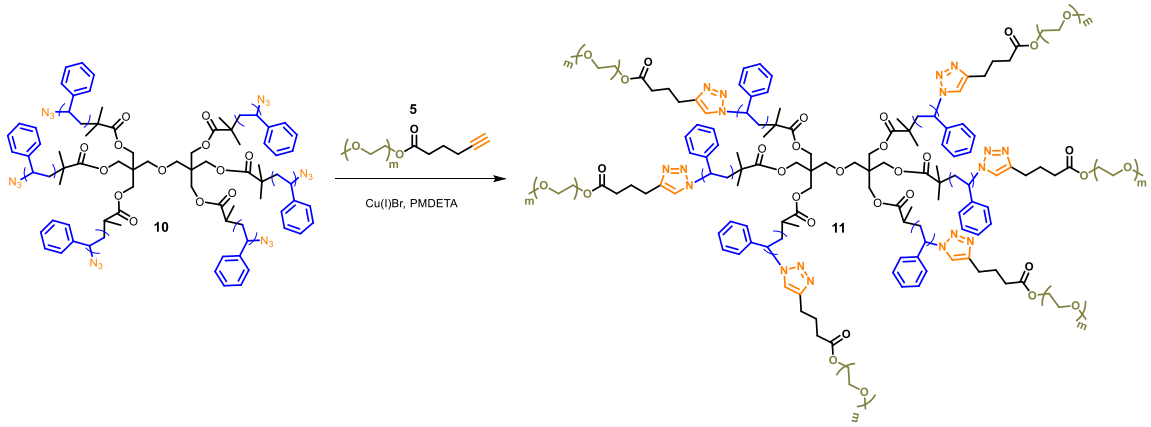

Cu(I)Br (0.1 eq.) was charged into a round bottom flask and purged with nitrogen. PEO-alkyne (**5**, 2 eq.), 6f-BiB-PS-N_3 (**9**, 1 eq.), and PMDETA (0.15 eq.) were added to a pear shaped flask, dissolved in THF, and bubbled with nitrogen for 30 minutes. The mixture in the pear shaped flask was transferred to the round bottom flask and stirred at 40 °C overnight. The reaction mixture was then concentrated to dryness, dissolved in dichloromethane. The solution was then precipitated into methanol two times. The product was collected by centrifuge and vacuum dried overnight. ^{1}H NMR (300 MHz, CD_3Cl_3): δ (ppm) 6.35-7.33 (br, Ar*H*), 4.22 (t, 2H, $CH_2CH_2COC(O)$), 3.4-3.8 (m, -OCH_2CH_2-), 3.35 (s, 3H, -OCH_3), 2.69 (s, 2H, CH_2CH), 2.48 (t, 2H, $C(O)CH_2CH_2$), 1.0-2.4 (br, -CH_2CH-)**.**

3.4 Results and Discussion

To prepare grafted and star block copolymers, similar synthetic routes were used, taking advantage of aforementioned controlled polymerization techniques and the copper-catalyzed Huisgen cycloaddition reaction. All architectures contained linear PS-

b-PEO block copolymer as side-chains or arms. Figure 3.1 shows the synthetic routes of the grafted (Figure 3.1A) and star (Figure 3.1 B) copolymers.

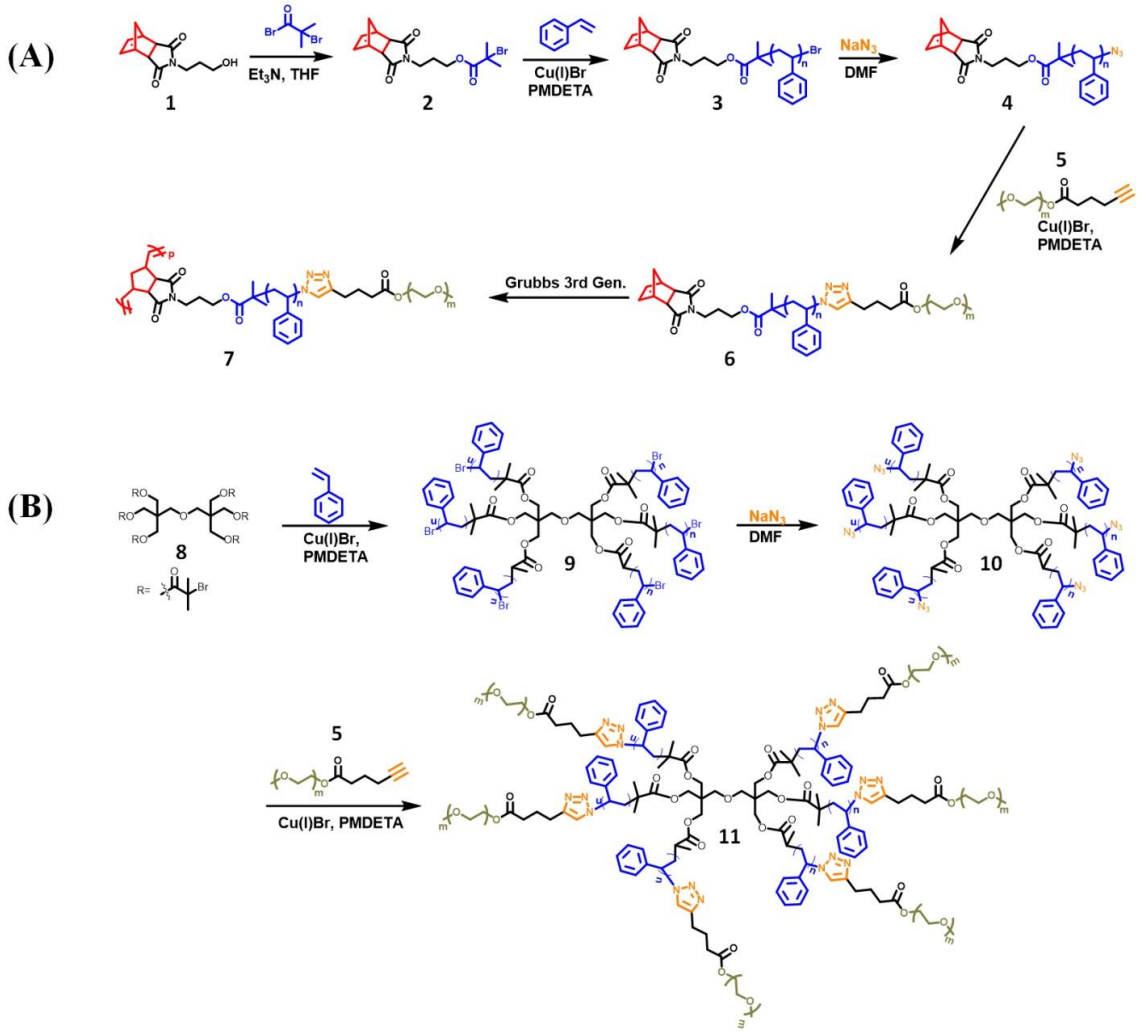

Figure 3.1 (**A**) Synthesis of Grafted Block Copolymer (PNP-g-(PS-b-PEO) (**B**) Synthesis of Star Block Copolymer 6f-PS-b-PEO.

As shown in Figure 3.1A, the synthesis of grafted block copolymer began by preparing a norbornene ATRP initiator (**2**) through an esterification reaction between norbornene alcohol (**1**) and 2-bromoisobutryl bromide in the presence of triethyl amine. NP-Br (**2**) was used to polymerize styrene through ATRP using Cu(I)Br and PMDETA as the catalyst system at 90 °C. The molecular weight of polystyrene was monitored by ^{1}H NMR (Figure 3.2A). The monomer conversion was obtained by calculating the decrease

of the vinyl peaks at 5.74 and 5.22 ppm to the aromatic peaks at 6.00 and 7.40 and the reaction was stopped at the desirable conversion. The molecular weight and dispersity are provided in Table 3.1. Displacement of the terminal bromide in NP-PS-Br (**3**) with sodium azide in DMF afforded NP-PS-N_3 (**4**). Furthermore, PEO-alkyne (**5**) (M_w-2000 Da) and NP-PS-N_3 (**4**) was coupled in a copper-catalyzed "click" reaction using Cu(I)Br and PMDETA as the catalyst system to afford linear NP-*g*-(PS-*b*-PEO) (**6**). Linear block copolymer (**6**) was confirmed by ^{1}H NMR (Figure 3.2A), and GPC (Figure 3.2B) Finally, ROMP was carried out on the linear block copolymer (**6**), using Grubbs 3rd generation catalyst in DMF. The polymerization was monitored by GPC (Figure 3.2B), and was quenched with ethyl vinyl ether once all macromonomer was consumed. PNb_{20}-*g*-(PS_{64}-*b*-PEO_{45}) (**7**) was confirmed by ^{1}H NMR (Figure 3.2A) through the disappearance of the monomer alkene protons at 6.30 ppm and through GPC (Figure 3.2B) that showed a clean shift to higher molecular weight. The polymer compositions are given in Table 3.1.

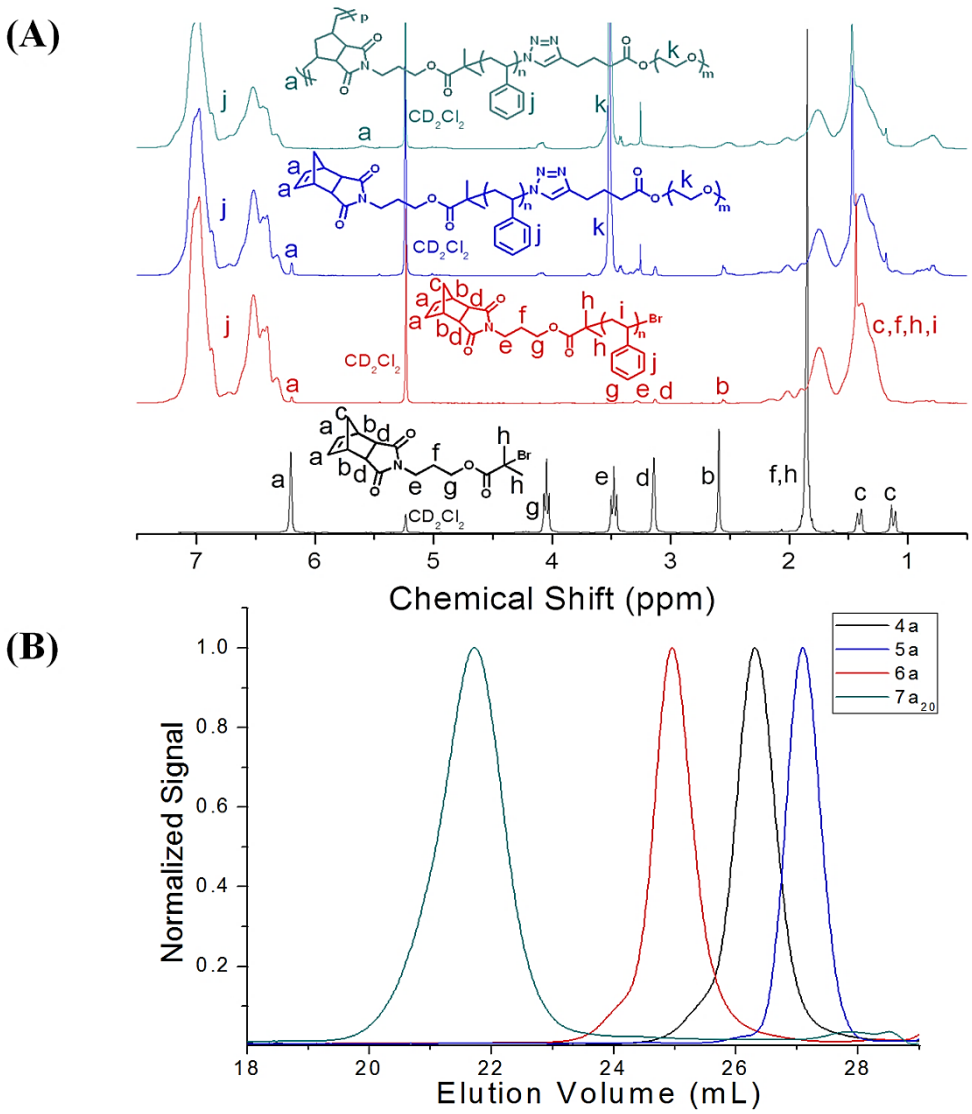

Figure 3.2 ^{1}H NMR spectra (**A**) and GPC traces (**B**) of grafted polymers.

In a similar fashion as shown in Figure 3.1B, the star block copolymer began with synthesis of PS-Br (**9**), by ATRP of styrene using commercially available dipentaerythritol hexakis (**8**), and Cu(I)Br and PMDETA as the catalyst system at 90 °C. Again, PEO-alkyne (**5**) (M_w-2000 Da) and PS-N_3 (**10**) was coupled in a "click" reaction to afford 6-arm-(PS-*b*-PEO) (**11**). The 6-arm star block copolymer (**11**) was confirmed through ^{1}H NMR (Figure 3.3A) and GPC (Figure 3.3B). The polymer compositions are given in Table 3.1.

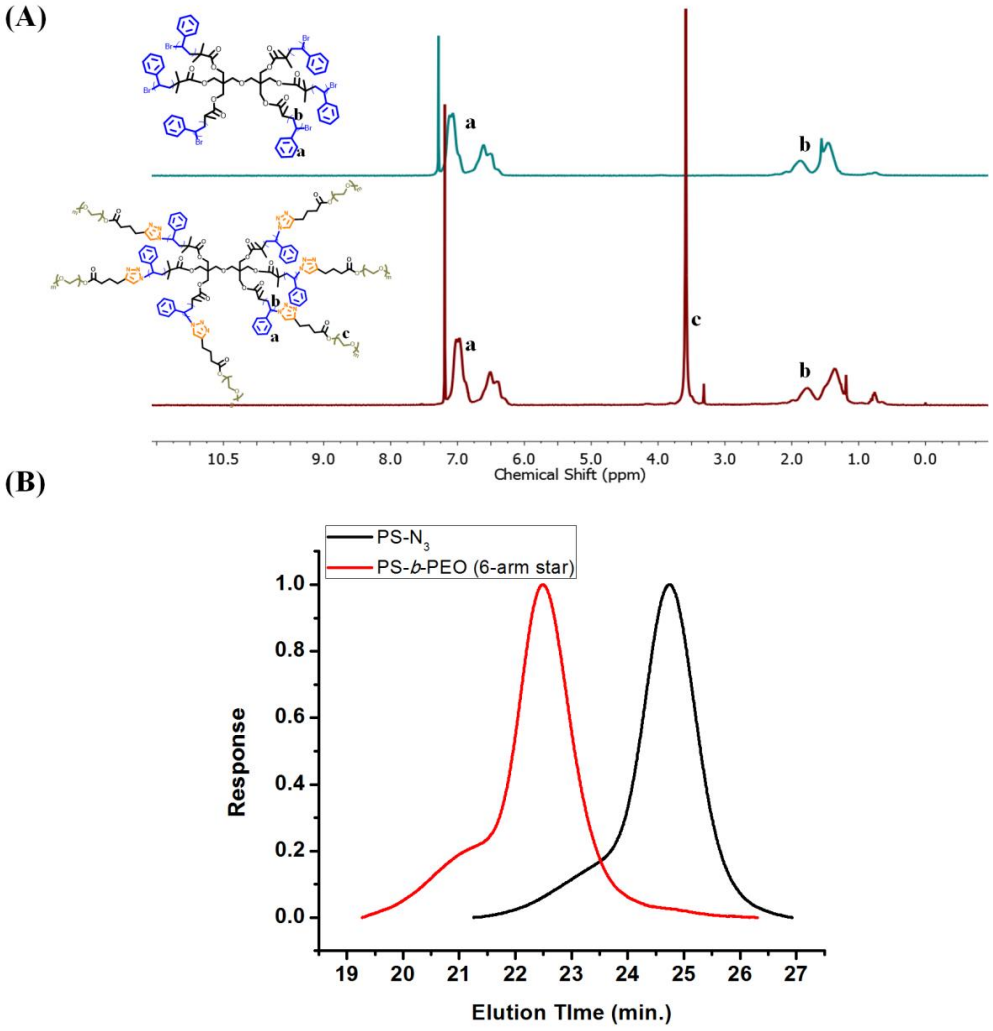

Figure 3.3 ^{1}H NMR spectra (**A**) and GPC traces (**B**) of star block polymers

Solvent annealing of PEO-*b*-PS diblock copolymers reported by other groups with the use of MW PEO = 2,000 g/mol and a weight percent close to 25% observed no microphase separation.[9, 10] This is due to the low the product of Flory-Huggins interaction and the degree of polymerization (χN). For PEO-*b*-PS systems, χ can be described by Equation3.1:

$$\chi_{\text{PS-}b\text{-PEO}} = -0.007 + 21.3/T \qquad \text{(Equation 3.1)}$$

where *T* is the temperature.[49] In our study on the linear block copolymer (MW_{total} = 8450 g·mol^{-1}), where χN ~8.11, (Table 3.1; linear block copolymer) we also observed no microphase separation.[25] This agrees with a previous report as weak microphase separated structures were observed for a PEO-*b*-PS polymer with χN ~16.8 and no microphase separated structures were observed when χN ~10.7.[10] Early work reported the increase of segregation strength, χ, by complexing the ether linkages in PEO domains with a salt additive (LiCl).[9, 10] This resulted in an apparent increase in χ by the formation of highly ordered microphase separated films. When the ether linkages in PEO complex with Li^+, the χ between PEO/Li and PS blocks increased due to the ionic nature of PEO/Li block. Furthermore, the lithium atoms can loosely coordinate between multiple PEO chains.[2, 10]

Self-assembly of grafted and star PEO-*b*-PS block copolymers in thin films were systematically studied and compared to the above-mentioned linear PS-*b*-PEO block copolymer. Solutions (1.5 wt%) of linear, grafted (**7**), and star (**11**) block copolymers in toluene were spun-cast onto silicon substrates and subsequently subjected to high-humidity solvent annealing to control orientation (Scheme 3.2). Annealing was conducted under a saturated toluene atmosphere overnight before exposure to a high relative humidity (RH) for 15 minutes (> 90% RH). The thin films were characterized by both optical microscopy and atomic force microscopy (AFM).

Scheme 3.2 A humidity-controlled solvent annealing process for block copolymer PEO-*b*-PS in thin films.

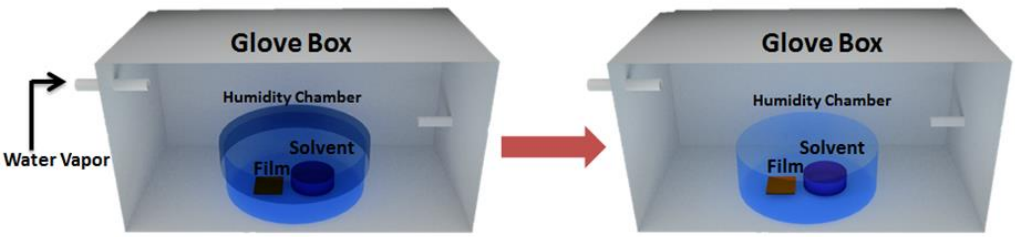

Hexagonally-packed surface domains with long-range order (2 μm × 2 μm) were obtained for all architectures (linear, grafted (**7**), and star (**11**)) (Figure 3.4A-C). All systems contained PEO with a molecular weight of 2000 Da. The grafted and star block copolymers counterparts (side-chains and arms) had nearly the same molecular weight as total molecular weight of the linear block copolymer (MW_{total}~8,700) with nearly identical PEO wt% = 24.0% (Table 3.1). Remarkably, the feature size (≈ 10 nm) and pitch (≈ 20 nm) of the hexagonally packed surface domains in both grafted (**7**) and star (**11**) block copolymers were the same as what was observed for the linear block copolymer complexed with LiCl. This demonstrates that when the length of the backbone or the number of arms is kept sufficiently low (< 20 repeat units), the feature size and pitch of the microphase separated structures are dictated by the block copolymers grafted onto the side chains of the polymer brush or as the extending arms on the star polymer.

Table 3.1: Characteristics of Block Copolymer Architectures

Sample	MW of BCP (g/mol)	MW of PEO (g/mol)	MW of PS (g/mol)	Wt. % PEO	Diameter (nm)	Pitch (nm)	Average Grain Size	DP Backbone	χN
Linear BCP	8450	2000	6450	23.7%	10	20	2 × 2 μm	Na	8.48
Grafted BCP	173,800	2000	6690	23.0%	10	20	2 × 2 μm	20	Max: 172.8
Star BCP	48,000	2000	5833	25.5%	10	20	2 × 2 μm	6	Max: 48.0

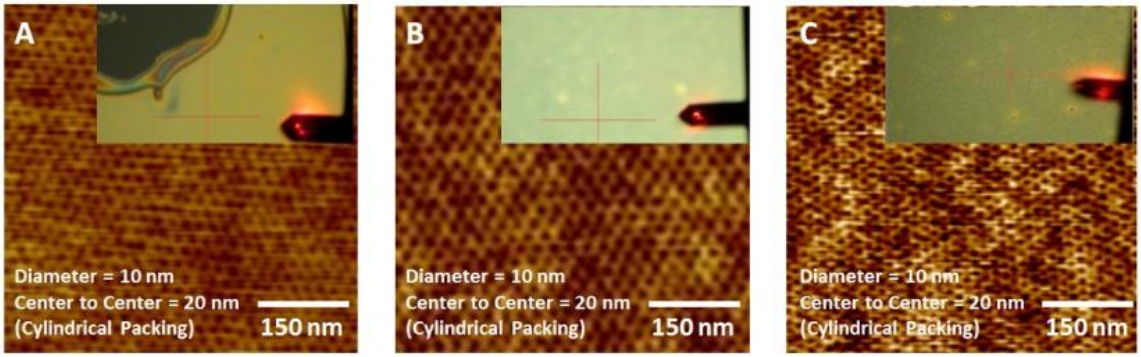

Figure 3.4 AFM and optical images of (**A**) linear, (**B**) grafted, and (**C**) star block copolymer

Another challenge we like to address is related with the stability of films of block copolymers. When the linear block copolymer was complexed with LiCl, there was still vast dewetting throughout the film as shown in Figure 3.4A (optical image). The additive, to an extent, allows for enhanced chain entanglement, as the lithium atoms serve as a type of binding agent between adjacent polymer chains. However, it seems the interactions are limited in increasing the entanglement from the dewetting observed. Astonishingly, the grafted and star block copolymers retained high quality films after solvent annealing as seen in Figure 3.4B and 3.4C (optical image). This comparison suggests the increase in overall molecular weight for the grafted and star block copolymers minimizes dewetting due to increased chain entanglement between adjacent polymer chains. As seen in Table 3.1, the χN values for the grafted and star are well above that of the linear block copolymer, and that each system has high chain entanglement which in turn helps with film stability.

3.5 Conclusion

In conclusion, we prepared grafted and star block copolymers with PS-b-PEO diblock copolymers as the side-chains and arms respectfully. By keeping the length of polymer backbone low or the number of arms low, the polymer films formed highly ordered hexagonally-packed surface domains of PEO within a matrix of PS upon solvent annealing. The feature sizes of grafted and star block copolymer systems were very close to those of the linear diblock copolymer complexed with LiCl, suggesting the block copolymer on the side-chain or arms determines the feature sizes. Furthermore, the high overall molecular weight prevents the macroscopic phase separation and retains highly quality films after solvent annealing. These novel architectures provide a solution to overcome decreasing feature size and pitch while maintaining high quality films.

3.6 References

1. Park, S.; Kim, B.; Xu, J.; Hofmann, T.; Ocko, B. M.; Russell, T. P., Lateral Ordering of Cylindrical Microdomains Under Solvent Vapor. *Macromolecules* **2009,** *42* (4), 1278-1284.
2. Park, S.; Lee, D. H.; Xu, J.; Kim, B.; Hong, S. W.; Jeong, U.; Xu, T.; Russell, T. P., Macroscopic 10-Terabit–per–Square-Inch Arrays from Block Copolymers with Lateral Order. *Science* **2009,** *323* (5917), 1030-1033.
3. Tang, C.; Lennon, E. M.; Fredrickson, G. H.; Kramer, E. J.; Hawker, C. J., Evolution of Block Copolymer Lithography to Highly Ordered Square Arrays. *Science* **2008,** *322* (5900), 429-432.
4. Bang, J.; Kim, S. H.; Drockenmuller, E.; Misner, M. J.; Russell, T. P.; Hawker, C. J., Defect-Free Nanoporous Thin Films from ABC Triblock Copolymers. *Journal of the American Chemical Society* **2006,** *128* (23), 7622-7629.
5. Bita, I.; Yang, J. K. W.; Jung, Y. S.; Ross, C. A.; Thomas, E. L.; Berggren, K. K., Graphoepitaxy of Self-Assembled Block Copolymers on Two-Dimensional Periodic Patterned Templates. *Science* **2008,** *321* (5891), 939-943.
6. Ross, C., Patterned Magnetic Recording Media. *Annual Review of Materials Research* **2001,** *31*, 203-235.
7. Ruiz, R.; Kang, H.; Detcheverry, F. A.; Dobisz, E.; Kercher, D. S.; Albrecher, T. R.; de Pable, J. J.; Nealey, P. F., Density Multiplication and Improved Lithography by Directed Block Copolymer Assembly. *Science* **2008,** *321*, 936-939.

8. Ryu, D. Y.; Ham, S.; Kim, E.; Jeong, U.; Hawker, C. J.; Russell, T. P., Cylindrical Microdomain Orientation of PS-b-PMMA on the Balanced Interfacial Interactions: Composition Effect of Block Copolymers. *Macromolecules* **2009,** *42* (13), 4902-4906.
9. Kim, H.-C.; Park, S.-M.; Hinsberg, W. D., Block Copolymer Based Nanostructures: Materials, Processes, and Applications to Electronics. *Chemical Reviews* **2010,** *110* (1), 146-177.
10. Xu, J.; Hong, S. W.; Gu, W.; Lee, K. Y.; Kuo, D. S.; Xiao, S.; Russell, T. P., Fabrication of Silicon Oxide Nanodots with an Areal Density Beyond 1 Teradots Inch−2. *Advanced Materials* **2011,** *23* (48), 5755-5761.
11. Borah, D.; Shaw, M. T.; Holmes, J. D.; Morris, M. A., Sub-10 nm Feature Size PS-b-PDMS Block Copolymer Structures Fabricated by a Microwave-Assisted Solvothermal Process. *ACS Applied Materials & Interfaces* **2013,** *5* (6), 2004-2012.
12. Jung, Y. S.; Chang, J. B.; Verploegen, E.; Berggren, K. K.; Ross, C. A., A Path to Ultranarrow Patterns Using Self-Assembled Lithography. *Nano Letters* **2010,** *10* (3), 1000-1005.
13. Jung, Y. S.; Ross, C. A., Solvent-Vapor-Induced Tunability of Self-Assembled Block Copolymer Patterns. *Advanced Materials* **2009,** *21* (24), 2540-2545.
14. Park, S.-M.; Liang, X.; Harteneck, B. D.; Pick, T. E.; Hiroshiba, N.; Wu, Y.; Helms, B. A.; Olynick, D. L., Sub-10 nm Nanofabrication via Nanoimprint Directed Self-Assembly of Block Copolymers. *ACS Nano* **2011,** *5* (11), 8523-8531.
15. Rasappa, S.; Schulte, L.; Borah, D.; Morris, M. A.; Ndoni, S., Rapid, Brushless Self-assembly of a PS-b-PDMS Block Copolymer for Nanolithography. *Colloids and Interface Science Communications* **2014,** *2* (0), 1-5.
16. Segalman, R. A.; Yokoyama, H.; Kramer, E. J., Graphoepitaxy of Spherical Domain Block Copolymer Films. *Advanced Materials* **2001,** *13* (15), 1152-1155.
17. Stein, G. E.; Kramer, E. J.; Li, X.; Wang, J., Single-Crystal Diffraction from Two-Dimensional Block Copolymer Arrays. *Physical Review Letters* **2007,** *98* (8), 086101.
18. Ouk Kim, S.; Solak, H. H.; Stoykovich, M. P.; Ferrier, N. J.; de Pablo, J. J.; Nealey, P. F., Epitaxial self-assembly of block copolymers on lithographically defined nanopatterned substrates. *Nature* **2003,** *424* (6947), 411-414.
19. Rockford, L.; Mochrie, S. G. J.; Russell, T. P., Propagation of Nanopatterned Substrate Templated Ordering of Block Copolymers in Thick Films. *Macromolecules* **2001,** *34* (5), 1487-1492.
20. Mansky, P.; DeRouchey, J.; Russell, T. P.; Mays, J.; Pitsikalis, M.; Morkved, T.; Jaeger, H., Large-Area Domain Alignment in Block Copolymer Thin Films Using Electric Fields. *Macromolecules* **1998,** *31* (13), 4399-4401.
21. Mansky, P.; Liu, Y.; Huang, E.; Russell, T. P.; Hawker, C., Controlling Polymer-Surface Interactions with Random Copolymer Brushes. *Science* **1997,** *275* (5305), 1458-1460.
22. Morkved, T. L.; Lu, M.; Urbas, A. M.; Ehrichs, E. E.; Jaeger, H. M.; Mansky, P.; Russell, T. P., Local Control of Microdomain Orientation in Diblock Copolymer Thin Films with Electric Fields. *Science* **1996,** *273* (5277), 931-933.
23. Tang, C.; Wu, W.; Smilgies, D.-M.; Matyjaszewski, K.; Kowalewski, T., Robust Control of Microdomain Orientation in Thin Films of Block Copolymers by Zone Casting. *Journal of the American Chemical Society* **2011,** *133* (30), 11802-11809.

24. Chuang, V. P.; Gwyther, J.; Mickiewicz, R. A.; Manners, I.; Ross, C. A., Templated Self-Assembly of Square Symmetry Arrays from an ABC Triblock Terpolymer. *Nano Letters* **2009,** *9* (12), 4364-4369.
25. Hardy, C. G. Functional Block Copolymers for Applications in Advanced Materials, Energy Storage, and Lithography. University of South Carolina, Columbia, SC, 2013.
26. Airaud, C. d.; Héroguez, V. r.; Gnanou, Y., Bicompartmentalized Polymer Particles by Tandem ROMP and ATRP in Miniemulsion. *Macromolecules* **2008,** *41* (9), 3015-3022.
27. Charvet, R.; Novak, B. M., One-Pot, One-Catalyst Synthesis of Graft Copolymers by Controlled ROMP and ATRP Polymerizations. *Macromolecules* **2004,** *37* (23), 8808-8811.
28. Cheng, C.; Khoshdel, E.; Wooley, K. L., One-Pot Tandem Synthesis of a Core−Shell Brush Copolymer from Small Molecule Reactants by Ring-Opening Metathesis and Reversible Addition−Fragmentation Chain Transfer (Co)polymerizations. *Macromolecules* **2007,** *40* (7), 2289-2292.
29. Feng, C.; Li, Y.; Yang, D.; Hu, J.; Zhang, X.; Huang, X., Well-defined graft copolymers: from controlled synthesis to multipurpose applications. *Chemical Society Reviews* **2011,** *40* (3), 1282-1295.
30. Kriegel, R. M.; Rees, W. S.; Weck, M., Synthesis and Hydrolysis of Poly(norbornene)/Poly(acrylic acid) Graft Copolymers Synthesized via a Combination of Atom-Transfer Radical Polymerization and Ring-Opening Metathesis Polymerization. *Macromolecules* **2004,** *37* (17), 6644-6649.
31. Le, D.; Montembault, V.; Soutif, J. C.; Rutnakornpituk, M.; Fontaine, L., Synthesis of Well-Defined ω-Oxanorbornenyl Poly(ethylene oxide) Macromonomers via Click Chemistry and Their Ring-Opening Metathesis Polymerization. *Macromolecules* **2010,** *43* (13), 5611-5617.
32. Le, D.; Morandi, G.; Legoupy, S.; Pascual, S.; Montembault, V.; Fontaine, L., Cyclobutenyl macromonomers: Synthetic strategies and ring-opening metathesis polymerization. *European Polymer Journal* **2013,** *49* (5), 972-983.
33. Li, Z.; Ma, J.; Cheng, C.; Zhang, K.; Wooley, K. L., Synthesis of Hetero-Grafted Amphiphilic Diblock Molecular Brushes and Their Self-Assembly in Aqueous Medium. *Macromolecules* **2010,** *43* (3), 1182-1184.
34. Xie, M.; Dang, J.; Han, H.; Wang, W.; Liu, J.; He, X.; Zhang, Y., Well-Defined Brush Copolymers with High Grafting Density of Amphiphilic Side Chains by Combination of ROP, ROMP, and ATRP. *Macromolecules* **2008,** *41* (23), 9004-9010.
35. Durmaz, H.; Dag, A.; Erdogan, E.; Demirel, A. L.; Hizal, G.; Tunca, U., Multiarm star block and multiarm star mixed-block copolymers via azide-alkyne click reaction. *Journal of Polymer Science Part A: Polymer Chemistry* **2010,** *48* (1), 99-108.
36. Hadjichristidis, N.; Pitsikalis, M.; Pispas, S.; Iatrou, H., Polymers with Complex Architecture by Living Anionic Polymerization. *Chemical Reviews* **2001,** *101* (12), 3747-3792.
37. Heroguez, V.; Gnanou, Y.; Fontanille, M., Novel Amphiphilic Architectures by Ring-Opening Metathesis Polymerization of Macromonomers. *Macromolecules* **1997,** *30* (17), 4791-4798.

38. Logan, J. L.; Masse, P.; Dorvel, B.; Skolnik, A. M.; Sheiko, S. S.; Francis, R.; Taton, D.; Gnanou, Y.; Duran, R. S., AFM Study of Micelle Chaining in Surface Films of Polystyrene-block-Poly(ethylene oxide) Stars at the Air/Water Interface. *Langmuir* **2005,** *21* (8), 3424-3431.
39. Park, J.; Jang, S.; Kon Kim, J., Morphology and microphase separation of star copolymers. *Journal of Polymer Science Part B: Polymer Physics* **2015,** *53* (1), 1-21.
40. Peleshanko, S.; Gunawidjaja, R.; Jeong, J.; Shevchenko, V. V.; Tsukruk, V. V., Surface Behavior of Amphiphilic Heteroarm Star-Block Copolymers with Asymmetric Architecture. *Langmuir* **2004,** *20* (22), 9423-9427.
41. Peleshanko, S.; Jeong, J.; Gunawidjaja, R.; Tsukruk, V. V., Amphiphilic Heteroarm PEO-b-PSm Star Polymers at the Air−Water Interface: Aggregation and Surface Morphology. *Macromolecules* **2004,** *37* (17), 6511-6522.
42. Peleshanko, S.; Jeong, J.; Shevchenko, V. V.; Genson, K. L.; Pikus, Y.; Ornatska, M.; Petrash, S.; Tsukruk, V. V., Synthesis and Properties of Asymmetric Heteroarm PEOn-b-PSm Star Polymers with End Functionalities. *Macromolecules* **2004,** *37* (20), 7497-7506.
43. Gu, W.; Huh, J.; Hong, S. W.; Sveinbjornsson, B. R.; Park, C.; Grubbs, R. H.; Russell, T. P., Self-Assembly of Symmetric Brush Diblock Copolymers. *ACS Nano* **2013,** *7* (3), 2551-2558.
44. Runge, M. B.; Bowden, N. B., Synthesis of High Molecular Weight Comb Block Copolymers and Their Assembly into Ordered Morphologies in the Solid State. *Journal of the American Chemical Society* **2007,** *129* (34), 10551-10560.
45. Babin, J.; Taton, D.; Brinkmann, M.; Lecommandoux, S., Synthesis and Self-Assembly in Bulk of Linear and Mikto-Arm Star Block Copolymers Based on Polystyrene and Poly(glutamic acid). *Macromolecules* **2008,** *41* (4), 1384-1392.
46. Hardy, C. G.; Islam, M. S.; Gonzalez-Delozier, D.; Morgan, J. E.; Cash, B.; Benicewicz, B. C.; Ploehn, H. J.; Tang, C., Converting an Electrical Insulator into a Dielectric Capacitor: End-Capping Polystyrene with Oligoaniline. *Chemistry of Materials* **2013,** *25* (5), 799-807.
47. Ren, L.; Zhang, J.; Bai, X.; Hardy, C. G.; Shimizu, K. D.; Tang, C., Preparation of cationic cobaltocenium polymers and block copolymers by "living" ring-opening metathesis polymerization. *Chemical Science* **2012,** *3* (2), 580-583.
48. Sanford, M. S.; Love, J. A.; Grubbs, R. H., A Versatile Precursor for the Synthesis of New Ruthenium Olefin Metathesis Catalysts. *Organometallics* **2001,** *20* (25), 5314-5318.
49. Zhu, L.; Cheng, S. Z. D.; Calhoun, B. H.; Ge, Q.; Quirk, R. P.; Thomas, E. L.; Hsiao, B. S.; Yeh, F.; Lotz, B., Phase structures and morphologies determined by self-organization, vitrification, and crystallization: confined crystallization in an ordered lamellar phase of PEO-b-PS diblock copolymer. *Polymer* **2001,** *42* (13), 5829-5839.

CHAPTER 4

SYMMETRIC POLY(2-VINYLPYRIDINE-*B*–STYRENE-*B*-ISOPRENE) TRIBLOCK COPOLYMERS: SYNTHESIS, CHARACTERIZATION, AND SELF-ASSEMBLY IN BULK AND THIN FILMS

4.1 Abstract

The synthesis, characterization, and self-assembly of a series of linear poly(2-vinylpyridine-*b*-styrene-*b*-isoprene) (P2VP-PS-PI or ISP) triblock copolymers is reported. The triblock copolymer contained nearly equal volume fractions of end blocks P2VP and PI ($f_{P2VP} \approx f_{PI}$), but varied in composition in the middle block PS ($f_{PS} \approx 0.67$-0.80). A series of alkyne functionalized poly(2-vinylpyridine-*b*-styrene) diblock copolymers were prepared by reversible-addition fragmentation chain transfer polymerization (RAFT) with different molecular weight styrene fractions. Monohydroxy-terminated poly(*cis*-1,4-isoprene) was first azide functionalized and then attached with the alkyne terminated P2VP-PS block copolymer via a copper catalyzed azide alkyne cycloaddition reaction to produce the triblock copolymer P2VP-PS-PI. Bulk and thin film morphology was studied using small angle X-ray scattering (SAXS), atomic force microscopy (AFM), transmission electron microscopy (TEM), and grazing incidence small angle X-ray scattering (GISAXS). Even though analysis showed promising results with the formation of microdomains, more analysis needs to be carried out on these systems before a true understanding of the self-assembly process occurring in these systems is achieved. Furthermore, this series of triblock copolymers provide a good foundation for further research to be conducted for this project.

4.2 Introduction

Block copolymers (BCP) are an intriguing class of polymers due to their ability to microphase separate into a variety of morphologies depending on their molecular characteristics.[1-3] The thermodynamic immiscibility between the blocks drives the self-assembly within the polymeric material. These polymers can self-assemble into various

morphologies (sphere, cylinders, lamella, etc.) with tuned periodicity in the range of 10-100 nm.[2-5] The ability of these materials to produce ordered nanostructures with varying periodicity enables them to be considered for numerous applications such as: photonic crystals, microelectronic templates, separation membranes, etc.[6-11] The phase behavior of block copolymers is controlled through three experimental parameters; Flory-Huggins interaction parameter (χ), degree of polymerization (N, total molecular weight), and volume fraction of each block (f).[12-18] The morphologies are primarily determined through f, while χN determines feature size and periodicity. When χN is greater the than the order-disorder transition (ODT), diblock copolymers can assemble into body-center cubic spheres, hexagonally packed cylinders, double gyroid structures, and lamella depending on f.[1, 3-5, 19]

A-B diblock copolymers have one binary interaction parameter, one volume fraction, and a single block sequence and have been extensively studied over the past decades to understand the self-assembly process.[2-5] Even though A-B diblock copolymers yield interesting self-assembled features, it is important to research other novel block copolymers systems to yield other ordered morphologies.[2, 3] Specifically, linear A-B-C triblock copolymers are an intriguing class of polymers due to their numerous obtainable morphologies, such as tetragonal lattices of cylinders, bi and tri-continuous mesophases, and periodic arrays of core shell spheres and cylinders.[2, 20-47] Unlike A-B diblock copolymers, linear A-B-C triblock copolymers have three distinct interaction parameters, two independent volume fractions, and three different block sequences that enable great diversity in morphology.[2, 24, 31-33, 35, 44, 48-51]

Symmetric ABC triblock copolymers have been explored to produce superlattice structures with integrated A and C segments.[28] The structures include tetragonally packed cylinders, spheres, and three-phase, four-layer lamella.[32, 33] Specifically, great work on the symmetric ABC triblock copolymer was introduced by Mogi et al., where the triblock copolymer consisted of polyisoprene (PI), poly(2-vinylpyridine) (P2VP), and polystyrene (PS) (ISP).[32, 33] Numerical, self-consistent theory (SCFT) predicts symmetric ABC triblock copolymers can form cylindrical superlattice structures in bulk if Flory-Huggins interaction parameter (χ) satisfy $\chi_{AB} = \chi_{BC} <<< \chi_{AC}$.[31, 35, 39] This fundamental prediction was confirmed through early work from above mentioned Mogi and coworkers, which reported their block copolymer system produced alternating cylinders of PI and P2VP as square arrays after self-assembly.[32, 33] In 2008, Tang et al., observed square packing of core shell spheres from poly(ethylene oxide)-*b*-poly(methyl methacrylate)-*b*-polystyrene ABC triblock copolymers.[44] Furthermore, Ross, Manners and coworkers attempted to produce square arrays of cylinder using polyisoprene-*b*-polystyrene-*b*-polyferrocenylsilane in thin films, however their systems were a mixture of hexagonal and square backed cylinders.[26, 43] Recently, Tang and coworkers, observed hexagonal packing of spheres from poly(ethylene oxide)-*b*-polystyrene-*b*-polyisoprene, as the PEO domains were in a matrix of mixed PS/PI.[52] The contribution from Tang's previous work prompted this work to target square arrays using another triblock composition.

Herein, we designed, synthesized, and characterized a series of linear poly(2-vinylpyridine)-*b*-polystyrene-*b*-polyisoprene (P2VP-PS-PI or ISP) triblock copolymers containing nearly equal volumes of P2VP and PI ($f_{P2VP} \approx f_{PI}$), but varied in composition in

PS (f_{PS} ≈ 0.67-0.80) that are designed to fall in the spherical or cylindrical morphologies.[4, 32, 33] The triblock copolymer was synthesized through a combination of reversible-addition fragmentation chain transfer polymerization (RAFT) and copper (I)-catalyzed azide-alkyne cycloaddition reaction.[53-58] Studies were carried out on both bulk and thin films. Bulk studies were done after thermal annealing for 7 days and thin film studies was done after solvent annealing. Analysis was conducted using atomic force microscopy (AFM), small angle X-ray scattering (SAXS), TEM, and gazing incidence small angle scattering (GISAXS). Bulk samples characterized by SAXS, showed insight to phase separation, however, results were rather ambiguous. Furthermore, thin films exhibit order domains at the surface via AFM and TEM measurements. More studies need to be carried out before a definitive assumption can be made on the self-assembly of this system.

4.3 Experimental Section

4.3.1 Materials

4-Cyano-4-(phenylcarbonothioylthio) pentanoic acid (97%, CPPA) was purchased from Aldrich and used directly. Hydroxy terminated Polyisoprene (1, 4 addition) was purchased from Polymer Source and used as received. Sodium azide was purchased from Acros Organics. Tetrahydrofuran (THF) and *N*,*N*-dimethylformamide (DMF) were dried over molecular sieves and distilled before use. Styrene was passed through a basic alumina column before use. 2-vinyl pyridine was passed through a basic alumina column and distilled before use (2VP, Alfa Aesar). *N,N,N',N'',N''*-pentamethyldiethylenetriamine (PMDETA, Aldrich) and triethylamine (Et_3N, 99%,

Aldrich) were distilled before use. Cu(I)Br (99.999% Aldrich) and all other reagents and solvents were purchased from Sigma Aldrich or Alfa Aesar and used as received.

4.3.2 Characterization

Gel permeation chromatography (GPC) was performed at 50 °C on a Varian system equipped with a Varian 356-LC refractive index detector and a Prostar 210 pump. The columns were STYRAGEL HR1, HR2 (300 × 7.5 mm) from Agilent. HPLC grade DMF was used as eluent flow rate of 1.0 mL/min. Polystyrene standards were used for calibration. DMF and samples were filtered through micro-filters with a pore size of 0.2 μm (Teflon, 17 mm Syringes Filters, National Scientific, USA). FT-IR spectra were recorded on a PerkinElmer Spectrum 100 FT-IR spectrometer equipped with a Universal ATR sampling accessory. ^{1}H NMR (300 MHz) spectra was recorded on a Bruker 300 spectrometer with tetramethylsilane (TMS) as an internal reference. Transmission electron microscopy (TEM) was conducted using a Hitachi 8000 TEM was applied to take images at an operating voltage of 150 kV.

4.3.3 Atomic Force Microscopy

Atomic force microscopy (AFM) was performed using a Multimode Nanoscope V system (Bruker, Santa Barbara, CA). Tapping mode AFM was used to map the topography by tapping the surface using an oscillating tip. The measurements were performed using commercial Si cantilevers with a nominal spring constant and resonance frequency at 20–80 N m^{-1} and 230–410 kHz, respectively (TESP, Bruker AFM Probes, Santa Barbara, CA).

4.3.4 Small-Angle X-ray Scattering

Small-angle scattering (SAXS) experiments were conducted using SAXS LAB Ganesha at the South Carolina SAXS center of the University of South Carolina. A Xencos GeniX3D mircofocus source was used with a copper target to generate a monochromic beam with 0.154 nm wavelength. The instrument was calibrated using a silver behenate reference with the first ordering scattering vector $q^* = 1.076\ nm^{-1}$, where $q = 4\ \pi\lambda\text{-}1 \sin\theta$ with total scattering angle of $2\ \theta$. A 300 K Pilatus detector (Dectris) was used to collect the two dimensional (2D) SAXS patterns. Radial integration of 2D patterns reduced the data to 1D profile. Polymer bulk sample were fixed to a mount such that only the sample was measured at the exclusion of any mounting tape. All data were acquired for ~3 hours at room temperature with incident X-ray flux pf ~1.5 M photons per second.

4.3.5 Grazing Incidence Small-Angle X-ray Scattering

Grazing incidence small-angle X-ray scattering (GISAXS) experiments were conducted using SAXS LAB Ganesha at the South Carolina SAXS Collaborative, University of South Carolina. The station at GI is equipped with a high flux X-ray beam of ~1.5 M photons per s. A Xenocs Genix3D microfocus source was used with a copper target to generate a monochromatic beam with a 0.154 nm wave length. A 300K Pilatus detector (Dectris) was used to collect the 2D SAXS pattern. All images were taken at incident angle (α_i) that varied from 0.14 to 0.26°, which is both below and above critical angle (α_{cp}) of the polymer film.

4.3.6 Preparation of Bulk Films

P2VP-PS-PI triblock copolymers were obtained by casting a 4% (w/v) polymer solution in tetrahydrofuran and slowly evaporating the solvent over a period of 3 days. The resulting films were thermally annealed under vacuum for 7 days at 150 °C and characterized by small-angle X-ray scattering.

4.3.7 Preparation of Thin Films

The P2VP-PS-PI triblock copolymer (1.5 wt %) toluene solution was spun cast (3000 RPM, 60 s) onto native oxide silicon substrates. The thin films were annealed in a covered jar at room humidity with toluene as the solvent. All films were saturated with solvent vapor in a chamber before exposure to the room humidity. Film thicknesses were measured with a J.A. Woollam spectroscopic ellipsometer with an incident angle of 70°. All film thicknesses were in the range of 55 to 65 nm.

4.3.8 Synthesis

Modification of 4-Cyano-4-(phenylcarbonothioylthio) pentanoic acid RAFT agent (RAFT-Alkyne): 4-Cyano-4-(phenylcarbonothiolthio) pentanoic acid (CPPA) was modified to afford an acetylene functionalized RAFT agent.[59] The modification proceeded through a DCC coupling reaction. CPPA (0.5 g, 1.75×10^{-2} mol), propargyl alcohol (0.19 mL, 3.3×10^{-2} mol), 4-dimethylaminopyridine (DMAP, 0.041g, 3.36×10^{-4} mol), and DCM (25 mL) were introduced into a round bottom flask and purged with nitrogen for 30 minutes. The solution was then cooled to 0 °C, and a mixture of DCM (1 mL) and *N*, *N*′-Dicyclohexylcarbodiimide (DCC; 0.69 g, 3.3×10^{-2} mol) was added dropwise over 30 minutes. After the overnight reaction at room temperature, the reaction was concentrated, and column chromatography was used to separate the products. The

final product was then concentrated and dried. ^{1}H NMR (300 MHz, $CDCl_3$, δ (ppm): 7.20-7.70 (Ar*H*), 4.2 (d, 2H, -OC*H*$_2$CH-), 3.00 (s, -CC*H*-), 2.82 (t, -CC*H*$_2$CH$_2$CO-), 2.35 (t, -CCH$_2$C*H*$_2$CO-), 1.73 (s, -SCCNC*H*$_3$).

Modification of Hydroxy-terminated Polyisoprene (PI-Br): Hydroxy terminated polyisoprene (PI 1, 4 addition) (0.35g, 5.38×10^{-5} mol), DMAP (2 mg, 1.64×10^{-5} mol), and 1.5mL of THF were introduced into a round bottom flask. The solution was cooled to 0 °C, and Et_3N (74 µL, 5.25×10^{-4} mol) was added dropwise. The solution was allowed to stir for 30 minutes. 4-bromobutyryl chloride (61µL, 5.32×10^{-4} mol), was then added dropwise to the solution and allowed to stir overnight. After the reaction the reaction solution was concentrated to dryness, dissolved in DCM, and extracted with water three times. The organic layer was dried was dried over anhydrous sodium sulfate, filtered, and concentrated.[52] The solution was then precipitated into hexane two times to remove residual PI. The solid product was collected by filtration and vacuum dried overnight. ^{1}H NMR (300 MHz, $CDCl_3$, δ (ppm): 5.39 (t, $CH_3CC\mathit{H}CH_2$), 4.5 (t, -C*H*$_2$OCO-), 2.8 (t, -CH$_2$C*H*$_2$Br), 2.7 (m, -CH$_2$C*H*$_2$CH$_2$Br), 2.1 (t, -COC*H*$_2$CH$_2$-), 1.7 (s, -C*H*$_3$CCH-)

Azide Terminated Polyisoprene (PI-N_3): The terminal bromide group was converted to azide by reacting sodium azide (NaN_3) in DMF/THF overnight.[60, 61] PI-Br (0.22 g, 3.35×10^{-5} mol) was dissolved in DMF (2 mL) and THF (2 mL) in a 10 mL round bottom flask. The reaction mixture was purged with nitrogen for 30 minutes. Sodium azide (22 mg, 3.38×10^{-4} mol) was then added to the reaction mixture. The reaction was stirred at 40 °C overnight. The product was concentrated and diluted with THF and precipitated in methanol. The product was centrifuged and vacuum dried overnight. ^{1}H NMR (300 MHz,

$CDCl_3$, δ (ppm): 5.39 (t, -CH_3CCHCH_2-), 4.5 (t, -CH_2OCO-), 2.7 (m, -$CH_2CH_2CH_2Br$), 2.1 (t, -$COCH_2CH_2$-), 1.7 (s, CH_3CCH-) 1.4 (t, -$CH_2CH_2N_3$). FT-IR (cm^{-1}): 2100

Bromide-terminated Polystyrene via RAFT (PS-Alkyne): To a 10 mL Schlenk flask, styrene (5.51 mL), end functionalized 4-cyano-4-phenylcarbonothiolthio) pentanoic acid (RAFT-Alkyne) (11 mg), Azobisisobutyronitrile (AIBN) (0.6 mg), and anisole (0.1mL; internal standard) were added. After three freeze-pump-thaw cycles, the flask was placed into a preheated oil bath set at 90 °C.[62-64] After the desired percent conversion was reached the reaction was removed from the oil bath and diluted with THF, and placed in an ice bath. The polymer was precipitated in methanol, filtered, and vacuum dried overnight. M_n (NMR) = 44,100 g/mol, PDI (GPC) = 1.10. ^{1}H NMR (300 MHz, $CDCl_3$ δ (ppm): 7.20-7.70 (Ar*H* RAFT agent), 6.35-7.33 (br, Ar*H* PS), **1.0-2.4 (**br, -CH_2CH-).

Chain-Extension to Prepare P2VP-PS-Alkyne via RAFT: To a 10 mL Schlenk flask, PS-Alkyne (0.5 g), 2-vinylpyridine (0.57 mL, 2VP), AIBN (0.5 mL, of 0.5mg/mL in THF), and anisole (0.5 mL; internal standard) were added. After three freeze-pump-thaw cycles, the flask was placed into a preheated oil bath set at 60 °C.[62-64] After the overnight reaction the flask was opened and diluted with THF and placed in an ice bath. The polymer was precipitated in methanol, filtered, and vacuumed dried overnight. M_n (NMR) = 52,500 g/mol, PDI (GPC) = 1.15. ^{1}H NMR (300 MHz, $CDCl_3$ δ (ppm): 8.2-8.5 (br, -C*H*NC-), 6.35-7.33 (br, Ar*H*), 1.0-2.4 (br, -CH_2CH-).

Triblock P2VP-PS-PI via "Click" Reaction: To a 10 mL Schlenk flask Cu(I)Br (0.15 eq.) was added a purged with nitrogen. P2VP-PS-Alkyne (1 eq.), PI-N_3 (2 eq.) and PMDETA (0.1 eq.) were dissolved in 2 mL of THF and added to a 10 mL pearl shaped flask and purged with nitrogen for 30 minutes.[65] The reaction mixture in the pearl shaped

flask was transferred to the 10 mL Schlenk flask containing the Cu(I)Br. The Schlenk flask was added to a preheated oil bath at 50 °C. After the overnight reaction the flask was opened and diluted with THF and placed in an ice bath. The polymer was precipitated in hexane twice, centrifuged, and vacuum dried overnight. M_n (NMR) = 58,500 g/mol, PDI (GPC) = 1.18. ^{1}H NMR (300 MHz, $CDCl_3$ δ (ppm): 6.2-8.5 (br, PS and P2VP aromatic groups), 4.2-5.2 (br, PI vinyl groups), 2.2-1.7 (br, PS, P2VP, and PI alkyl groups).

4.4 Results and Discussion

The synthetic strategy of triblock copolymer P2VP-PS-PI was outlined in Scheme 4.1. Briefly an alkyne end-functionalized RAFT agent was used for polymerization of styrene to obtain the RAFT macroinitator (PS-Alkyne) at 90 °C.[62-64] The molecular weight of polystyrene was monitored by ^{1}H NMR, through monomer conversion by calculating the decrease of the vinyl peaks at 5.74 and 5.22 ppm to the aromatic peaks at 6.00 and 7.40 and the reaction was stopped at the desired percent conversion. The macroinitiator PS-Alkyne was used for chain extension of 2-vinylpyridine to give diblock copolymer P2VP-PS-Alkyne in preparation for the click reaction.[62-64] Again, the molecular weight of 2-vinylpyridine was monitored by ^{1}H NMR, through monomer conversion by calculating the decrease of vinyl peaks at 5.74 and 5.22 ppm, to the aromatic peaks at 6.00 and 7.40 ppm.

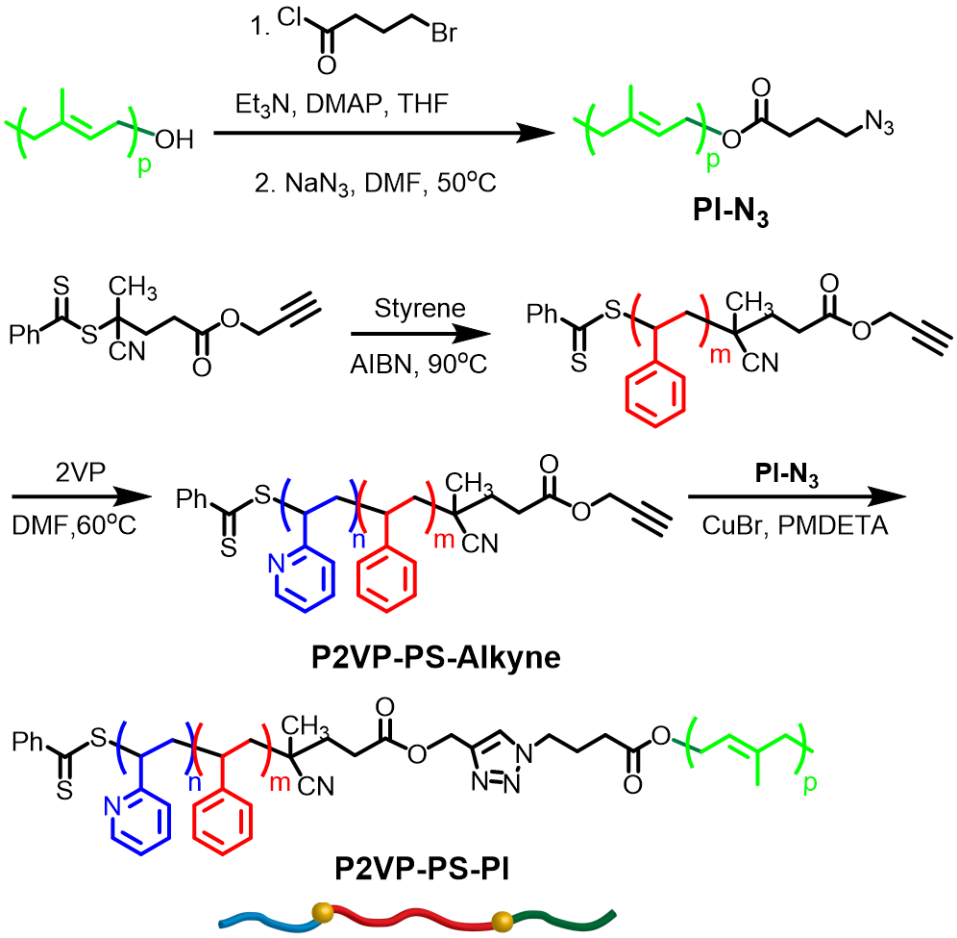

Scheme 4.1 General Synthesis Procedure for P2VP-PS-PI Triblock Copolymer

On the other hand, the monohydroxy polyisoprene (1, 4 addition), was prepared via living anionic polymerization (Polymer Source) was esterified with 4-bromobutyryl chloride (Figure 4.1) followed by reacting sodium azide to convert the bromine end group to azide for the click reaction.[52]

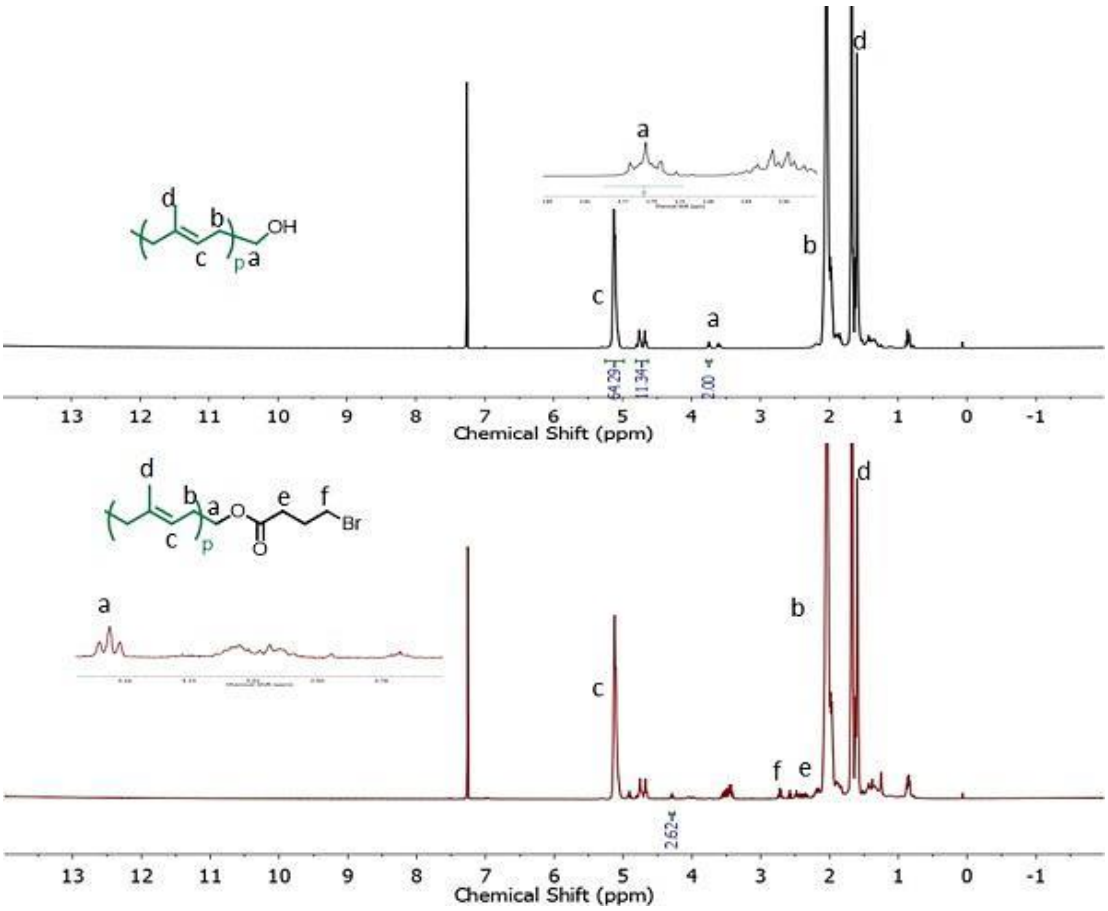

Figure 4.1 ^{1}H NMR spectrum of PI-OH and PI-Br

The use of the standard Huisgen cycloaddition conditions mediated by Cu(I)Br and PMDETA produced the triblock copolymer P2VP-PS-PI. (ISP).[52, 65] A series of triblock copolymers with nearly the same volume fractions of P2VP and PI ($f_{P2VP} \approx f_{PI}$) and various volume fractions of the middle PS block were prepared in order to investigate the influence of volume fractions of the triblock system in both bulk and thin films. GPC measurements confirmed no residual hompolymer was present as shown in Figure 4.2; monomodal GPC traces with an increase in molecular weight were obtained for each chain extension.

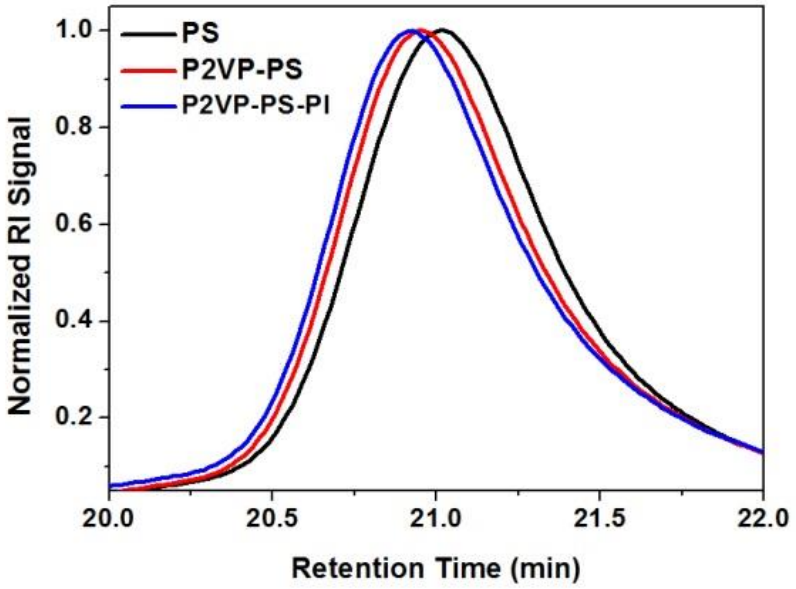

Figure 4.2 GPC traces following the synthesis of P2VP-PS-PI (ISP) in DMF

The relative degree of polymerization and molecular weight of each block was determined using ^{1}H NMR based on the molecular weight of the homopolymer PS-Alkyne in each series. The representative ^{1}H NMR spectrum for ISP is shown in Figure 4.3.

The relative integrals of PS and P2VP aromatic protons (7.43-6.1 ppm) and PI vinyl groups (5.27-4.45 ppm) provide the relative volume fractions of each block. The total molecular weight of P2VP-PS-PI was calculated based on ^{1}H NMR and also confirmed through GPC. The dispersity (Đ) was obtained from the GPC in DMF. Both triblock copolymers systems have a Đ ~ 1.15. The experimental data for each triblock series in described in Table 4.1.

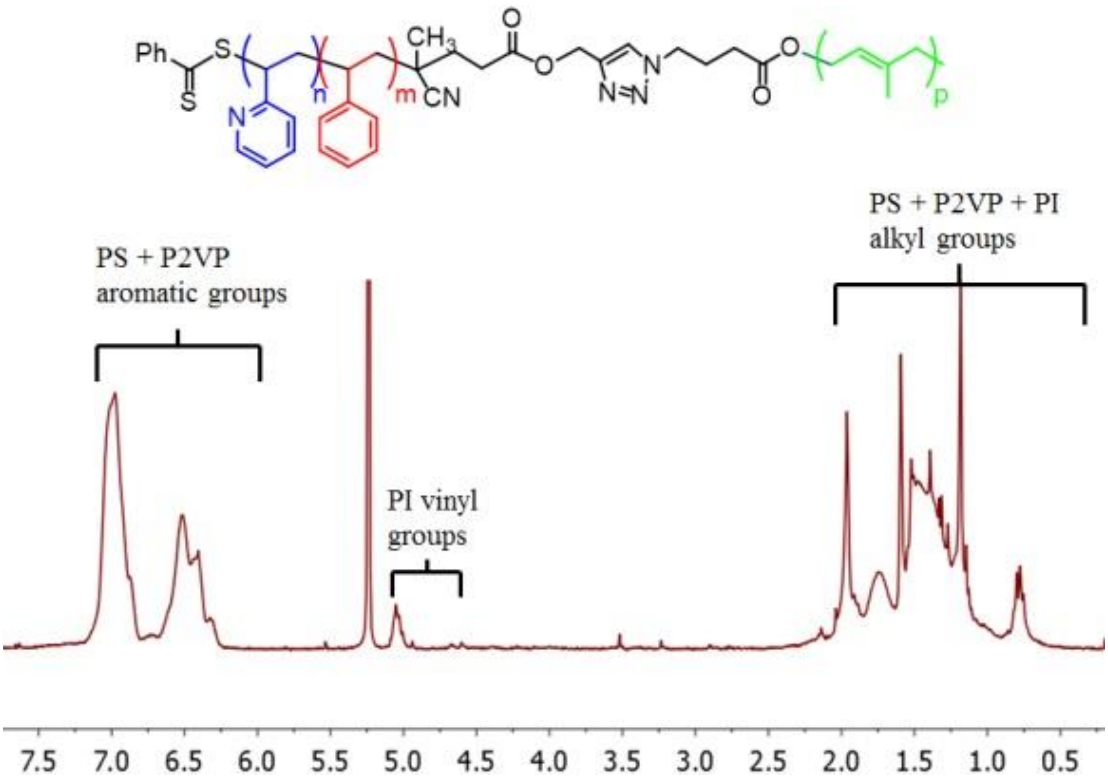

Figure 4.3 ^{1}H NMR spectrum of P2VP-PS-PI (ISP) triblock copolymer in CD_2Cl_2

The self-assembly of the triblock copolymers was studied in both bulk and thin films. The bulk material from both series were prepared by film casting from tetrahydrofuran (4 wt %) similar to earlier work.[32, 33] The morphology of the bulk material was characterized with the aid of small angle X-ray scattering (SAXS), after the film casts were completely dried and thermal annealed for 7 days at T = 150 °C under nitrogen**.** Figure 4.4 depicts the SAXS data for both series JH-4-96 (A) and JH-5-54 (B).

Table 4.1 Characteristics of P2VP-PS-PI (ISP) Triblock Copolymers

Sample	M_n (g/mol) (^{1}H NMR)	Đ (GPC)	P2VP M_n (g/mol, vol %)	PS M_n (g/mol, vol %)	PI M_n (g/mol, vol %)
(A) $P2VP_{76}$-PS_{423}-PI_{96} (JH-4-96)	58,500	1.15	8,000, 12.4	44,000, 74.9	6, 500, 12.6
(B) $P2VP_{80}$-PS_{480}-PI_{96} (JH-5-54)	64,700	1.15	8,500, 11.9	50,200, 76.7	6, 500, 11.4

The presence of distinctive scattering peaks in each of the systems suggest that phase separation is occurring, however, both systems only show a distinct q* peaks indicating no presences of periodic microdomain morphology. The q* values of each system are nearly identical at $q^* \approx 0.02$ nm^{-1}. The d-pacing of the material was 33-34 nm. Even though SAXS determined phase separation in the bulk state, we observed shallow to no higher order peaks which render the determination of the bulk morphology rather ambiguous.

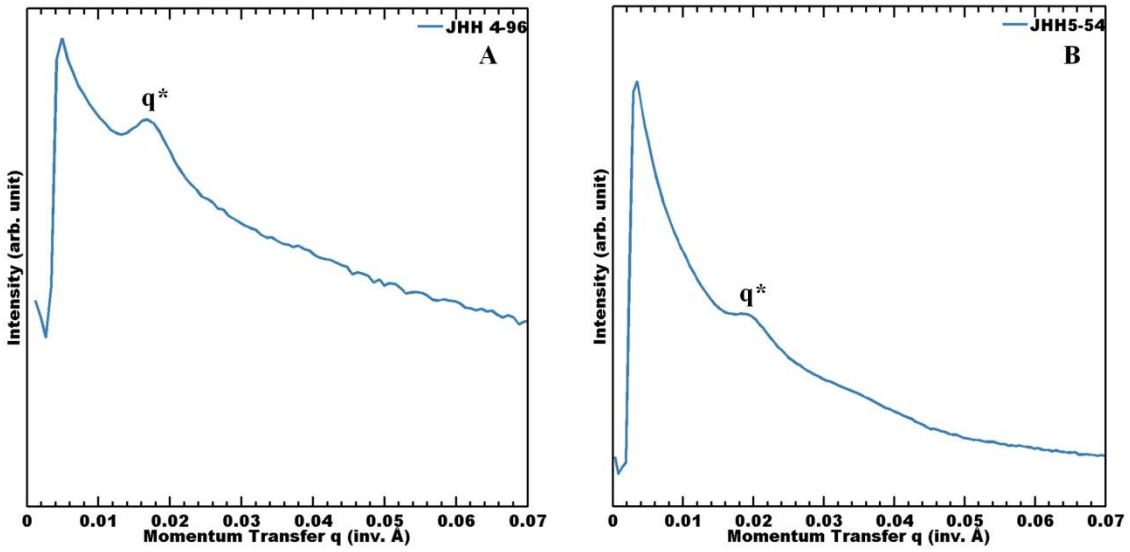

Figure 4.4 SAXS intensity profiles of P2VP-PS-PI (ISP). **(A**) JH-4-96; PS: 44,000 g/mol. (**B**) JH 5-54; PS: 50,000 g/mol after thermal annealing at t = 150 °C for 7 days under nitrogen.

Thus, we rationalize a conclusion the bulk material is dependent on the volume fractions of each block in both systems. Since each system has $f_{P2VP} \approx f_{PI}$ (both 11-12 %), and PS block ($f_{PS} \approx 0.67$-0.80), we can assume the morphology should be either spherical or cylindrical. To support this assumption, thin-film studies were conducted on both systems.

Thin films (1.5 wt %) of both systems were prepared by spin-casting the material onto native oxide silicon wafers (50-60 nm). The thin-films were annealed at room temperature overnight under low-humidity using toluene as the solvent. The ordering at the film-air interface was measure using AFM as can be seen in Figure 4.5.

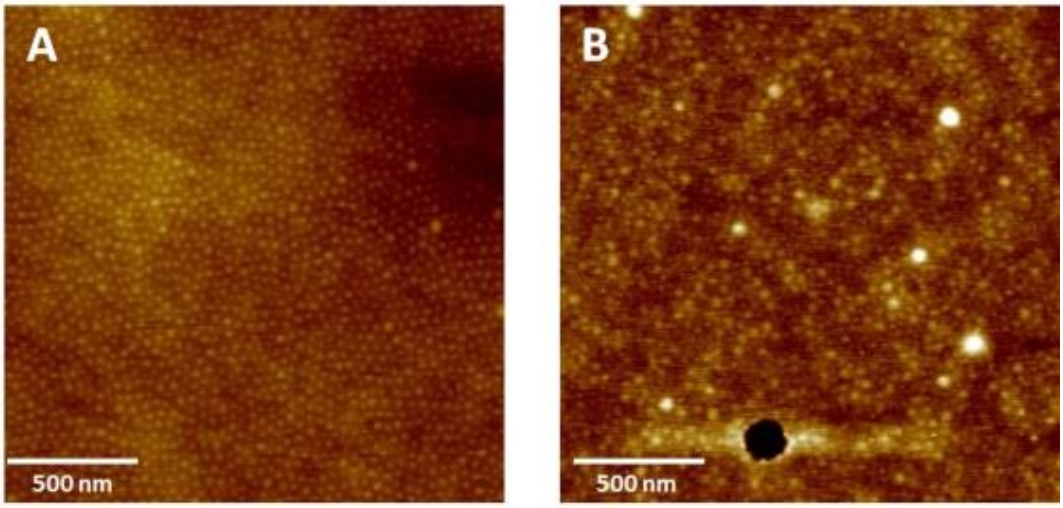

Figure 4.5 AFM height images of P2VP-PS-PI. (**A**) JH 4-96; PS: 44,000 g/mol; (**B**) JH 5-54; PS: 50,000 g/mol.

The AFM image of P2VP-PS-PI Figure 4.5 (**A**) clearly shows lateral ordering domains at the air interface. As seen in (**B**) only a minor degree of surface domains was apparent after annealing. Furthermore, the domain spacing and nearest-neighbor distance measured by AFM for Figure 4.5 (**A**) is around 25 nm and 37 nm, respectively. The spacing in AFM was somewhat larger than the values obtained by SAXS, but still relatively close. However, it was hard to distinguish and identify the different blocks (either P2VP or PI). It is important to note here that further characterization was done on sample (**A**) since lateral ordered surface domains were clearly present and superior to that of (**B**).

GISAXS measurements were performed to evaluate the ordering and morphology in Figure 4.5A, induced from low-humidity solvent annealing. Films were measured by varying the incident angle near the polymers critical angle ($\alpha_c \approx 0.16°$), which produces controlled penetration depths of a few nanometers up to full film thickness.[66] The

scattering profiles for the P2VP-PS-PI (ISP: 58,500 g/mol; Fig. 4.5A) show the appearance of higher order peaks (ratios of 1: √3: √4: √7) as shown in the 1D GISAXS data in Figure 4.6. The distance between the close packed rows is around 37 nm, which is nearly identical to the outcome of the solvent annealed sample of P2VP-PS-PI with PS molecular weight of 44,000 g/mol,. These higher ordering scattering peaks are consistent with hexagonal packed domains on the surface.

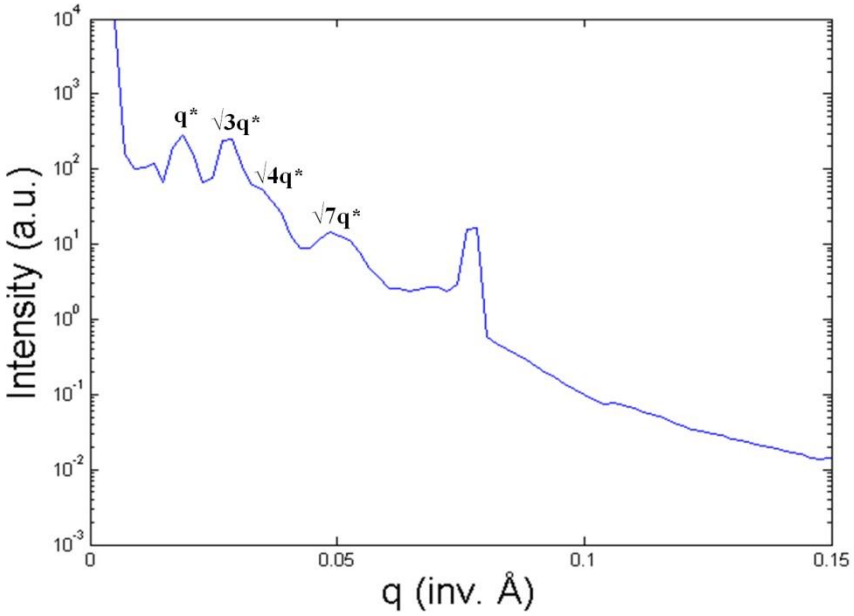

Figure 4.6 GISAXS measurement of P2VP-PS-PI (JH-4-96) by low humidity annealing.

To understand the domains block in P2VP-PS-PI (JH 4-96) transmission electron microscopy (TEM) was used. According to previous literature staining P2VP-PS-PI with OsO_4, the TEM micrographs of the film displayed black, white, and gray regions denoted by PI, PS, and P2VP, respectively.[32, 33] This process was done using annealed thin films of P2VP-PS-PI (JH 4-96). The thin films layer was removed from the silicon wafers by immersing it in a dilute solution of hydrofluoric acid. Once immersed, the thin film

would etch away from the silicon wafer. TEM grids were used to catch the thin films from the solution. Upon drying, the films were stained using OsO_4 for 18 hours in a vial. As shown in Figure 4.7, although very ambiguous, it seems the TEM image of P2VP-PS-PI shows varying regions of black and gray domains throughout the sample.

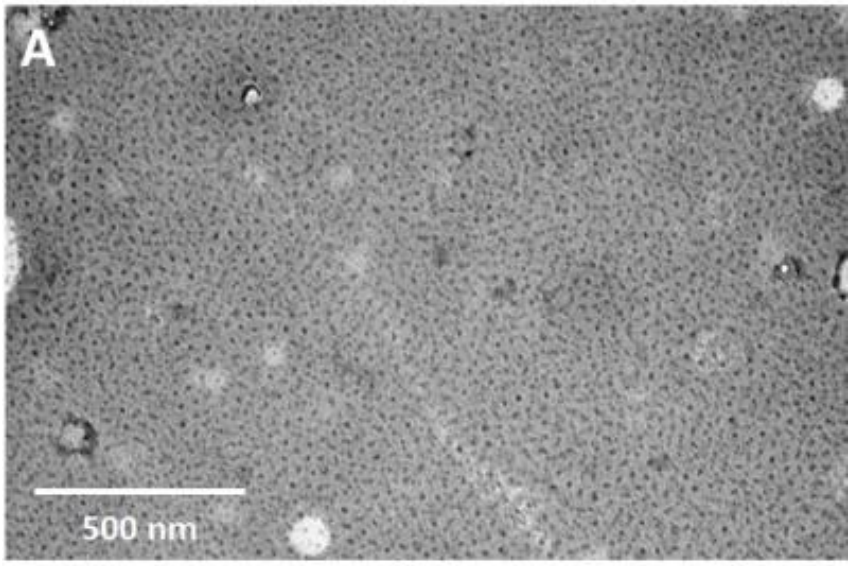

Figure 4.7 TEM image of P2VP-PS-PI (JH-4-96)

Even though the image is not conclusive in representing perfectly alternating domains, it does however provide an insight to a mixture of PI and P2VP domains as the black and gray regions correspond to both PI and P2VP domains, respectively. It is interesting to note here that the TEM image shows no degree of ordering in contrast to the AFM images shown before. This could attribute to the TEM film preparation as the dilute HF solution could have an effect or during when the film was picked up using the TEM grid some of the film could have folded back on itself. However this study helps demonstrate a potential mixture of domains is present via TEM. Further analysis needs to done to make an accurate assumption.

P2VP-PS-PI triblock copolymer systems were synthesized and characterized using a variety of techniques. Both bulk and thin film analysis were done to determine the morphology of the triblock copolymer. Alternating cylinders of P2VP and PI in a tetragonal lattice was the overall goal for this system; however, after characterizing by AFM, GISAXS, and TEM we observed potential alternating hexagonally packed domains of P2VP and PI. AFM measurements proved that hexagonally ordered domains were present at the air-interface; however, the measurements fail to distinguish the domain blocks. TEM was utilized to determine the domain composition, indicating that (although low contrast and lack of ordering) that the system potentially had alternating P2VP and PI block in a PS matrix. Finally, GISAXS was used to determine the scattering profiles of the thin film used in solvent annealing. The appearance of higher order scattering profiles further provide that hexagonal packed domains were at the air interface. Both AFM and GISXS data were consistent in d spacing between the close pack rows.

4.5 Conclusion

In conclusion, a series of P2VP-PS-PI triblock copolymers were successfully produced via RAFT polymerization and "click" chemistry. The lower molecular weight system of the triblock copolymer produced better phase seperation as opposed to their higher molecular weight counterparts. The problem for the higher molecular system could be caused by the $f_{P2VP} \approx f_{PI}$ being relatively low which could have caused these systems to be on the boundary of sphere and cylinders, however in depth χN value studies need to be carried out using Linkam via SAXS to fully understand the system . Further investigation on sample (**A**) using GISAXS provided insight that this system has

hexagonal packed domains at the air interface. TEM, even though somewhat ambiguous, shows there is a potential mixture of P2VP and PI domains in the thin films. More analysis needs to be done on these systems before a true understanding of the self-assembly process occurs in these systems. This series of triblock copolymers provides a good foundation for further research to be conducted for this project.

4.6 References

1. Bates, F. S.; Fredrickson, G. H., Block Copolymer Thermodynamics: Theory and Experiment. *Annual Review of Physical Chemistry* **1990,** *41*, 525-557.
2. Bates, F. S.; Fredrickson, G. H., Block Copolymers---Designer Soft Materials. *Physics Today* **1999,** *52* (2), 32-38.
3. Fredrickson, G. H.; Bates, F. S., Dynamics of Block Copolymers: Theory and Experiment. *Annual Review of Materials Research* **1996,** *26* (1), 501-550.
4. Helfand, E., Block Copolymer Theory .3. Statistical-Mechanics of Microdomain Structure. *Macromolecules* **1975,** *8* (4), 552-556.
5. Leibler, L., Theory of Microphase Separation in Block Copolymers. *Macromolecules* **1980,** *13*, 1602-1617.
6. Hadjichristidis, N.; Pispas, S.; Floudas, G., *Block Copolymers: Synthetic Strategies, Physical Properties, and Applications*. John Wiley & Sons, Inc.: Hoboken, NJ, 2003.
7. Hamley, I. W., *The Physics of Block Copolymers*. Oxford University Press: Oxford, U.K., 1998.
8. Hawker, C. J.; Russell, T. P., Block Copolymer Lithography: Merging "Bottom-Up" with "Top-Down" Processes. *MRS Bulletin* **2005,** *30* (12), 952-966.
9. Lazzari, M.; Liu, G.; Lecommandoux, S., *Block Copolymers in Nanoscience*. Wiley-VCH: Weinheim, 2007.
10. Park, C.; Yoon, J.; Thomas, E. L., Enabling Nanotechnology with Self Assembled Block Copolymer Patterns. *Polymer* **2003,** *44* (22), 6725-6760.
11. Ross, C., Patterned Magnetic Recording Media. *Annual Review of Materials Research* **2001,** *31*, 203-235.
12. Bates, C. M.; Maher, M. J.; Janes, D. W.; Ellison, C. J.; Willson, C. G., Block Copolymer Lithography. *Macromolecules* **2013,** *47* (1), 2-12.
13. Hajduk, D. A.; Harper, P. E.; Gruner, S. M.; Honeker, C. C.; Kim, G.; Thomas, E. L.; Fetters, L. J., The Gyroid: a New Equlibrium. *Macromolecules* **1994,** *27*, 4063-4075.
14. Helfand, E.; Wasserman, Z. R., Block Copolymer Theory .5. Spherical Domains. *Macromolecules* **1978,** *11* (5), 960-966.
15. Helfand, E.; Wasserman, Z. R., Block Co-Polymer Theory .6. Cylindrical Domains. *Macromolecules* **1980,** *13* (4), 994-998.
16. Luo, M.; Epps, T. H., Directed Block Copolymer Thin Film Self-Assembly: Emerging Trends in Nanopattern Fabrication. *Macromolecules* **2013,** *46* (19), 7567-7579.

17. Matsushita, Y.; Mori, K.; Saguchi, R.; Nakao, Y.; Noda, I.; Nagasawa, M., Molecular-Weight Dependence of Lamellar Domain Spacing of Diblock Copolymers in Bulk. *Macromolecules* **1990,** *23* (19), 4313-4316.
18. Seo, M.; Hillmyer, M. A., Reticulated Nanoporous Polymers by Controlled Polymerization-Induced Microphase Separation. *Science* **2012,** *336* (6087), 1422-1425.
19. Tang, C.; Wu, W.; Smilgies, D.-M.; Matyjaszewski, K.; Kowalewski, T., Robust Control of Microdomain Orientation in Thin Films of Block Copolymers by Zone Casting. *Journal of the American Chemical Society* **2011,** *133* (30), 11802-11809.
20. Albalak, R. J.; Thomas, E. L., Roll-Casting of block copolymers and of block copolymer-homopolymer blends. *Journal of Polymer Science Part B: Polymer Physics* **1994,** *32* (2), 341-350.
21. Angelescu, D. E.; Waller, J. H.; Adamson, D. H.; Deshpande, P.; Chou, S. Y.; Register, R. A.; Chaikin, P. M., Macroscopic Orientation of Block Copolymer Cylinders in Single-Layer Films by Shearing. *Advanced Materials* **2004,** *16* (19), 1736-1740.
22. Bita, I.; Yang, J. K. W.; Jung, Y. S.; Ross, C. A.; Thomas, E. L.; Berggren, K. K., Graphoepitaxy of Self-Assembled Block Copolymers on Two-Dimensional Periodic Patterned Templates. *Science* **2008,** *321* (5891), 939-943.
23. Chen, H.-L.; Lu, J.-S.; Yu, C.-H.; Yeh, C.-L.; Jeng, U. S.; Chen, W.-C., Tetragonally Packed Cylinder Structure via Hierarchical Assembly of Comb−Coil Diblock Copolymer. *Macromolecules* **2007,** *40* (9), 3271-3276.
24. Chen, H.-Y.; Fredrickson, G. H., Morphologies of ABC triblock copolymer thin films. *Journal of Chemical Physics* **2002,** *116*, 1137-1146.
25. Cheng, J. Y.; Ross, C. A.; Smith, H. I.; Thomas, E. L., Templated Self-Assembly of Block Copolymers: Top-Down Helps Bottom-Up. *Advanced Materials* **2006,** *18* (19), 2505-2521.
26. Chuang, V. P.; Gwyther, J.; Mickiewicz, R. A.; Manners, I.; Ross, C. A., Templated Self-Assembly of Square Symmetry Arrays from an ABC Triblock Terpolymer. *Nano Letters* **2009,** *9* (12), 4364-4369.
27. De Rosa, C.; Park, C.; Thomas, E. L.; Lotz, B., Microdomain patterns from directional eutectic solidification and epitaxy. *Nature* **2000,** *405* (6785), 433-437.
28. Hardy, C. G.; Tang, C., Advances in square arrays through self-assembly and directed self-assembly of block copolymers. *Journal of Polymer Science Part B: Polymer Physics* **2013,** *51* (1), 2-15.
29. Hur, S.-M.; García-Cervera, C. J.; Kramer, E. J.; Fredrickson, G. H., SCFT Simulations of Thin Film Blends of Block Copolymer and Homopolymer Laterally Confined in a Square Well. *Macromolecules* **2009,** *42* (15), 5861-5872.
30. Mansky, P.; Liu, Y.; Huang, E.; Russell, T. P.; Hawker, C., Controlling Polymer-Surface Interactions with Random Copolymer Brushes. *Science* **1997,** *275* (5305), 1458-1460.
31. Matsen, M. W., Gyroid versus double-diamond in ABC triblock copolymer melts. *The Journal of Chemical Physics* **1998,** *108* (2), 785-796.
32. Mogi, Y.; Kotsuji, H.; Kaneko, Y.; Mori, K.; Matsushita, Y.; Noda, I., Preparation and Morphology of Triblock Copolymers of the ABC Type. *Macromolecules* **1992,** *25*, 5408-5411.

33. Mogi, Y.; Nomura, M.; Kotsuji, H.; Ohnishi, K.; Matsushita, Y.; Noda, I., Superlattice Structures in Morphologies of the ABC Triblock Copolymers. *Macromolecules* **1994,** *27*, 6755-6760.
34. Morkved, T. L.; Lu, M.; Urbas, A. M.; Ehrichs, E. E.; Jaeger, H. M.; Mansky, P.; Russell, T. P., Local Control of Microdomain Orientation in Diblock Copolymer Thin Films with Electric Fields. *Science* **1996,** *273* (5277), 931-933.
35. Nakazawa, H.; Ohta, T., Microphase Separation of ABC-Type Triblock Copolymers. *Macromolecules* **1993,** *26*, 5503-5511.
36. Park, M.; Harrison, C.; Chaikin, P. M.; Register, R. A.; Adamson, D. H., Block Copolymer Lithography: Periodic Arrays of ~1011 Holes in 1 Square Centimeter. *Science* **1997,** *276* (5317), 1401-1404.
37. Park, S.; Lee, D. H.; Xu, J.; Kim, B.; Hong, S. W.; Jeong, U.; Xu, T.; Russell, T. P., Macroscopic 10-Terabit–per–Square-Inch Arrays from Block Copolymers with Lateral Order. *Science* **2009,** *323* (5917), 1030-1033.
38. Park, S.-M.; Craig, G. S. W.; La, Y.-H.; Solak, H. H.; Nealey, P. F., Square Arrays of Vertical Cylinders of PS-b-PMMA on Chemically Nanopatterned Surfaces. *Macromolecules* **2007,** *40* (14), 5084-5094.
39. Phan, S.; Fredrickson, G. H., Morphology of Symmetric ABC Triblock Copolymers in the Strong Segregation Limit. *Macromolecules* **1998,** *31* (1), 59-63.
40. Ruiz, R.; Kang, H.; Detcheverry, F. A.; Dobisz, E.; Kercher, D. S.; Albrecher, T. R.; de Pable, J. J.; Nealey, P. F., Density Multiplication and Improved Lithography by Directed Block Copolymer Assembly. *Science* **2008,** *321*, 936-939.
41. Ryu, D. Y.; Shin, K.; Drockenmuller, E.; Hawker, C. J.; Russell, T. P., A Generalized Approach to the Modification of Solid Surfaces. *Science* **2005,** *308* (5719), 236-239.
42. Segalman, R. A.; Yokoyama, H.; Kramer, E. J., Graphoepitaxy of Spherical Domain Block Copolymer Films. *Advanced Materials* **2001,** *13* (15), 1152-1155.
43. Son, J. G.; Gwyther, J.; Chang, J.-B.; Berggren, K. K.; Manners, I.; Ross, C. A., Highly Ordered Square Arrays from a Templated ABC Triblock Terpolymer. *Nano Letters* **2011,** *11* (7), 2849-2855.
44. Tang, C.; Bang, J.; Stein, G. E.; Fredrickson, G. H.; Hawker, C. J.; Kramer, E. J.; Sprung, M.; Wang, J., Square Packing and Structural Arrangement of ABC Triblock Copolymer Spheres in Thin Films. *Macromolecules* **2008,** *41*, 4328-4339.
45. Tang, C.; Hur, S.-m.; Stahl, B. C.; Sivanandan, K.; Dimitriou, M.; Pressly, E.; Fredrickson, G. H.; Kramer, E. J.; Hawker, C. J., Thin Film Morphology of Block Copolymer Blends with Tunable Supramolecular Interactions for Lithographic Applications. *Macromolecules* **2010,** *43* (6), 2880-2889.
46. Tang, C.; Lennon, E. M.; Fredrickson, G. H.; Kramer, E. J.; Hawker, C. J., Evolution of Block Copolymer Lithography to Highly Ordered Square Arrays. *Science* **2008,** *322* (5900), 429-432.
47. Tang, C.; Sivanandan, K.; Stahl, B. C.; Fredrickson, G. H.; Kramer, E. J.; Hawker, C. J., Multiple Nanoscale Templates by Orthogonal Degradation of a Supramolecular Block Copolymer Lithographic System. *ACS Nano* **2009,** *4* (1), 285-291.
48. Bailey, T. S.; Pham, H. D.; Bates, F. S., Morphological Behavior Bridging the Symmetric AB and ABC States in the Poly(styrene-b-isoprene-b-ethylene oxide) Triblock Copolymer System. *Macromolecules* **2001,** *34*, 6994-7008.

49. Bang, J.; Kim, S. H.; Drockenmuller, E.; Misner, M. J.; Russell, T. P.; Hawker, C. J., Defect-Free Nanoporous Thin Films from ABC Triblock Copolymers. *Journal of the American Chemical Society* **2006,** *128* (23), 7622-7629.
50. Rzayev, J.; Hillmyer, M. A., Nanochannel Array Plastics with Tailored Surface Chemistry. *Journal of the American Chemical Society* **2005,** *127*, 13373-13379.
51. Rzayev, J.; Hillmyer, M. A., Nanoporous Polystyrene Containing Hydrophilic Pores from an ABC Triblock Copolymer Precursor. *Macromolecules* **2005,** *38* (1), 3-5.
52. Qiao, Y.; Ferebee, R.; Lee, B.; Mitra, I.; Lynd, N. A.; Hayat, J.; Stein, G. E.; Bockstaller, M. R.; Tang, C., Symmetric Poly(ethylene oxide-b-styrene-b-isoprene) Triblock Copolymers: Synthesis, Characterization, and Self-Assembly in Bulk and Thin Film. *Macromolecules* **2014,** *47* (18), 6373-6381.
53. Barner-Kowollik, C., *Handbook of RAFT Polymerization*. Wiley: 2008.
54. Chiefari, J.; Chong, Y. K.; Ercole, F.; Krstina, J.; Jeffery, J.; Le, T. P. T.; Mayadunne, R. T. A.; Meijs, G. F.; Moad, C. L.; Moad, G.; Rizzardo, E.; Thang, S. H., Living Free-Radical Polymerization by Reversible Addition−Fragmentation Chain Transfer: The RAFT Process. *Macromolecules* **1998,** *31* (16), 5559-5562.
55. Chiefari, J.; Mayadunne, R. T. A.; Moad, C. L.; Moad, G.; Rizzardo, E.; Postma, A.; Thang, S. H., Thiocarbonylthio Compounds (SC(Z)S−R) in Free Radical Polymerization with Reversible Addition-Fragmentation Chain Transfer (RAFT Polymerization). Effect of the Activating Group Z. *Macromolecules* **2003,** *36* (7), 2273-2283.
56. Hein, J. E.; Fokin, V. V., Copper-catalyzed azide-alkyne cycloaddition (CuAAC) and beyond: new reactivity of copper(i) acetylides. *Chemical Society Reviews* **2010,** *39* (4), 1302-1315.
57. Rostovtsev, V. V.; Green, L. G.; Fokin, V. V.; Sharpless, K. B., A Stepwise Huisgen Cycloaddition Process: Copper(I)-Catalyzed Regioselective "Ligation" of Azides and Terminal Alkynes. *Angewandte Chemie International Edition* **2002,** *41* (14), 2596-2599.
58. Sumerlin, B. S.; Vogt, A. P., Macromolecular Engineering through Click Chemistry and Other Efficient Transformations. *Macromolecules* **2010,** *43* (1), 1-13.
59. Ranjan, R.; Brittain, W. J., Combination of Living Radical Polymerization and Click Chemistry for Surface Modification. *Macromolecules* **2007,** *40* (17), 6217-6223.
60. Hardy, C. G.; Ren, L.; Ma, S.; Tang, C., Self-assembly of well-defined ferrocene triblock copolymers and their template synthesis of ordered iron oxide nanoparticles. *Chemical Communications* **2013,** *49* (39), 4373-4375.
61. Kang, M.; Moon, B., Synthesis of Photocleavable Poly(styrene-block-ethylene oxide) and Its Self-Assembly into Nanoporous Thin Films. *Macromolecules* **2008,** *42* (1), 455-458.
62. Convertine, A. J.; Sumerlin, B. S.; Thomas, D. B.; Lowe, A. B.; McCormick, C. L., Synthesis of Block Copolymers of 2- and 4-Vinylpyridine by RAFT Polymerization. *Macromolecules* **2003,** *36* (13), 4679-4681.
63. Jang, S. G.; Khan, A.; Hawker, C. J.; Kramer, E. J., Morphology Evolution of PS-b-P2VP Diblock Copolymers via Supramolecular Assembly of Hydroxylated Gold Nanoparticles. *Macromolecules* **2012,** *45* (3), 1553-1561.
64. Zhang, K.; Gao, L.; Chen, Y., Organic/inorganic nanoobjects with controlled shapes from gelable triblock copolymers. *Polymer* **2010,** *51* (13), 2809-2817.

65. Hardy, C. G. Functional Block Copolymers for Applications in Advanced Materials, Energy Storage, and Lithography. University of South Carolina, Columbia, SC, 2013.
66. Stein, G. E.; Kramer, E. J.; Li, X.; Wang, J., Layering Transitions in Thin Films of Spherical-Domain Block Copolymers. *Macromolecules* **2007,** *40* (7), 2453-2460.

CHAPTER 5

GRAFTED BLOCK COPOLYMER PNB-*G*-(PS-*B*-PMMA)

5.1 Abstract

This chapter addresses the synthesis, characterization, and preliminary thin film studies of grafted block copolymer polystyrene-*block*-poly(methyl methacrylate) (PNb-*g*-(PS-*b*-PMMA)). Polystyrene-*block*-poly(methyl methacrylate) (PS-*b*-PMMA) diblock copolymers served as the side chains on a norbornene based backbone of the grafted block copolymer. The grafted block copolymer was synthesized through a combination of atom transfer radical polymerization (ATRP), reversible-addition fragmentation chain transfer polymerization (RAFT), ring-opening metathesis polymerization (ROMP) and copper(I)-catalyzed azide-alkyne cycloaddition reactions. The polymers were synthesized with low dispersity, however self-assembly studies under thermal annealing showed minimal phase separation. This study, illustrates a general strategy to prepare a novel class of grafted PNb-g-(PS-*b*-PMMA) block copolymers, however further characterization needs to be carried out.

5.2 Introduction

Block copolymers (BCP) are a class of materials that are widely studied due to their unique capabilities to self-assemble into ordered morphologies with precisely controlled size and pitch.[1-7] Block copolymers have gained tremendous interest for the use in many technical applications such as photonic crystals, separation membranes, and microelectronics patterning.[4, 8-12] Specifically, microelectronics require small features to be used as templates in current devices which is a problem that current photolithography is trying to overcome. The ability of block copolymers to self- assemble into sub-20 nm scale features provides an advantage over current photolithography techniques employed

today. These advances are feasible due to great insight in BCP synthesis and polymer engineering over the past decades.[7, 13-31]

The phase behavior of block copolymers are controlled through three experimental pararmeters:[13, 32-36] Flory-Huggins interaction parameter (χ), degree of polymerization (similar to molecular weight) (N), and volume fractions of the block (f).[32] When χN is sufficiently high, diblock copolymer will self-assemble in body-centered cubic spheres, hexagonal packed cylinders, or lamella depending on their volume fractions (f).[29, 32, 34, 37-39] Most applications incorporating block copolymers require controlled order, which depends on interfacial energetics between the polymer and substrate. External structure directing potentials are a popular way to control parallel or perpendicular ordering. Examples include chemoepitaxy (chemical pattern substrates), graphoepitaxy (topographically pattern substrates), or surface treatment.[40-52]

One of the most prevalent block copolymers studied is poly(styrene-*block*-methyl methacrylate), due to the simple synthetic route, attractive etch selectivity, and ability to form perpendicular domains when the surface chemistry is controlled.[23, 30, 31] Furthermore, surface chemistry in respect to controlling the interfacial energetics has been well documented in literature, especially for PS-*b*-PMMA by using random brush copolymers.[40-47, 50, 53, 54] It has been shown that, neutral surfaces (surface displaying equal interaction) energies with both blocks, will enable perpendicular cylinders,[40-42, 44, 47, 53] while non-neutral surfaces will promote horizontal.[43, 45, 46, 53] Most commonly, hydroxy-terminated random brush polymers (HO-PS-*r*-PMMA) can be used to align PS-*b*-PMMA.[41, 43, 53]

The only drawback of PS-*b*-PMMA is the low Flory-Huggins interaction parameter; $\chi_{PS\text{-}PMMA}$ ~0.06 at room temperature, which limits the size of the microdomain that can be formed.[55] This limitation is overcome using block copolymers with higher χ values, like PS-*b*-PDMS,[56, 57] and PEO-*b*-PS[58]. However, expanding research with PS-*b*-PMMA diblock copolymer within other polymeric architectures (grafted) may present an interesting insight to overcome its low χ hinderance.

Grafted block copolymers (or brush copolymers) are interesting architectures of block copolymers as they have the ability to form nanostructures that are not capable by simple linear diblock copolymers.[59-66] The large cross-sectional area and dense side chains inherent with grafting from ultimately high molecular weight polymers, limit intermolecular chain entanglement, and thus, form wormlike structures.[67] Additionally, spherical, cylindrical, and lamellae structures have been prepared with domain size > 100 nm for various applications.[68-70] These grafted block copolymer systems have long backbones between 1000 – 2000 repeat units, with relatively low molecular side-chains between 3,000 – 10,000 g/mol.

In this work, we prepared grafted block copolymers in which the side-chains consist of low molecular weight PS-*b*-PMMA linear diblock copolymers. These polymers were prepared via ATRP, RAFT, ROMP, and "click" chemistry. Additionally, anchoring a random copolymer OH-PS-*r*-PMMA was done to promote perepndicular ordering.[41, 43, 53]

5.3 Experimental Section

5.3.1 Materials

All reagents were purchased from Alfa Aesar and Aldrich was used as received unless otherwise noted. Styrene and methyl methacrylate was passed through a basic alumina column before use. Tetrahydrofuran (THF) and dimethylformamide (DMF) were dried over molecular sieves and distilled before use. *N,N,N',N'',N''*-pentamethyldiethylenetriamine (PMDETA, Aldrich) and triethylamine (Et_3N, 99%, Aldrich) were distilled before use. Grubbs 3rd generation catalyst (G3), N-[3-Hydroxylpropyl]-*cis*-5-Norbornene-*exo*-2,3-Dicarboximide (NPH) were prepared according to previous reports.[71-73] 4-Cyano-4-(phenylcarbonothioylthio) pentanoic acid (97%, CPPA) was purchased from Aldrich and used directly. Random copolymer composed of styrene (S) and methyl methacrylate (MMA), denoted as P(S-*r*-MMA) was purchased from Polymer Source with PS mol % = ~67% was used as received.

5.3.2 Characterization

^{1}H NMR spectra were recorded on Brucker ARX300 and ARX400 spectrometers with tetramethylsilane (TMS) as an internal reference. Gel permeation chromatography (GPC) was performed at room temperature on a Varian system equipped with a Varian 356-LC refractive index detector and a Prostar 210 pump. The columns were STYRAGEL HR1, HR2 (300×7.5 mm) from Varian. HPLC grade THF was used as eluent at a flow rate of 1 mL/min. Samples were filtered over a microfilter with pore size of 0.2 μm (Nylon, Millex-HN 13 mm Syringes Filters, Millipore, USA). GPC was calibrated using polystyrene as standards. FTIR spectra were recorded on a PerkinElmer

Spectrum 100 FTIR spectrometer equipped with a universal ATR sampling accessory. Thermal transitions were recorded using differential scanning calorimetry (DSC) on a TA Q200 calorimeter in a temperature range from 0 to 200 °C at a heating rate of 10 °C min^{-1} under continuous nitrogen flow. All the data was collected during the second heating process after cooling at 10 °C min^{-1} from 200 °C. The average sample mass was about 5 mg, and the nitrogen flow rate was 50 mL min^{-1}. Atomic force microscopy (AFM) was performed using a Multimode Nanoscope V system (Bruker, Santa Barbara, CA). Tapping mode AFM was used to map the topography by tapping the surface using an oscillating tip. The measurements were performed using commercial Si cantilevers with a nominal spring constant and resonance frequency at 20–80 N m^{-1} and 230–410 kHz, respectively (TESP, Bruker AFM Probes, Santa Barbara, CA).

5.3.3 Synthesis

Norbornene-terminated ATRP initiator (N-[3-propyl-2-bromo-2-methylproponate]-*cis*-5-Norbornene-*exo*-2,3-Dicarboximide, NP-Br: NPH (**1**, 0.31 g, 1.4×10^{-3} mol) was added to a 100 mL round bottom flask equipped with a stir bar and purged with nitrogen. Dry tetrahydrofuran (25 mL) was added and the reaction was cooled to 0 °C before triethylamine (0.39 mL, 2.8×10^{-3} mol) was added. A solution of 2-bromoisobutyryl bromide (0.26 mL, 2.1×10^{-3} mol) in dry tetrahydrofuran (15 mL) was added drop wise to the cooled solution. The solution was stirred at 0 °C for 30 minutes, then at room temperature overnight. The mixture was filtered and concentrated to dryness. The solids were then dissolved in either DCM or water. The DCM was extracted with deionized H_2O twice. The aqueous layers were combined and extracted with DCM three times. The organic layers were combined, dried over anhydrous sodium sulfate, filtered,

concentrated, and the products were separated using column chromatography (silica gel, eluent: DCM). The product was collected, concentrated, and vacuum dried**.** ^{1}H NMR (CD_2Cl_2), δ (TMS, ppm): 6.30 (s, 2H, C*H*=C*H*), 4.15 (t, 2H, $CH_2CH_2OC(O)$), 3.59 (t, 2H, NCH_2CH_2), 3.33 (s, 2H, C*H*C(O)N), 2.69 (s, 2H, CH_2CH), 1.88-2.08 (m, 8s, $CH_2CH_2CH_2$ + $(CH_3)_2C(O)$), 1.51 and 1.23 (d, 2H, CH_2CH)**.** FTIR (cm^{-1}): 2980, 1760, 1690, 1465, 1440, 1390, 1340, 1110, 1170, 890, 720.

Bromine-terminated NP-polystyrene (NP-PS-Br): Copper (I) bromide (1 eq.) was charged into a 10 mL schlenk line flask and purged with nitrogen. NP-Br (1 eq.), styrene (*n* eq.), and N,N,N',N'',N''-pentamethyldiethylenetriamine (PMDETA, 1.5 eq.) were added to a 5 mL pearl shaped flask, degassed by bubbling nitrogen through the solution for 20 minutes, and transferred to the schlenk line flask. The schlenk line flask was then added to an oil bath preheated to 90 ^{o}C. The polymerization was monitored by proton NMR and the reaction was stopped at the desired monomer conversion by cooling in an ice bath and then diluting the solution with THF. The solution was then precipitated into methanol twice. The solid white product was collected by filtration and vacuum dried**.** ^{1}H NMR (CD_2Cl_2), δ (TMS, ppm): 6.35-7.33 (br, Ar*H*), 6.30 (s, 2H, C*H*=C*H*), 3.59 (t, 2H, NCH_2CH_2), 3.33 (s, 2H, C*H*C(O)N), 2.69 (s, 2H, CH_2CH), 1.0-2.4 **(**br, -CH_2CH-).

Azide-terminated NP-polystyrene (NP-PS-N_3): The terminal bromine groups were converted to azide groups through reaction with NaN_3 in DMF as previously reported.[71] ^{1}H NMR (CD_2Cl_2), δ (TMS, ppm): 6.35-7.33 (br, Ar*H*), 6.30 (s, 2H, C*H*=C*H*), 3.59 (t, 2H, NCH_2CH_2), 3.33 (s, 2H, C*H*C(O)N), 2.69 (s, 2H, CH_2CH), 1.0-2.4 **(**br, -CH_2CH-). FTIR (cm^{-1}): 3090, 3050, 3020, 2960, 2840, 2100, 1700, 1590, 1490, 1460.

Alkyne-terminated 4-Cyano-4-(phenylcarbonothioylthio) pentanoic acid: 4-cyano-4-(phenylcarbonothiolthio) pentanoic acid (CPPA) was modified to afford an alkyne functionalized RAFT agent. The modification proceeded through a DCC coupling reaction. CPPA (0.5 g, 1.75×10^{-2} mol), propargyl alcohol (0.19 mL, 3.3×10^{-2} mol), 4-dimethylaminopyridine (DMAP, 0.041g, 3.36×10^{-4} mol), and DCM (25 mL) were introduced into a round bottom flask and purged with nitrogen for 30 minutes. The solution was then cooled to 0 °C, and a mixture of DCM (1 mL) and *N*, *N*'-Dicyclohexylcarbodiimide (DCC; 0.69 g, 3.3×10^{-2} mol) was added dropwise over 30 minutes. After the overnight reaction at room temperature, the reaction was concentration, and column chromatography was used to separate the products. The final product was then concentration and dried. ^{1}H NMR (300 MHz, $CDCl_3$, δ (ppm**):** 7.20-7.70 (Ar*H*), 4.2 (d, 2H, -OC*H*$_2$CH-), 3.00 (s, -CC*H*-), 2.82 (t, -CC*H*$_2$CH$_2$CO-), 2.35 (t, -CCH$_2$C*H*$_2$CO-), 1.73 (s, -SCCNC*H*$_3$).

Alkyne-terminated poly(methyl methacrylate) (PMMA-Alkyne): To a 10 mL Schlenk flask, methyl methacrylate (*n* eq.**),** end functionalized RAFT-Alkyne (1 eq.**),** Azobisisobutyronitrile (AIBN) (0.1 eq.), and anisole (0.1 mL; internal standard) were added. After three freeze-pump-thaw cycles, the flask was placed into a preheated oil bath set at 60 °C. The polymerization was monitored by proton NMR and the reaction was stopped at the desired monomer conversion by cooling in an ice bath and then diluting the solution with THF. The solution was then precipitated into methanol twice. The solid product was collected by filtration and vacuum dried. ^{1}H NMR (300 MHz, $CDCl_3$ δ (ppm): 7.70-7.20 (Ar*H* RAFT agent), 3.4-3.8 **(**3H, -OC*H*$_3$),), 1.0-2.4 **(**br, -C*H*$_2$C*H*-).

Norbornene-terminated diblock copolymer PS-*b*-PMMA (NB-*g*-(PS-*b*-PMMA): Cu(I)Br (0.1 equiv.) was charged into a round bottom flask and purged with nitrogen. PMMA-alkyne (2 equiv.), NP-PS-N_3 (1 equiv.), and PMDETA (0.15 equiv.) were added to a pear shaped flask, dissolved in THF, and bubbled with nitrogen for 30 minutes. The mixture in the pear shaped flask was transferred to the round bottom flask and stirred at 40 °C overnight. The reaction mixture was then diluted with, DCM, and precipitated into methanol two times. The product was collected by centrifuge and vacuum dried overnight. ^{1}H NMR (CD_2Cl_2), δ (TMS, ppm): 6.35-7.33 (br, Ar*H*), 6.30 (s, 2H, C*H*=C*H*), 3.4-3.8 (3H, -OCH_3),), 1.0-2.4 **(**br, -CH_2C*H*-), 1.0-2.4 **(**br, -CH_2C*H*-).

Grafted block copolymer poly(norbornene-graft-(PS-*b*-PMMA)) (PNB-*g*-(PS-*b*-PMMA): Grubbs 3rd generation catalyst (1 equiv.) and anhydrous DMF (1 mL) were added to a schlenk line flask and bubbled with nitrogen for 10 minutes. NP-*g*-(PS-*b*-PEO) (*p* equiv.) was added to a pear shaped flask, dissolved in DMF (4 mL), and bubbled with nitrogen for 10 minutes. The mixture in the pear shaped flask was transferred to the schlenk line flask and stirred at 60 °C. The polymerization was monitored by GPC and terminated by addition of ethyl vinyl ether (5 equiv.) when all macromonomer was consumed. The reaction mixture was precipitated into diethyl ether two times. The solid product was collected by centrifuge and vacuum dried overnight. ^{1}H NMR (CD_2Cl_2), δ (TMS, ppm**):** 6.35-7.33 (br, Ar*H*), 5.42 and 5.60 (br, C*H*=C*H*), 3.4-3.8 (3H, -OCH_3), 1.0-2.4 **(**br, -CH_2C*H*-), 1.0-2.4 **(**br, -CH_2C*H*-).

Preparation of Modified Substrates. Surface modification of the silicon wafers with random brush copolymer P(S-*r*-MMA) with PS mol % = ~67%., was done by spin casting a 1.0 wt % of P(S-*r*-MMA) onto the wafer and then thermally annealed under

vacuum at 170 °C, which is well above the T_g for both PS (100 °C) and PMMA (115 °C) for 5 days.[74] This time allows for the end functional hydroxyl groups to diffuse into the substrate and react with oxide layer on the substrate, resulting in anchored polymer brushes.[74] Residual brush layers were removed by sonicating in toluene three times. The resulting anchored brush layer was confirmed through water contact angle measurements of un-treated silicon wafer with modified surfaces.

Preparation of Thin Films. The NP-*g*-(PS-*b*-PMMA) linear diblock copolymer and PNP-*g*-(PS-*b*-PMMA) grafted block copolymer was spin-cast (3000 RPM, 60 s) from toluene solutions (1.5 wt%) onto modified silicon substrates that were coated with the random copolymer layer. The thin films were then thermally annealed for various times at 150 °C.

5.4 Results and Discussion

Polystyrene-*block*-poly(methyl methacrylate) PS-*b*-PMMA diblock copolymers were grafted from a norbornene backbone through a combination of ATRP, RAFT, ROMP, and "click" chemistry. The synthetic route is shown in Scheme 5.1 and begins by synthesizing compound **2**, which has a norbornene unit that can be polymerized through ROMP, as well as having an ATRP initiating site. This compound is synthesized by reacting the primary alcohol of compound 1 with 2-bromoisobutyryl bromide in the presence of triethylamine. The product was confirmed through NMR. The chemical shift of the methylene protons adjacent to the alcohol in compound **1** clearly shifted downfield from 3.53 ppm to 4.15 ppm as the ester formed for compound **2** (Figure 5.1). Additionally, a singlet appeared at 1.90 ppm, which corresponds to the methyl groups of the tertiary alkyl halide.

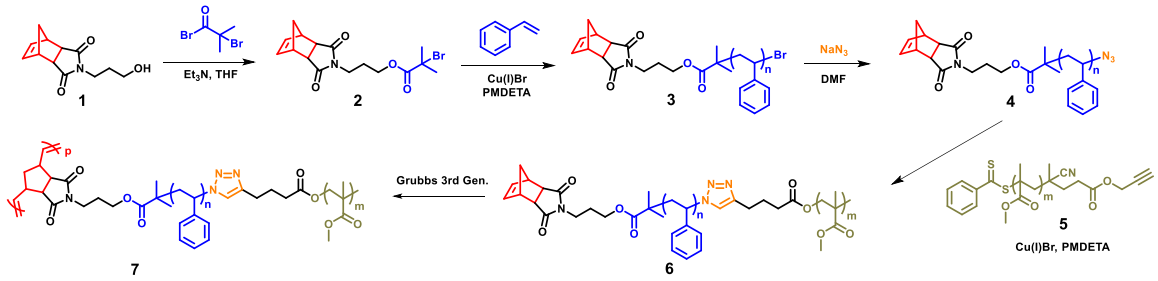

Scheme 5.1 Synthesis of grafted block copolymer PNb-*g*-(PS-*b*-PMMA) (**7**)

Nb-Br (**2**) was then used to initiate the polymerization of styrene using Cu(I)Br and PMDETA at 90 °C. The polymerization was monitored by ^{1}H NMR, as monomer conversion was calculated by comparing the ratio of the decrease of vinyl peaks at 5.74 and 5.22 ppm to the aromatic peaks between 6.00 and 7.40 ppm. The chain extensions were stopped at the desired percent conversion. The molecular weight was confirmed through ^{1}H NMR (Figure 5.1) and GPC. The dispersity was also confirmed through GPC. Nb-PS-N_3 (**3**) was obtained after reacting the terminal bromine group of Nb-PS-Br (**2**) with sodium azide in DMF. Extractions against water and precipitation into diethyl ether removed residual DMF. The azide was confirmed through FTIR, as a sharp peak at 2100 cm^{-1} appeared which is indicative of an azide stretch (Figure 5.2).

Simultaneously, an alkyne end-functionalized RAFT agent was used for polymerization of methyl methacrylate using AIBN in bulk at 60 °C. The polymerization was monitored by ^{1}H NMR, as monomer conversion was calculated by comparing the ratio of the decrease of double bond peaks at 6.20 and 5.70 ppm to the aromatic end group from the RAFT agent between 7.70-7.20 ppm. The polymerizations were stopped at the desired percent conversion. The molecular weight was confirmed through ^{1}H NMR (Figure 5.3) and GPC. The dispersity was also confirmed through GPC.

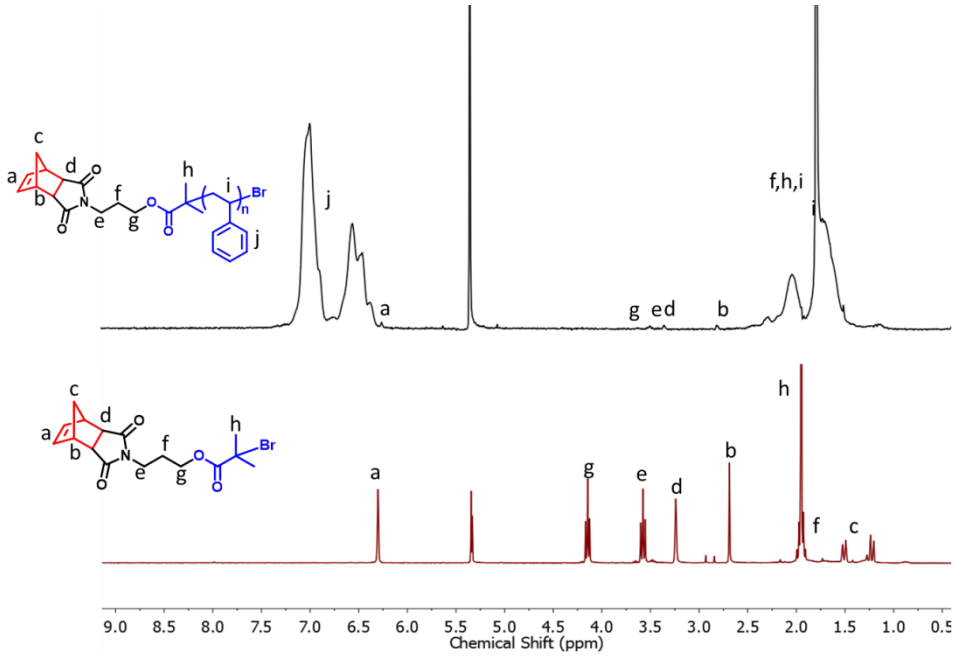

Figure 5.1 ^{1}H NMR spectra for compound **2** and polymer **3**

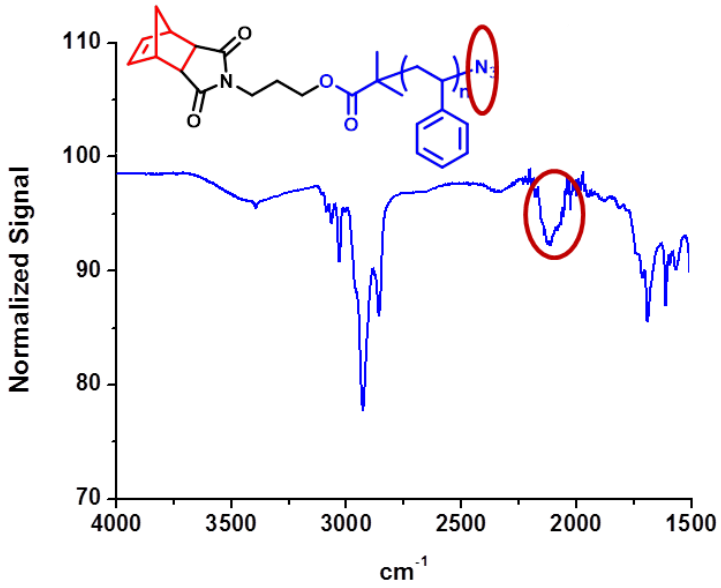

Figure 5.2 FTIR spectra for polymer **3**

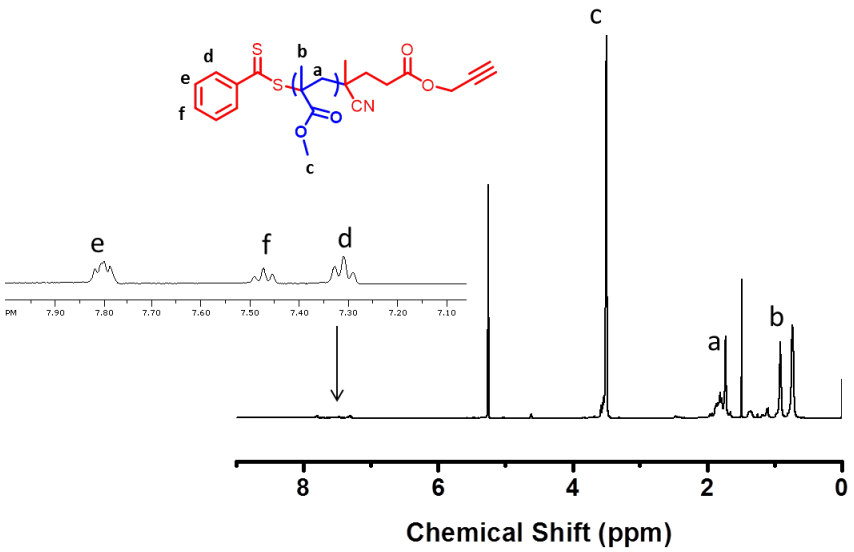

Figure 5.3 ^{1}H NMR spectra for polymer **5**

PMMA-alkyne (**5**) was then reacted with Nb-PS-N_3 (**4**) in a copper catalyzed alkyne-azide cycloaddition using a Cu(I)Br/PMDETA catalyst system. The reaction was monitored by GPC, and was stopped when all Nb-PS-N_3 (**4**) was consumed. Residual PMMA-alkyne was removed by precipitating in methanol twice. ^{1}H-NMR revealed the peaks characteristic for both PS (6.35-7.33, 1.0-2.4 ppm) and PMMA (3.4-3.8, and 1.0-2.4 ppm), while also having the norbornene end-functionalized groups (6.30 ppm) as seen in Figure 5.4. Additionally, clean shifts to higher molecular weight from homopolymer (**4**) and (**5**), to end-functionalized diblock copolymer (**6**) was observed in GPC (Figure 5.5 and 5.6).

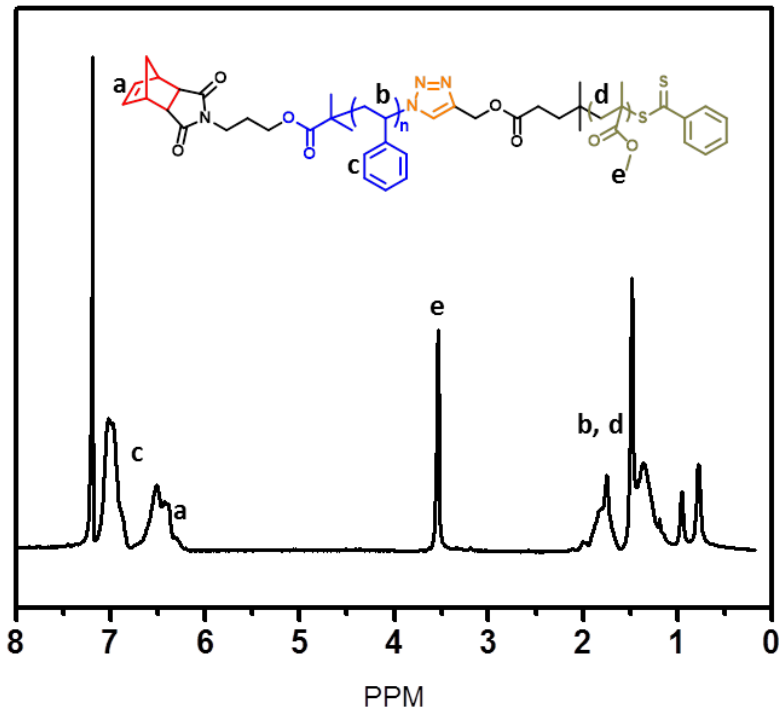

Figure 5.4 ^{1}H NMR spectra for polymer **6**

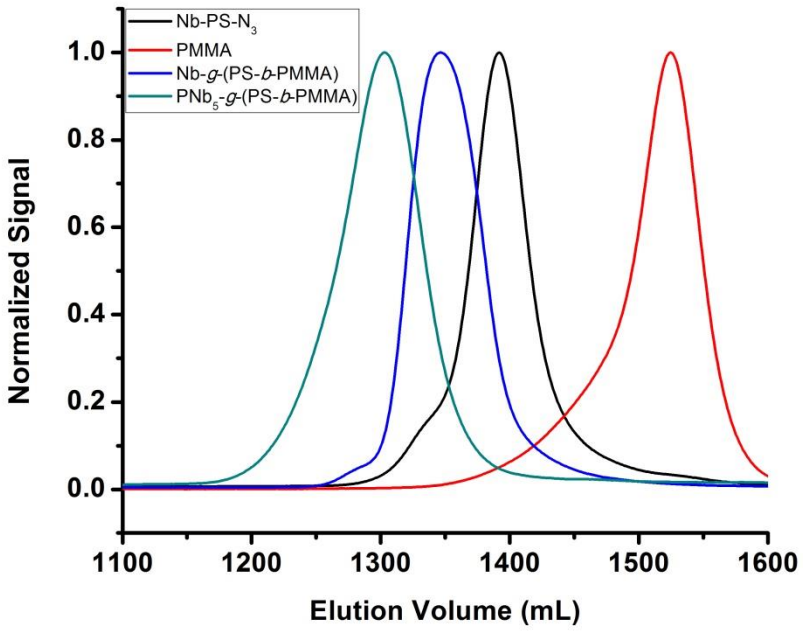

Figure 5.5 GPC traces for polymer **4a-7a**

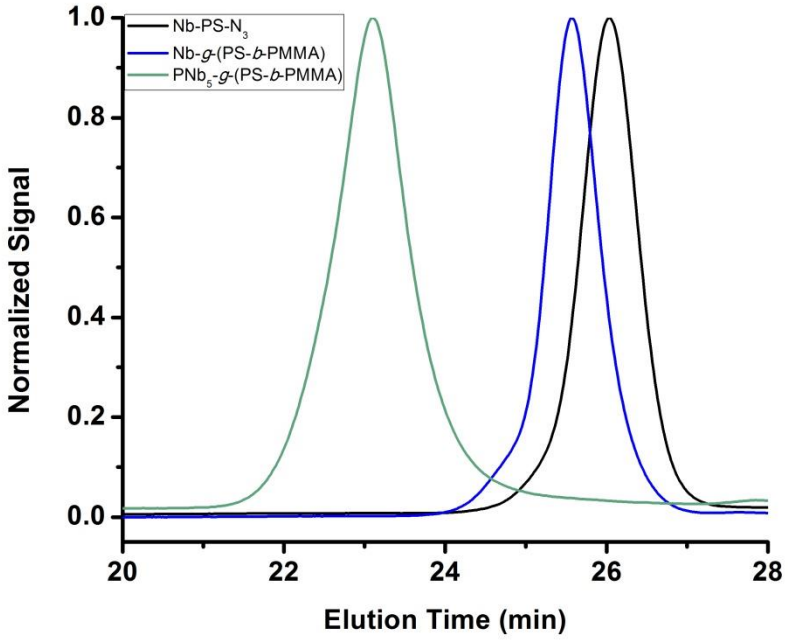

Figure 5.6 GPC traces for polymer **4b-7b**

Grubbs 3rd generation catalyst was used to polymerize the norbornene functionalized diblock copolymer **6** in DMF at 60 °C. The polymerization was monitored by GPC, and was quenched with ethyl vinyl ether once all macromonomer was consumed. The polymer was precipitated into methanol twice. ^{1}H NMR showed the disappearance of the initial norbornene alkene protons at 6.30, and the appearance of two new small peaks at 5.4 and 5.2, which indicate the new polymer alkenes (Figure 5.7). Furthermore, GPC also showed a 5x molecular weight increase which corresponds to the degree of polymerization targeted for this reaction. Additionally, there was also a clean shift from to the higher molecular weight grafted block copolymer, indicating no residual macromonomer (Figure 5.5 and 5.6). Furthermore, the dispersity of the final grafted block copolymer was 1.2-1.3, demonstrating that the combination of RAFT, ATRP,

ROMP, and "click" chemistry resulted in well-defined polymers. Table 5.1 provides the polymer compositions with their respected wt % and experimental χ_N values.

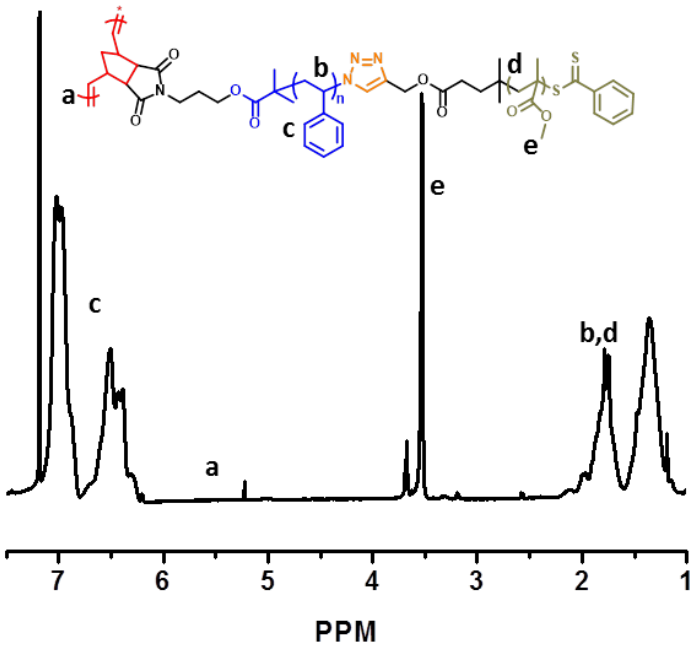

Figure 5.7 ^{1}H NMR spectra for polymer **7**

Surface modification of silicon wafers to help control the interfacial energetics was done by spin casting a 1.0 wt % solution of random brush copolymer (HO-PS-*r*-PMMA) from toluene. The thin film of random brush copolymer was thermally annealed under vacuum at 170 °C for 5 days. Films were then removed and sonicated in a solution of toluene to remove any unreacted brush copolymer. Water contact angles measurements were done to ensure the random brush copolymer diffused onto the surface of the oxide silicon wafer (Figure 5.8).

Table 5.1 Characterization of polymers **4-7**

Polymer Entry	M_n	PDI [a]	DP PNP	Wt. % PMMA	Wt. % PS	Wt. % Backbone	$\chi N \approx 0.06$ @ (rt)
4a	21100[a]	1.15	--	--	--	--	--
4b	11500 [a]	1.11	--	--	--	--	--
5a	6800 [a]	1.12	--	--	--	--	--
5b	3000 [a]	1.08	--	--	--	--	--
6a	27500	1.13	--	24.70	76.73	1.05	16.2
6b	14200	1.18	--	21.11	80.90	2.04	8.4
7a$_5$	136000[c]	1.23	5	25.00	77.21	1.06	81.2
7b$_5$	72100[c]	1.32	5	20.80	79.70	0.40	42.1

[a]Determined from GPC calibrated by PS standards. [b]From supplier. [c]Calculated from feed ratio.

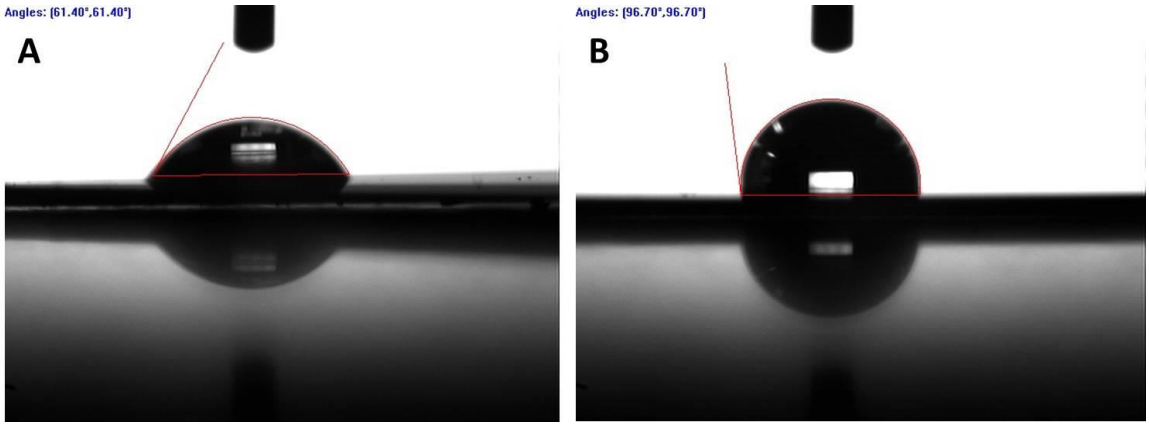

Figure 5.8 Water contact angle measurements for untreated silicon wafer (**A**); and HO-PS-*r*-PMMA random brush layer, PS mol % = ~67% (**B**).

The treated silicon wafer with the random brush copolymer had a water contact angle of (~96°), whereas the untreated was (~61°). The increase in water contact must be attributed to the presence of the more hydrophobic random brush copolymer layer. 1.5 wt % solutions of block copolymers **6** and **7** were spin casted onto the treated silicon wafers. The films were then thermally annealed under vacuum for 3 days at 150 °C. AFM measurements were done on both **6a** and **7a**, since both systems Flory-Huggins interaction parameter was well above the order-disorder transition (ODT). However, phase segregation was very ambiguous as illustrated in Figure 5.9 for both systems.

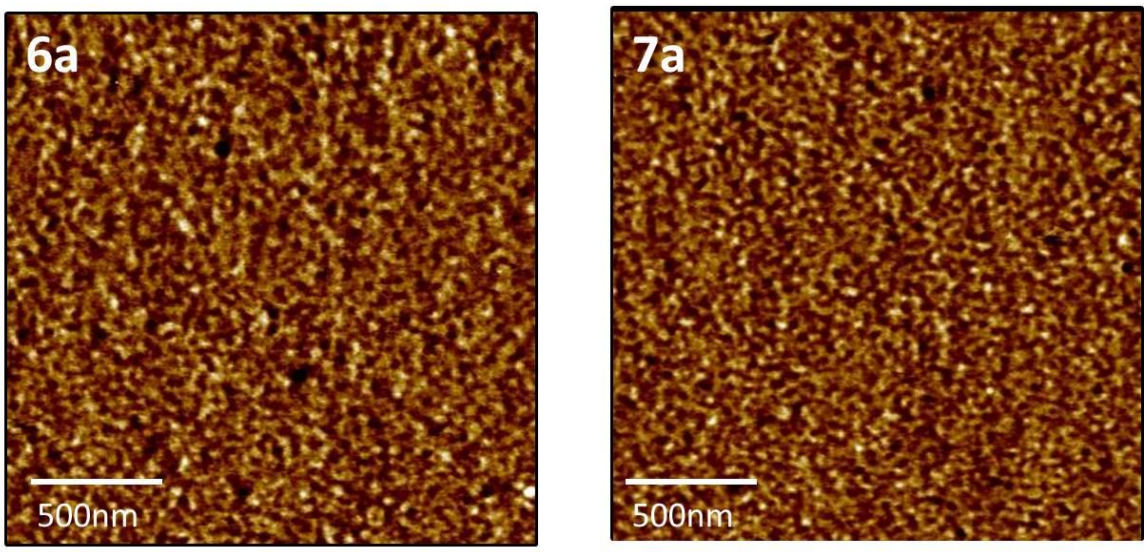

Figure 5.9 AFM images for diblock copolymer (**6a**) and grafted block copolymer (**7a**)

The lack of phase separation in both systems could be due to processing conditions such as thermal annealing or preparation of the films. Thermal annealing was also conducted on the lower molecular weight linear and grafted block copolymer (**6b** and **7b**), however, as expected, phase separation was ambiguous. Current work is focusing on SAXS measurements of all samples in bulk, as well as thin film GISAXS

measurements. These measurements will help us determine if phase in these polymeric systems. Furthermore, commercially available linear PS-*b*-PMMA diblock copolymer with similar molecular weight to our systems will be purchased and thermally annealed to see if our processing methods could be the problem. These simple measurements and tests should provide an insight to why our linear and grafted block copolymer systems are lacking phase separation.

5.5 Conclusion

In conclusion, we prepared both linear and grafted block copolymers using a combination of ATRP, RAFT, ROMP, and "click" chemistry. The grafted block copolymer consisted of a polynorbornene based backbone with PS-*b*-PMMA diblock copolymers as side-chains. Even though a complex synthetic strategy was employed and characterization confirmed all polymers were made in moderate yield, thin-film studies showed very ambiguous phase separation after thermal annealing. Further measurements and processing studies need to be carried out to fully understand how the system is behaving.

5.6 References

1. Bang, J.; Kim, S. H.; Drockenmuller, E.; Misner, M. J.; Russell, T. P.; Hawker, C. J., Defect-Free Nanoporous Thin Films from ABC Triblock Copolymers. *Journal of the American Chemical Society* **2006,** *128* (23), 7622-7629.
2. Bita, I.; Yang, J. K. W.; Jung, Y. S.; Ross, C. A.; Thomas, E. L.; Berggren, K. K., Graphoepitaxy of Self-Assembled Block Copolymers on Two-Dimensional Periodic Patterned Templates. *Science* **2008,** *321* (5891), 939-943.
3. Park, S.; Lee, D. H.; Xu, J.; Kim, B.; Hong, S. W.; Jeong, U.; Xu, T.; Russell, T. P., Macroscopic 10-Terabit–per–Square-Inch Arrays from Block Copolymers with Lateral Order. *Science* **2009,** *323* (5917), 1030-1033.
4. Ross, C., Patterned Magnetic Recording Media. *Annual Review of Materials Research* **2001,** *31*, 203-235.

5. Ruiz, R.; Kang, H.; Detcheverry, F. A.; Dobisz, E.; Kercher, D. S.; Albrecher, T. R.; de Pable, J. J.; Nealey, P. F., Density Multiplication and Improved Lithography by Directed Block Copolymer Assembly. *Science* **2008,** *321*, 936-939.
6. Ryu, D. Y.; Ham, S.; Kim, E.; Jeong, U.; Hawker, C. J.; Russell, T. P., Cylindrical Microdomain Orientation of PS-b-PMMA on the Balanced Interfacial Interactions: Composition Effect of Block Copolymers. *Macromolecules* **2009,** *42* (13), 4902-4906.
7. Tang, C.; Lennon, E. M.; Fredrickson, G. H.; Kramer, E. J.; Hawker, C. J., Evolution of Block Copolymer Lithography to Highly Ordered Square Arrays. *Science* **2008,** *322* (5900), 429-432.
8. Hadjichristidis, N.; Pispas, S.; Floudas, G., *Block Copolymers: Synthetic Strategies, Physical Properties, and Applications*. John Wiley & Sons, Inc.: Hoboken, NJ, 2003.
9. Hamley, I. W., *The Physics of Block Copolymers*. Oxford University Press: Oxford, U.K., 1998.
10. Hawker, C. J.; Russell, T. P., Block Copolymer Lithography: Merging "Bottom-Up" with "Top-Down" Processes. *MRS Bulletin* **2005,** *30* (12), 952-966.
11. Lazzari, M.; Liu, G.; Lecommandoux, S., *Block Copolymers in Nanoscience*. Wiley-VCH: Weinheim, 2007.
12. Park, C.; Yoon, J.; Thomas, E. L., Enabling Nanotechnology with Self Assembled Block Copolymer Patterns. *Polymer* **2003,** *44* (22), 6725-6760.
13. Bates, F. S., Polymer-Polymer Phase Behavior. *Science* **1991,** *251* (4996), 898-905.
14. Bates, F. S.; Fredrickson, G. H., Block Copolymer Thermodynamics: Theory and Experiment. *Annual Review of Physical Chemistry* **1990,** *41*, 525-557.
15. Ghoshal, T.; Maity, T.; Godsell, J. F.; Roy, S.; Morris, M. A., Large Scale Monodisperse Hexagonal Arrays of Superparamagnetic Iron Oxides Nanodots: A Facile Block Copolymer Inclusion Method. *Advanced Materials* **2012,** *24* (18), 2390-2397.
16. Glagola, C. P.; Miceli, L. M.; Milchak, M. A.; Halle, E. H.; Logan, J. L., Polystyrene–Poly(ethylene oxide) Diblock Copolymer: The Effect of Polystyrene and Spreading Concentration at the Air/Water Interface. *Langmuir* **2012,** *28* (11), 5048-5058.
17. Hardy, C. G.; Ren, L.; Ma, S.; Tang, C., Self-assembly of well-defined ferrocene triblock copolymers and their template synthesis of ordered iron oxide nanoparticles. *Chemical Communications* **2013,** *49* (39), 4373-4375.
18. Hardy, C. G.; Tang, C., Advances in square arrays through self-assembly and directed self-assembly of block copolymers. *Journal of Polymer Science Part B: Polymer Physics* **2013,** *51* (1), 2-15.
19. Hillmyer, M., Nanoporous Materials from Block Copolymer Precursors. In *Block Copolymers II*, Abetz, V., Ed. Springer Berlin Heidelberg: 2005; Vol. 190, pp 137-181.
20. Hobbs, R. G.; Farrell, R. A.; Bolger, C. T.; Kelly, R. A.; Morris, M. A.; Petkov, N.; Holmes, J. D., Selective Sidewall Wetting of Polymer Blocks in Hydrogen Silsesquioxane Directed Self-Assembly of PS-b-PDMS. *ACS Applied Materials & Interfaces* **2012,** *4* (9), 4637-4642.
21. Jung, Y. S.; Chang, J. B.; Verploegen, E.; Berggren, K. K.; Ross, C. A., A Path to Ultranarrow Patterns Using Self-Assembled Lithography. *Nano Letters* **2010,** *10* (3), 1000-1005.

22. Jung, Y. S.; Ross, C. A., Solvent-Vapor-Induced Tunability of Self-Assembled Block Copolymer Patterns. *Advanced Materials* **2009,** *21* (24), 2540-2545.
23. Shin, K.; Leach, K. A.; Goldbach, J. T.; Kim, D. H.; Jho, J. Y.; Tuominen, M.; Hawker, C. J.; Russell, T. P., A Simple Route to Metal Nanodots and Nanoporous Metal Films. *Nano Letters* **2002,** *2* (9), 933-936.
24. Tang, C.; Bang, J.; E. Stein, G.; Fredrickson, G. H.; Hawker, C. J.; Kramer, E. J.; Sprung, M.; Wang, J., Square Packing and Structural Arrangement of ABC Triblock Copolymer Spheres in Thin Films. *Macromolecules* **2008,** *41* (12), 4328-4339.
25. Tang, C.; Bang, J.; Stein, G. E.; Fredrickson, G. H.; Hawker, C. J.; Kramer, E. J.; Sprung, M.; Wang, J., Square Packing and Structural Arrangement of ABC Triblock Copolymer Spheres in Thin Films. *Macromolecules* **2008,** *41*, 4328-4339.
26. Tang, C.; Hur, S.-m.; Stahl, B. C.; Sivanandan, K.; Dimitriou, M.; Pressly, E.; Fredrickson, G. H.; Kramer, E. J.; Hawker, C. J., Thin Film Morphology of Block Copolymer Blends with Tunable Supramolecular Interactions for Lithographic Applications. *Macromolecules* **2010,** *43* (6), 2880-2889.
27. Tang, C.; Sivanandan, K.; Stahl, B. C.; Fredrickson, G. H.; Kramer, E. J.; Hawker, C. J., Multiple Nanoscale Templates by Orthogonal Degradation of a Supramolecular Block Copolymer Lithographic System. *ACS Nano* **2010,** *4* (1), 285-291.
28. Tang, C.; Tracz, A.; Kruk, M.; Zhang, R.; Smilgies, D.-M.; Matyjaszewski, K.; Kowalewski, T., Long-Range Ordered Thin Films of Block Copolymers Prepared by Zone-Casting and Their Thermal Conversion into Ordered Nanostructured Carbon. *Journal of the American Chemical Society* **2005,** *127* (19), 6918-6919.
29. Tang, C.; Wu, W.; Smilgies, D.-M.; Matyjaszewski, K.; Kowalewski, T., Robust Control of Microdomain Orientation in Thin Films of Block Copolymers by Zone Casting. *Journal of the American Chemical Society* **2011,** *133* (30), 11802-11809.
30. Thurn-Albrecht, T.; Schotter, J.; Kästle, G. A.; Emley, N.; Shibauchi, T.; Krusin-Elbaum, L.; Guarini, K.; Black, C. T.; Tuominen, M. T.; Russell, T. P., Ultrahigh-Density Nanowire Arrays Grown in Self-Assembled Diblock Copolymer Templates. *Science* **2000,** *290* (5499), 2126-2129.
31. Yang, X.; Wan, L.; Xiao, S.; Xu, Y.; Weller, D. K., Directed Block Copolymer Assembly versus Electron Beam Lithography for Bit-Patterned Media with Areal Density of 1 Terabit/inch2 and Beyond. *ACS Nano* **2009,** *3* (7), 1844-1858.
32. Bates, F. S.; Fredrickson, G. H., Block Copolymers---Designer Soft Materials. *Physics Today* **1999,** *52* (2), 32-38.
33. Bates, F. S.; Hillmyer, M. A.; Lodge, T. P.; Bates, C. M.; Delaney, K. T.; Fredrickson, G. H., Multiblock Polymers: Panacea or Pandora's Box? *Science* **2012,** *336* (6080), 434-440.
34. Fredrickson, G. H.; Bates, F. S., Dynamics of Block Copolymers: Theory and Experiment. *Annual Review of Materials Research* **1996,** *26* (1), 501-550.
35. Hawker, C. J.; Wooley, K. L., The Convergence of Synthetic Organic and Polymer Chemistries. *Science* **2005,** *309* (5738), 1200-1205.
36. Stuparu, M. C.; Khan, A.; Hawker, C. J., Phase separation of supramolecular and dynamic block copolymers. *Polymer Chemistry* **2012,** *3* (11), 3033-3044.
37. Helfand, E.; Wasserman, Z. R., Block Copolymer Theory .5. Spherical Domains. *Macromolecules* **1978,** *11* (5), 960-966.

38. Helfand, E.; Wasserman, Z. R., Block Co-Polymer Theory .6. Cylindrical Domains. *Macromolecules* **1980,** *13* (4), 994-998.
39. Leibler, L., Theory of Microphase Separation in Block Copolymers. *Macromolecules* **1980,** *13*, 1602-1617.
40. Haensch, C.; Hoeppener, S.; Schubert, U. S., Chemical modification of self-assembled silane based monolayers by surface reactions. *Chemical Society Reviews* **2010,** *39* (6), 2323-2334.
41. Ham, S.; Shin, C.; Kim, E.; Ryu, D. Y.; Jeong, U.; Russell, T. P.; Hawker, C. J., Microdomain Orientation of PS-b-PMMA by Controlled Interfacial Interactions. *Macromolecules* **2008,** *41* (17), 6431-6437.
42. Han, E.; Stuen, K. O.; La, Y.-H.; Nealey, P. F.; Gopalan, P., Effect of Composition of Substrate-Modifying Random Copolymers on the Orientation of Symmetric and Asymmetric Diblock Copolymer Domains. *Macromolecules* **2008,** *41* (23), 9090-9097.
43. Huang, E.; Russell, T. P.; Harrison, C.; Chaikin, P. M.; Register, R. A.; Hawker, C. J.; Mays, J., Using Surface Active Random Copolymers To Control the Domain Orientation in Diblock Copolymer Thin Films. *Macromolecules* **1998,** *31* (22), 7641-7650.
44. Liu, P.-H.; Thébault, P.; Guenoun, P.; Daillant, J., Easy Orientation of Diblock Copolymers on Self-Assembled Monolayers Using UV Irradiation. *Macromolecules* **2009,** *42* (24), 9609-9612.
45. Mansky, P.; Liu, Y.; Huang, E.; Russell, T. P.; Hawker, C., Controlling Polymer-Surface Interactions with Random Copolymer Brushes. *Science* **1997,** *275* (5305), 1458-1460.
46. Mansky, P.; Russell, T. P.; Hawker, C. J.; Mays, J.; Cook, D. C.; Satija, S. K., Interfacial Segregation in Disordered Block Copolymers: Effect of Tunable Surface Potentials. *Physical Review Letters* **1997,** *79* (2), 237-240.
47. Niemz, A.; Bandyopadhyay, K.; Tan, E.; Cha, K.; Baker, S. M., Fabrication of Nanoporous Templates from Diblock Copolymer Thin Films on Alkylchlorosilane-Neutralized Surfaces. *Langmuir* **2006,** *22* (26), 11092-11096.
48. Ouk Kim, S.; Solak, H. H.; Stoykovich, M. P.; Ferrier, N. J.; de Pablo, J. J.; Nealey, P. F., Epitaxial self-assembly of block copolymers on lithographically defined nanopatterned substrates. *Nature* **2003,** *424* (6947), 411-414.
49. Rockford, L.; Mochrie, S. G. J.; Russell, T. P., Propagation of Nanopatterned Substrate Templated Ordering of Block Copolymers in Thick Films. *Macromolecules* **2001,** *34* (5), 1487-1492.
50. Ryu, D. Y.; Shin, K.; Drockenmuller, E.; Hawker, C. J.; Russell, T. P., A Generalized Approach to the Modification of Solid Surfaces. *Science* **2005,** *308* (5719), 236-239.
51. Segalman, R. A.; Yokoyama, H.; Kramer, E. J., Graphoepitaxy of Spherical Domain Block Copolymer Films. *Advanced Materials* **2001,** *13* (15), 1152-1155.
52. Stein, G. E.; Kramer, E. J.; Li, X.; Wang, J., Single-Crystal Diffraction from Two-Dimensional Block Copolymer Arrays. *Physical Review Letters* **2007,** *98* (8), 086101.
53. Ryu, D. Y.; Wang, J.-Y.; Lavery, K. A.; Drockenmuller, E.; Satija, S. K.; Hawker, C. J.; Russell, T. P., Surface Modification with Cross-Linked Random Copolymers: Minimum Effective Thickness. *Macromolecules* **2007,** *40* (12), 4296-4300.

54. Rzayev, J.; Hillmyer, M. A., Nanochannel Array Plastics with Tailored Surface Chemistry. *Journal of the American Chemical Society* **2005,** *127*, 13373-13379.
55. Bucholz, T. L.; Loo, Y.-L., Phase Behavior of Near-Monodisperse Semifluorinated Diblock Copolymers by Atom Transfer Radical Polymerization. *Macromolecules* **2006,** *39* (18), 6075-6080.
56. Jung, Y. S.; Ross, C. A., Orientation-Controlled Self-Assembled Nanolithography Using a Polystyrene−Polydimethylsiloxane Block Copolymer. *Nano Letters* **2007,** *7* (7), 2046-2050.
57. Son, J. G.; Gotrik, K. W.; Ross, C. A., High-Aspect-Ratio Perpendicular Orientation of PS-b-PDMS Thin Films under Solvent Annealing. *ACS Macro Letters* **2012,** *1* (11), 1279-1284.
58. Kim, S. H.; Misner, M. J.; Xu, T.; Kimura, M.; Russell, T. P., Highly Oriented and Ordered Arrays from Block Copolymers via Solvent Evaporation. *Advanced Materials* **2004,** *16* (3), 226-231.
59. Airaud, C. d.; Héroguez, V. r.; Gnanou, Y., Bicompartmentalized Polymer Particles by Tandem ROMP and ATRP in Miniemulsion. *Macromolecules* **2008,** *41* (9), 3015-3022.
60. Charvet, R.; Novak, B. M., One-Pot, One-Catalyst Synthesis of Graft Copolymers by Controlled ROMP and ATRP Polymerizations. *Macromolecules* **2004,** *37* (23), 8808-8811.
61. Cheng, C.; Khoshdel, E.; Wooley, K. L., One-Pot Tandem Synthesis of a Core−Shell Brush Copolymer from Small Molecule Reactants by Ring-Opening Metathesis and Reversible Addition−Fragmentation Chain Transfer (Co)polymerizations. *Macromolecules* **2007,** *40* (7), 2289-2292.
62. Feng, C.; Li, Y.; Yang, D.; Hu, J.; Zhang, X.; Huang, X., Well-defined graft copolymers: from controlled synthesis to multipurpose applications. *Chemical Society Reviews* **2011,** *40* (3), 1282-1295.
63. Kriegel, R. M.; Rees, W. S.; Weck, M., Synthesis and Hydrolysis of Poly(norbornene)/Poly(acrylic acid) Graft Copolymers Synthesized via a Combination of Atom-Transfer Radical Polymerization and Ring-Opening Metathesis Polymerization. *Macromolecules* **2004,** *37* (17), 6644-6649.
64. Le, D.; Montembault, V.; Soutif, J. C.; Rutnakornpituk, M.; Fontaine, L., Synthesis of Well-Defined ω-Oxanorbornenyl Poly(ethylene oxide) Macromonomers via Click Chemistry and Their Ring-Opening Metathesis Polymerization. *Macromolecules* **2010,** *43* (13), 5611-5617.
65. Le, D.; Morandi, G.; Legoupy, S.; Pascual, S.; Montembault, V.; Fontaine, L., Cyclobutenyl macromonomers: Synthetic strategies and ring-opening metathesis polymerization. *European Polymer Journal* **2013,** *49* (5), 972-983.
66. Xie, M.; Dang, J.; Han, H.; Wang, W.; Liu, J.; He, X.; Zhang, Y., Well-Defined Brush Copolymers with High Grafting Density of Amphiphilic Side Chains by Combination of ROP, ROMP, and ATRP. *Macromolecules* **2008,** *41* (23), 9004-9010.
67. Cheng, J. Y.; Ross, C. A.; Smith, H. I.; Thomas, E. L., Templated Self-Assembly of Block Copolymers: Top-Down Helps Bottom-Up. *Advanced Materials* **2006,** *18* (19), 2505-2521.
68. Chiefari, J.; Chong, Y. K.; Ercole, F.; Krstina, J.; Jeffery, J.; Le, T. P. T.; Mayadunne, R. T. A.; Meijs, G. F.; Moad, C. L.; Moad, G.; Rizzardo, E.; Thang, S. H.,

Living Free-Radical Polymerization by Reversible Addition−Fragmentation Chain Transfer: The RAFT Process. *Macromolecules* **1998,** *31* (16), 5559-5562.
69. Gu, W.; Huh, J.; Hong, S. W.; Sveinbjornsson, B. R.; Park, C.; Grubbs, R. H.; Russell, T. P., Self-Assembly of Symmetric Brush Diblock Copolymers. *ACS Nano* **2013,** *7* (3), 2551-2558.
70. Runge, M. B.; Bowden, N. B., Synthesis of High Molecular Weight Comb Block Copolymers and Their Assembly into Ordered Morphologies in the Solid State. *Journal of the American Chemical Society* **2007,** *129* (34), 10551-10560.
71. Hardy, C. G.; Islam, M. S.; Gonzalez-Delozier, D.; Morgan, J. E.; Cash, B.; Benicewicz, B. C.; Ploehn, H. J.; Tang, C., Converting an Electrical Insulator into a Dielectric Capacitor: End-Capping Polystyrene with Oligoaniline. *Chemistry of Materials* **2013,** *25* (5), 799-807.
72. Ren, L.; Zhang, J.; Bai, X.; Hardy, C. G.; Shimizu, K. D.; Tang, C., Preparation of cationic cobaltocenium polymers and block copolymers by "living" ring-opening metathesis polymerization. *Chemical Science* **2012,** *3* (2), 580-583.
73. Sanford, M. S.; Love, J. A.; Grubbs, R. H., A Versatile Precursor for the Synthesis of New Ruthenium Olefin Metathesis Catalysts. *Organometallics* **2001,** *20* (25), 5314-5318.
74. In, I.; La, Y.-H.; Park, S.-M.; Nealey, P. F.; Gopalan, P., Side-Chain-Grafted Random Copolymer Brushes as Neutral Surfaces for Controlling the Orientation of Block Copolymer Microdomains in Thin Films. *Langmuir* **2006,** *22* (18), 7855-7860.

CHAPTER 6

SUMMARY AND OUTLOOK

6.1 Dissertation Summary

Block copolymers have been recognized as potential candidates for various applications based on their ability to form nano-scale patterns. Specifically, these materials can be used as templates in nanolithography since the length scales are in the range of 5-30 nm. Furthermore, the ability to incorporate functional groups into the chain-ends, side-chains, or as linkers between chains allows for confinement of the functional group either in a specific domain or at the interface between domains in microphase separated block copolymers. Also, specific morphologies can be obtained by simply altering parameters in the block copolymer system. The general objective of research done in this thesis project focuses on developing highly ordered arrays of domains which could be used as templates for future microelectronic devices, with the aim in reducing feature size and pitch. Specifically, this dissertation covers two main objectives: (1) addressing critical issues in solvent annealing of polystyrene-*block*-(ethylene oxide) in thin films; reduction of annealing time and implementation of industrially compatible solvents; (2) the design, synthesis, and characterization of various functional block copolymers architectures using controlled radical polymerization techniques and robust chemistry.

The first facet of this dissertation is described in chapter 2 where the reduction of annealing time by nearly an order of magnitude was done with PS-*b*-PEO under high humidity solvent annealing with toluene by simply decreasing the annealing chamber size was achieved. Furthermore the utilization of two industry-benign solvents, MEK and PGMEA, allowed the formation of ordered surface patterns under high humidity, however, these solvents reduced the incompatibility between each block, thus requiring

longer annealing time. These simple changes to high-humidity solvent annealing protocols can be easily implemented.

The second part of this dissertation involved design of various diblock and triblock copolymer architectures. Chapter 3 elaborates on work on decreasing feature size while retaining the films stability. This was done using grafted and star block copolymers in which PS-*b*-PEO diblock copolymers served as side-chains or arms respectively from a backbone or a core. By limiting the backbone length, and number of arms, enhanced inter-chain entanglement led to enhanced quality of films with high degrees of order. For both systems the feature size and spacing were dictated by the molecular weight of the side-chains or arms, while the overall molecular weight of each system ensures film stability. In another facet, chapter 4 addresses a series of P2VP-PS-PI triblock copolymers to target alternating square arrays of cylinders. Again, this work stemmed from previous work involving PEO-PS-PI triblock copolymers. A series of triblock copolymers was successfully synthesized through RAFT polymerization and "click" chemistry. Although square arrays of cylinders were not obtained, AFM and TEM measurements showed hexagonally packed domains at the surface. Finally, chapter 5 describes grafted block copolymers in which PS-*b*-PMMA diblock copolymers served as side chains grafted from a backbone. A series of grafted copolymers were successfully synthesized by a combination of ATRP, RAFT, ROMP, and "click" chemistry. Even though highly ordered arrays were not obtained, these materials have the potential to create a toolbox of low molecular weight PS-*b*-PMMA diblock copolymers as side chains to decrease the feature size and pitch in thin films while still maintaining film stability.

6.2 Future Work

To expand the reduction of annealing time, further research could be explored through microwave solvent annealing. This would further reduce annealing time down to seconds.[1-4] Also, expanding research with other industry-benign solvents for solvent annealing of other polymer compositions would make this process more industrially friendly.

Other polymeric architectures like multi-segmented block copolymers and miktoarm star block can be prepared to allow low feature sizes and high film stability. These systems utilize a central core to link the low molecular weight polymers. Furthermore, other work could be focused on using star copolymers with high Flory-Huggins interaction parameters (χ) such as PS-*b*-PDMS ($\chi \approx 0.26$). This could enable us to use even lower molecular weight linear block copolymers as the side-chains than that of PS-*b*-PEO.

6.3 References

1. Borah, D.; Senthamaraikannan, R.; Rasappa, S.; Kosmala, B.; Holmes, J. D.; Morris, M. A., Swift Nanopattern Formation of PS-b-PMMA and PS-b-PDMS Block Copolymer Films Using a Microwave Assisted Technique. *ACS Nano* **2013,** *7* (8), 6583-6596.
2. Borah, D.; Shaw, M. T.; Holmes, J. D.; Morris, M. A., Sub-10 nm Feature Size PS-b-PDMS Block Copolymer Structures Fabricated by a Microwave-Assisted Solvothermal Process. *ACS Applied Materials & Interfaces* **2013,** *5* (6), 2004-2012.
3. Mokarian-Tabari, P.; Cummins, C.; Rasappa, S.; Simao, C.; Sotomayor Torres, C. M.; Holmes, J. D.; Morris, M. A., Study of the Kinetics and Mechanism of Rapid Self-Assembly in Block Copolymer Thin Films during Solvo-Microwave Annealing. *Langmuir* **2014,** *30* (35), 10728-10739.
4. Hardy, C. G. Functional Block Copolymers for Applications in Advanced Materials, Energy Storage, and Lithography. University of South Carolina, Columbia, SC, 2013.

APPENDIX A

COPYRIGHT RELEASES

Dear Mr. Jeffery Hayat,

Thank you for placing your order through Copyright Clearance Center's RightsLink service. Elsevier has partnered with RightsLink to license its content. This notice is a confirmation that your order was successful.

Your order details and publisher terms and conditions are available by clicking the link below:
http://s100.copyright.com/CustomerAdmin/PLF.jsp?ref=b382360f-720f-400e-84a0-42c59cd843c7

Order Details
Licensee: Jeffery Hayat
License Date: Sep 22, 2015
License Number: 3714310408805
Publication: European Polymer Journal
Title: Improving humidity-controlled solvent annealing processes for block copolymer poly(ethylene oxide)-b-polystyrene
Type Of Use: reuse in a thesis/dissertation
Total: 0.00 USD

To access your account, please visit https://myaccount.copyright.com.

Please note: Online payments are charged immediately after order confirmation; invoices are issued daily and are payable immediately upon receipt.

To ensure that we are continuously improving our services, please take a moment to complete our customer satisfaction survey.

B.1:v4.2

Figure A.1. Copyright release for Chapter 2